# On Sizing and Control of a Renewables-based Hybrid Power Supply System for Stand-Alone Applications in an Island Context

Tony El Tawil

UNIVERSITE SCIENCES
BRETAGNE DE LA MER
LOIRE ET DU LITTORAL

Thèse préparée à l'Université de Bretagne Occidentale

pour obtenir le diplôme de DOCTEUR délivré de façon partagée par L'Université de Bretagne Occidentale et l'Université de Bretagne Loire

*Spécialité : Génie Electrique*

**École Doctorale Sciences de la Mer et du Littoral**


présentée par

Tony EL TAWIL

Préparée au sein de l'Institut de Recherche de l'Ecole Navale (EA 3634 IRENav) et au sein de l'Institut de Recherche Dupuy de Lôme (FRE CNRS 3744 IRDL)


# On sizing and control of a renewables-based hybrid power supply system for stand-alone applications in an island context


This project has received financial support from Brest Metropole and Ecole Navale


**Thèse soutenue le 11 Janvier 2018**
devant le jury composé de :

**Seddik BACHA**
Professeur, Université Grenoble Alpes, Grenoble / *président*

**Manuela SECHILARIU**
Professeur, Université de Technologie de Compiègne / *rapporteur*

**Quoc Tuan TRAN**
Professeur INSTN et CEA-INES, Chambéry / *rapporteur*

**Chritopher FRANQUET**
Ingénieur, ENTECH Smart Energies, Quimper / *invité*

**Jean Frédéric CHARPENTIER**
Maître de Conférence - HDR, Ecole Navale / *directeur de thèse*

**Mohamed BENBOUZID**
Professeur, Université de Bretagne Occidentale / *co-directeur de thèse*

UBO Université de Bretagne Occidentale

*"Therefore let your soul exalt your reason to the height of passion, that it may sing; and let it direct your passion with reason, that your passion may live through its own daily resurrection, and like the phoenix rise above its own ashes."*

KHALIL GIBRAN

# *Abstract*

This PhD thesis models a renewable-based hybrid power supply system applied in an islanded context and investigates sizing and regulation strategies of such a hybrid system. First, various marine energy production technologies were reviewed and compared to common renewable resources. As well, various energy storage technologies were reviewed, compared, and evaluated to fit the chosen site characteristics. A brief investigation on offshore energy transmission and inverter regulations methods is presented. Then, a study of the site characteristics, and the availability of the different renewable energy resources in the area are presented. This energy study constitutes the basis of the proposed system sizing method, where minimizing the cost and the CO2 emissions are considered as the main objectives. Furthermore, a fuzzy logic power management approach is proposed for the islanded microgrid. Finally, a detailed study of the system components grid-side inverter regulation is presented. Three regulation levels were investigated: the single inverter, the renewable farm, and the hybrid system. In this context, different regulation strategies are considered at each level.

# *Acknowledgements*

This work has been carried out at French Naval Academy Research Institute (EA 3436 IRENav) and at the Institut de Recherche Dupuy de Lôme (FRE CNRS 3744 IRDL) of the University of Brest. The financial support provided by Brest Métropole (BM) is gratefully acknowledged.

I wish to express my gratitude to my main supervisor Dr. Jean Frédéric CHARPENTIER for the consistently inspiration, encouragement and guidance throughout this work. I also wish to thank my supervisor Prof. Mohamed BENBOUZID for his valuable comments, suggestions and discussions related to this thesis and the published papers.

I wish to thank the pre-examiners Prof. Manuela SECHILARIU from 'Université de Technologie de Compiègne' and Prof. Quoc Tuan TRAN from INSTN and CEA-INES, Chambéry for their valuable comments and corrections. I am also grateful to Prof. Seddik BACHA from the University of Grenoble Alpes for examining my work. Finally, i wish to thank Mr. Christopher FRANQUET from ENTECH Smart energies for representing industrial interest in my work and giving practical comments.

Special thanks are due to Prof. Ibrahim MOUKARZEL for his help, council, and encouragement during my entire academic studies.

I wish to thank my colleagues Dhafar, Zakarya, Youness, Ousmane, Zhibin, Sofiane, Ali, Hajj-Ahmad, and Wissame; the helps given by them have been very important to me. As well I wish to thank my friends Peter, Elie, and Joe; their friendship is a great support in my life. also I wish to thank Ms. Solenne DERIGOND for her support and company.

Finally, I am deeply indebted to my parents Nazira EL HAGE and Adel EL TAWIL, and my siblings Chady EL TAWIL and Rozy EL TAWIL, for their infinite love and untiring support.

Brest
MÉTROPOLE & VILLE

# List of Publications

Main results of this PhD thesis have lead to the following publications:

International journals:

1. T. El Tawil, J. F. Charpentier, and M. E. H. Benbouzid, "Tidal energy site characterization for marine turbine optimal installation: Case of the Ouessant island in France," International Journal of Marine Energy, vol. 18, pp. 57-64, June 2017.
2. T. El Tawil, J.F. Charpentier and M.E.H. Benbouzid, “Sizing and rough optimization of a hybrid renewable-based farm in a stand-alone marine context,” Renewable Energy, vol. 115, pp. 1134–1143, January 2018.

International conferences:

1. T. El Tawil, J. F. Charpentier, and M. E. H Benbouzid, "Sizing and rough optimization of a hybrid power generation system based on renewables in a stand-alone marine context," in Proceedings of the 2017 ELECTRIMACS, Toulouse (France), pp. 1-7, July 2017.
2. T. El Tawil, J. F. Charpentier, M. E. H Benbouzid, and G. Yao, "Design, analysis, and comparison of inverter control methods for microgrid application for stand-alone sites," in Proceedings of the 2017 IEEE IEMDC, Miami (USA), pp. 1-8, May 2017.

# Contents

# List of Figures

# List of Tables

# Introduction

In our modern era, pollution presents the greatest threat for the entire human society. Deforestation and greenhouse gazes emission are changing the climate of the planet. More than $25\%$ of global greenhouse gazes emission is due to electrical power production. Therefore, the presence of renewable green energy sources (wind, sunlight, geothermal heat, hydro-power, ...) has been growing, and will keep their accelerated growth for many decades. Furthermore, renewable power production can present a final solution for greenhouse gazes emission. In fact, using electricity, many applications related to agriculture, industry, and transportation that contribute to $24\%$, $21\%$, and $14\%$ of global greenhouse gazes emission respectively, can be transformed to pollution free applications.

In this context, islands are extremely affected by climate change. They are even more affected then continents by such climate variations and the consequences are higher for these sites. Moreover, such sites are dependent on imported combustion resources, which presents even high cost in addition to their greenhouse gazes emission. Furthermore, the west Atlantic-European shore, where Ouessant island is situated, present an access to abundant renewable energies, most notably ocean based ones. Therefore, an inclusion of renewable energy sources on such islanded sites can present great advantages. However, small islanded sites present a critical grid stability since they are completely separated from the main continental grid. Such stability constraint presents a key feature for the success of this study.

Oceans and seas present high potential for supporting renewable power production systems, counting: offshore wind energy, tidal energy, marine thermal energy, wave energy, marine osmosis energy, and marine biomass energy. French western coast presents a high tidal power production potential. For example, France present a high tidal energy potential around $42\ \%$ of the $24\ TWh/year$ total energy potential of the European coast [20]. Moreover, oceans present large unused spaces, where offshore wind turbine farms with a high power production potential can be installed. In fact, such offshore

projects can avoid two major wind farms constraints. Firstly, the noise emitted from wind turbines can disturb the population living nearby. Offshore wind farms are far enough from populated areas so to minimize such noise disturbances. Secondly, large scale wind farms occupy huge space, and therefore large amount of land must be sacrified. However, oceans present a lot of unused spaces, and therefore large scale offshore wind farms can be constructed with less space constraints.

However, there are still some difficulties in offshore applications. Firstly, offshore energy transmission cables are costly, while losses are significant. Secondly, the total cost of offshore projects can be significantly higher than onshore ones. Finally, offshore technology is not yet as mature as its onshore counterpart. View the advantages and disadvantage of marine renewable energies, such application can be very effective if used in a well studied project and in a suitable site.

The main objective of this Ph.D. thesis is therefore to study the cost and $CO_2$ emission efficiency of such marine based renewable energy production systems, when used in stand-alone marine site. Some inverter control strategies where as well applied in this thesis, in order to simulate the technical efficiency (the stability of the electrical signal from both voltage and frequency aspects) of such systems.

The contribution of this thesis are:

- Proposal of using a hybrid energy production system for a small stand-alone maritime site located in the north Atlantic like the island of Ouessant. All potential energy production sources were investigated and a suitable multi-source system was chosen.
- Proposal of a simple approach for a rough optimization of the hybrid system sizing, where a power network was established between the different elements of the system, and used to determine the efficiency of each element.
- Proposal of a fuzzy logic power management strategy, in order to regulate the power production of the hybrid system elements.
- Comparing a virtual synchronous generator control approach to other traditional inverter regulation methods, when applied to hybrid energy production system in a stand-alone context.

- Development of two simulation platforms (under Matlab/Simulink) for a full hybrid energy production system, including: wind turbines, tidal turbines, pumped hydroelectric energy storage system, diesel generator, fuzzy logic controller, and a dynamic load. The first simulator considers a power network exchange and is used for long simulations, where the fuel consumption and the $CO_2$ emission are evaluated. The second simulator considers the electrical systems with a time step of $5.10^{-6}\ s$ and is developed for the study of the microgrid stability.

This thesis is organized as follows:

**Chapter 1** presents the up-to-date information on the achievements in marine renewable energy technologies, while exploring their possible adaptation to stand-alone maritime context. It reviews and compares various energy storage technologies used for large energy storage capacity, under the same stand-alone maritime context. It reviews as well different offshore energy transmission methods and various inverter regulation methods, which can be adapted for such islanded sites.

**Chapter 2** presents the different marine energies and their potential power production on a chosen typical islanded site.

**Chapter 3** deals with a rough optimization method in order to minimize both cost and $CO_2$ emission for the studied site.

**Chapter 4** details various regulation methods for grid side inverter in a renewable energy production system with a multi-source aspect. These methods are finally adapted in the case of a stand-alone installation.

# 1. State of the Art of Renewable Energy and Energy Storage Systems Technologies in a Stand Alone Maritime Context

## 1.1 Introduction

This thesis studies a power supply hybrid system, including: renewable energy sources, diesel generators, and an energy storage system. The study will focus on two major parts; the first part will be a power management and system sizing in order to minimize the $CO_2$ emission and the system cost, while the second part will focus on the regulation of the system elements. Mainly, the stability of the electrical signal voltage and frequency of the grid have to be controlled. One of the originalities in this study is the stand-alone context of the site. This factor changes the concept of renewable energy control from a maximal power transfer-based regulation to a voltage and frequency-based regulations.

The state of art, presented in this chapter, will focus on four major parts. In a first part, the most common and some marine renewable energy technologies will be presented while focusing on a management and applicability point of view (cost, production, maturity, existing installations) and adaptation to the study case. In a second part, the possible energy storage systems (ESS) will be investigated and a study similar to the renewable energies technologies case will be presented for the ESS technologies. In a third part, the energy transmission for offshore applications will be addressed. This part will focus on the offshore energy transmission and it will be based on previous studies and publications. In a final part, different regulation strategies for renewable energy sources will be investigated. Pros and cons of the more classical

regulation methods will be presented, with their possible adaptation to the studied case.

## 1.2 Stand-Alone Maritime Site Suitable Renewable Energy Systems

This thesis focuses on stand-alone maritime sites situated in the north Atlantic near the western European shore. The load of such islanded sites varies with its nature and population. For example, the load in Ouessant island varies around a few $MW$. Therefore, three possible renewable energy sources will be presented: offshore wind turbines, tidal turbines, and wave generators. Furthermore, and in order to better understand the performance of such maritime systems, the two most common onshore renewable energy sources will be also presented: onshore wind turbines and photo-voltaic solar panels.

### 1.2.1 Onshore wind turbine

An onshore wind turbine is a turbine based electrical generator, it transforms the kinetic energy of the wind to electrical energy, and it is located onshore. Wind turbines are well developed and mature system, reaching a mark of $9$ on the TRL scale (technology readiness level) [21, 22], which makes it one of the most developed renewable energy systems. The largest operating wind farm is the Gansu wind farm in china (fig.1.1), with a production capacity of $5160\ MW$ [23, 24].

FIGURE 1.1: Gansu wind farm [1].

In addition to its high maturity and large scale existing installations, onshore wind turbines are one of the cheapest renewable energy systems. In fact, referring to IRENA (international renewable energy agency) the cost of a wind

turbine depends heavily on the site characteristics, but it is roughly estimated by a total capital cost between $1.85$ \$ and $2.1$ \$ per $W$ of installation and a total production cost of $0.08$ \$ to $0.14$ \$ per $kWh$ of production [25,26].

Onshore wind turbine is the most used renewable energy technology, it presents the lowest costs and the highest maturity. Furthermore, wind energy is a very reliable source of energy in the chosen site location. However, wind turbine farms needs large space to be built, which might present difficulties in a small stand-alone islanded site as Ouessant. Moreover, they can cause noise due to vibrations. For the reasons cited above, onshore wind turbines will be avoided in this study.

### 1.2.2 Photovoltaic panel

Solar panels transform the solar energy to electrical energy. They present high efficiency in sunny regions. Solar panels are well developed and mature systems, reaching a mark of $9$ on the TRL scale [21,22]. The largest operating solar panel station is the Topaz solar farm in the U.S.A.(fig.1.2), its DC peak power is $375$ $MW$ [27].


FIGURE 1.2: the Topaz solar farm.

One disadvantage of solar panels is their cost. In fact, referring to IRENA, the cost of solar panels can be roughly estimated by a total capital cost between $3.8$ \$ and $5.8$ \$ per $W$ of installation and a total production cost of $0.25$ \$ to $0.65$ \$ per $kWh$ or production [25].

Solar panels are a very mature renewable energy technology. As sited earlier, large solar farms can be found. Furthermore, solar radiations present

the highest source of renewable energy worldwide [28]. However as onshore wind turbines, solar panels need large space to be built, which can present difficulties in a small stand-alone islanded site as Ouessant. Furthermore, the studied location presents low solar radiations, which limits the effectiveness of this technology. Moreover, PV panels recycling methods are still limited and underdeveloped [29, 30]. For the reasons cited above, photovoltaic panels will be avoided in this study.

### 1.2.3 Offshore wind turbine

Offshore wind turbines are wind turbines installed in the ocean or the sea (fig.1.3). In fact, one of the greatest problems of wind turbines is the noise produced due to the vibrations, and the unsteady characteristics of the wind. View their distance from habitation, offshore wind turbines presents an advantage over onshore ones for that concern. But at the other hand, the offshore wind turbine presents many disadvantages: higher prices, harder to install, and lower TRL level.

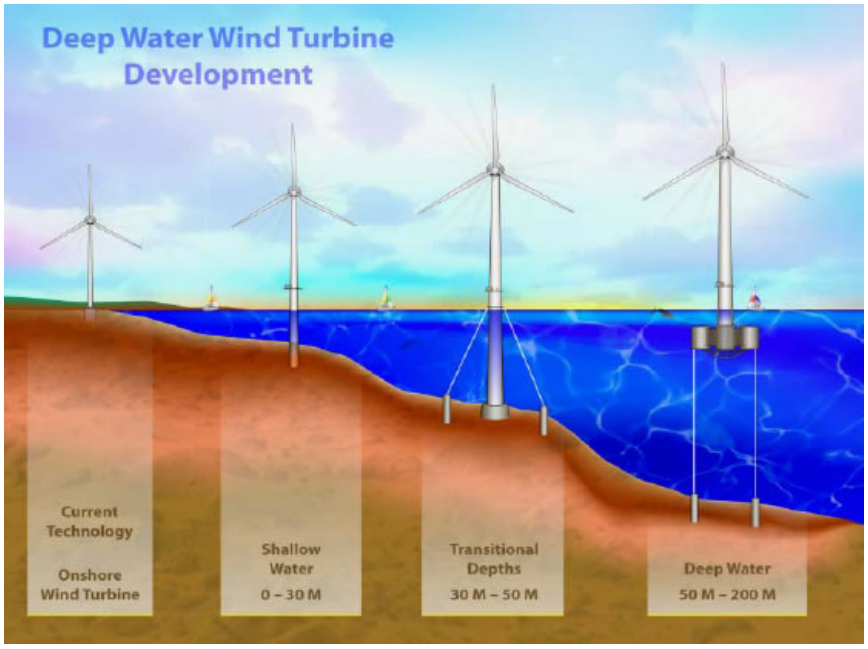


FIGURE 1.3: Offshore wind turbines [2].

Two kinds of offshore wind turbines can be found: fixed bottom offshore wind turbines and floating offshore wind turbines. First, fixed bottom offshore wind turbines are fixed to the sea floor using foundation (pile, tripod, jacket) as shown in figure 1.3. They reach a mark of 8 on the TRL scale [21,22] with the offshore wind farm of London array in the U.K. as the largest in the

world, it presents a capacity of $630\ MW$ [31]. For the cost of a fixed bottom offshore wind turbine, IRENA gives the following rough estimations: a total capital cost between $4\ \$$ and $4.5\ \$$ per $W$ of installation and a total production cost of $0.08\ \$$ to $0.14\ \$$ per $kWh$ of production [25,26]. However, fixed bottom offshore wind turbines are limited to shallow water sites, with a depth lower then $50\ m$ (figure 1.3) [2].

Floating offshore wind turbines are setup in a floating platform, which is moored to the seabed. Such technology allows to setup turbines in deeper waters, as shown in figure 1.3. This technology reaches a mark of $6$ on the TRL scale [21, 22]. The largest offshore floating wind turbine farm is in the U.S.A. with a capacity of $20\ MW$ [32], and the largest project is located in japan with 6 turbines of $2\ MW$ up to 80 turbines till 2020 [33]. The cost of floating offshore wind turbines is hard to estimate. In fact, IRENA does not give any approximation. But other studies show the following rough estimations: a total capital cost between $3.5\ \$$ and $4.5\ \$$ per $W$ of installation and a total production cost of $0.15\ \$$ to $0.19\ \$$ per $kWh$ or production [25,26].

The chosen site present several advantages that help offshore wind turbine technology. In fact, a large zone of shallow water around is present near the island, such zone allows the usage of the more mature fixed bottom offshore wind turbines. Furthermore, the site presents relatively high wind potential. For the reasons cited above, offshore wind turbines will be considered as a potential energy source for this study.

### 1.2.4 Tidal turbine

Tidal turbine technology is still under development, only research-based applications can be found around the world. It transforms the kinetic energy of the underwater tidal currents to electricity via a turbine (fig.1.4). However, tidal energy is promising, view the high density of water (about 1000 times the density of the air) and the predictability of tidal currents. Tidal turbines reach a mark of $7$ on the TRL scale [21, 22]. An example of precommercial tidal turbine farm is the Sabella project in France [34], and the biggest turbine are around $2\ MW$ [35].

Tidal turbines cost is hard to estimate. In fact, IRENA does not give any approximation. But other studies [36] show a total capital cost between $4\ \$$ and $4.5\ \$$ per $W$ of installation and a total production cost of $0.13\ \$$ to $0.18\ \$$ per

FIGURE 1.4: Sabella tidal turbine [3].

$kWh$ of production. Furthermore, two tidal turbine technologies can be identified: the yaw driven tidal turbine and the bidirectional tidal turbine. The yaw driven tidal turbines is able to rotate and change its axis direction in order to follow the direction of the tidal current.The bidirectional tidal turbine present a fixed axis direction, and therefore can use the tidal energy resulting of the current projection on its axis. View their difference, the yaw driven technology can present higher efficiency compared to the bidirectional one, however it needs further maintenance view the complex mechanical systems it presents.

Tidal turbines present an interesting source of energy in the studied site, which presents very high tidal currents [37]. However, tidal turbines still face many challenges, for example: the biofouling and underwater operations. The biofouling is a major problem that can cause disturbances on the tidal system, and can even stop turbine rotation [38]. Underwater operations present most of the installation and maintenance of tidal turbines, such operations can be costly and dangerous due to the submerged nature of tidal turbines [39]. View the advantages tidal turbines present in the considered site, they will be considered as a potential energy source in this study.

### 1.2.5 Wave power

Electric energy can be created by transforming the kinetic energy of the waves into electricity. This technology is still under development and little applied


FIGURE 1.5: Wave energy farm in Scotland [4].

around the world. Its TRL level is around $5$ [21, 22] the lowest between the presented technologies. The largest farm is located in Scotland with a capacity of $3\ MW$ (fig.1.5) [40].

Wave energy farms are the most expensive to build between the studied systems. In fact, referring to IRENA, wave energy farms present a total capital cost between $6.2$ \$ and $11.2$ \$ per $W$ of installation and a total production cost of $0.264$ \$ to $0.622$ \$ per $kWh$.

Wave energy farms can be easily accessed, since they are mainly offshore floating system. therefore installation and maintenance of such technology is easier compared to tidal current systems that must be underwater at all time. However, wave energy presents the lowest maturity in the investigated renewable energy systems, and studies are still needed in order to industrialize such technology. For all these reasons, wave energy will be avoided in this study.

## 1.3 Energy Storage Systems Suitable for Stand-Alone Maritime Site

In this studied, an islanded site is considered. In such study case, both the load of the island and the renewable energy production will be highly intermittent. Therefore, balancing the production and the load on the gird presents a key feature. For these reasons, it is necessary to optimize the system behavior by associating an energy storage system to the renewable

energy sources. In fact, energy storage systems can store electricity or transform electrical energy into other forms of energy and storing it in the process. Different energy storage systems can be applied to an islanded site. The more used ones will be presented in this part of the study.

### 1.3.1 Pumped hydroelectric storage

Pumped hydroelectric storage (PHS) (fig.1.6) presents the largest energy storage capacity form for grid applications (about $95\%$ of the total energy stored) [41, 42]. Such systems use the gravity potential energy of the water for storage purposes. In fact, at times of low demand, excess generation capacity is used to pump water from a lower reservoir into a higher one. When power is needed, water is released back into the lower reservoir threw a turbine, generating electricity [43]. The largest PHS station is the Bath country station in the U.S.A., with a production capacity of $3\ GW$ [41, 42].

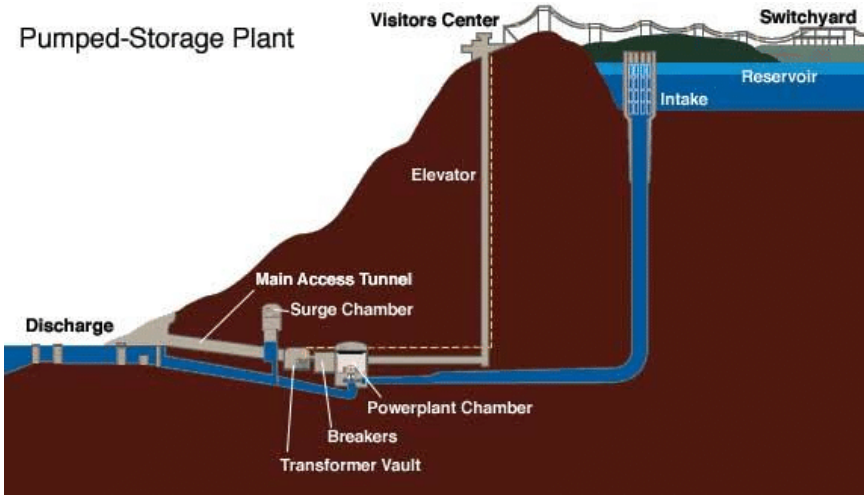


FIGURE 1.6: PHS station [1].

The energy stored in a PHS station is related to the volume $V$ of water stored in the upper reservoir and the altitude difference $h$ between the upper and lower reservoirs. In fact, the gravity potential energy respects the following equation:

$$E_p = mgh \tag{1.1}$$

where, $E_p$ is the gravity potential energy, $m$ is the mass of the water stored in the upper reservoir, and $g$ is gravitational constant. The mass of water is considered proportional to its volume,

$$m = \rho V \tag{1.2}$$

where $\rho$ is the density of the water. Therefore,

$$E_p = \rho V g h \tag{1.3}$$

finally, by adding the efficiency of the PHS $\mu_{phs}$

$$E_{PHS} = \mu_{phs} \rho V g h \tag{1.4}$$

The PSH is the most developed between the different storage systems in this study. It scores a $9$ TRL level [44]. PHS systems present also two key features: their long discharge time and their remarkable lifetime [43]. However, PHS systems present a low efficiency per volume unit since it needs two reservoirs, and each reservoir volume must be higher or equal to the one presented in equation (1.4), which presents a problem when applied in small islanded sites.

Referring to IRENA [15], PHS presents a total capital cost between $1$ \$ and $4$ \$ per $W$ of installation and a total production cost of $0.05$ \$ to $0.15$ \$ per $kWh$.

FIGURE 1.7: SWPHS station in Japan.

Sea water pumped hydroelectric storage (SWPHS) is an alternative choice

derived from the PHS, where the lower reservoir is replaced by the ocean or the sea (fig.1.7). This technology is still researched, since it is not yet fully mature, and therefore it is yet rarely used [45]. Therefore cost estimations are very vague and not yet published. However, SWPHS technology is subject of many research studies [45–48], and it can present the solution of the low volume efficiency of PHS systems.

To conclude, PHS has been used in islanded projects with a big success. But the chosen island presents limited free space. Therefore, a SWPHS will be considered even tho it is less mature then its PHS counterpart.

### 1.3.2 Compressed air

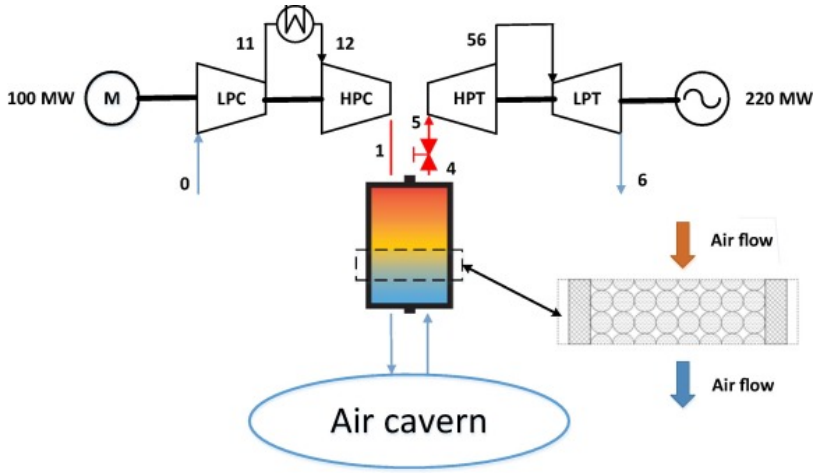


FIGURE 1.8: Advanced adiabatic compressed air storage (AA-CAES) [5].

Compressed air energy storage (CAES), is an energy storing method where the air is compressed in underground reservoir, so it can be released in the future for re-transforming the pressure to electrical power. Knowing that compressing the gas creates thermal energy, CAES presents high losses. Therefore it has a lower efficiency compared to PHS systems. The advanced adiabatic compressed air storage (AA-CAES) (fig.1.8) adds a second storage system to the CAES to be able to store the heat and reuse it, it is more efficient then the CAES system [18].

Referring to IRENA [15], CAES presents a total capital cost between $0.8\ \$$ and $1\ \$$ per $W$ of installation and a total production cost of $0.1\ \$$ to $0.2\ \$$ per $kWh$ of production.


FIGURE 1.9: Ocean-base underwater compressed air storage [6].

CAES systems are advantageous in sites where natural reservoirs can be found, for example depleted gaze fields. But the chosen site does not include such properties. A more interesting alternative is the ocean-base underwater compressed air energy storage (OCAES) technology. Such technology is being developed for offshore renewable energy applications. OCAES utilizes the hydrostatic pressure to keep the compressed air (in an air bag/accumulator) under constant high pressure at the bottom of the ocean (fig.1.9). In this way, the expensive pressure tanks or underground cavern can be avoided [18]. However, waters surrounding Ouessant island are shallow, and long distances must be crossed in order to find suitable location for OCAES. Moreover, the chosen site presents high tidal currents which decreases the lifespan of such systems and increases their maintenance cost.

### 1.3.3 Batteries

Batteries are systems that store electricity in the form of chemical energy. A battery is comprised of a cathode (positive electrode), an anode (negative electrode), and an electrolyte that provides the electrons transfer between the electrodes. During discharge, electrochemical reactions at the two electrodes generate a flow of electrons through an external circuit with the cathode accepting electrons and the anode providing electrons. During charging process, the electrochemical reactions are reversed and the battery absorbs electrical energy from the external circuit.

Batteries are known for their lower power usage [18, 44]. Therefore they are used in large variety of applications, from electronic systems to electric cars. They present high efficiency in low power DC applications. But in higher power gird applications, batteries present a lower maturity compared to PHS

and CAES. Reference [15] present a various maturity values scoring between $6$ and $8$ on the TRL scale for different kinds of batteries. In fact, reference [15] indicates that Lead-acid batteries score the highest maturity, $8$ on TRL scale. Li-ion and NaS (sodium sulfur) batteries score a $7$ and the redox flow batteries score a $6$ on the same TRL scale. Furthermore, batteries present a notable self discharge problem [7, 15], which reduces their efficiency when charging for long time periods. Finally, batteries used for gird applications present a high cost and a short lifetime. In fact, according to reference [15], batteries capital cost, production cost, and lifetime can vary from $0.3$ to $4$ $\$/W$, from $0.05$ to $0.45$ $\$/kWh$, and from $3$ to $15$ years respectively 1.1.

TABLE 1.1: Summary of batteries technology and cost [15].

| | Lead-acid | Li-ion | NaS | Redox flow |
|---|---|---|---|---|
| Lifetime (years) | 3 - 10 | 10 - 15 | 15 | 5 - 15 |
| Capital cost ($/W) | 0.3 - 0.8 | 0.4 - 1 | 1 - 2 | 3 - 4 |
| Production cost ($/kWh) | 0.25 - 0.35 | 0.3 - 0.45 | 0.05 - 0.15 | 0.25 - 0.3 |

However, in recent years, batteries technology for grid applications starts appearing in real projects. Reference [7] presents an up to date survey on technological developments in batteries for grid applications. One of the highest power for such batteries applications, is the 'Santa Rita Jail Smart Grid Advanced Energy Storage System' in California based on a Li-ion technology, with a $32\ MW/0.25\ h$ storage capacity. As for the application with the highest storage capacity, the 'Sumitomo Electric Industries' in Hokkaido-Japan based on the Vanadium Redox Flow technology, present a $15\ MW/60\ MWh$ storage capacity. According to the Navigant research and the U.S. department of energy's global database [7], figure 1.10 presents the estimated worldwide battery storage installed capacity, and estimation on the evolution of this technology for the near future.

Even tho battery technology for grid applications presents lower maturity compared to PHS and CAES, with a notable self discharge problem, a high cost, and a short lifetime. This technology can still be very effective for small stand-alone sites, mostly the Vanadium redox technology which presents higher storage capacity. Such systems can even be considered in this studied site, however a SWPHS was chosen and developed.

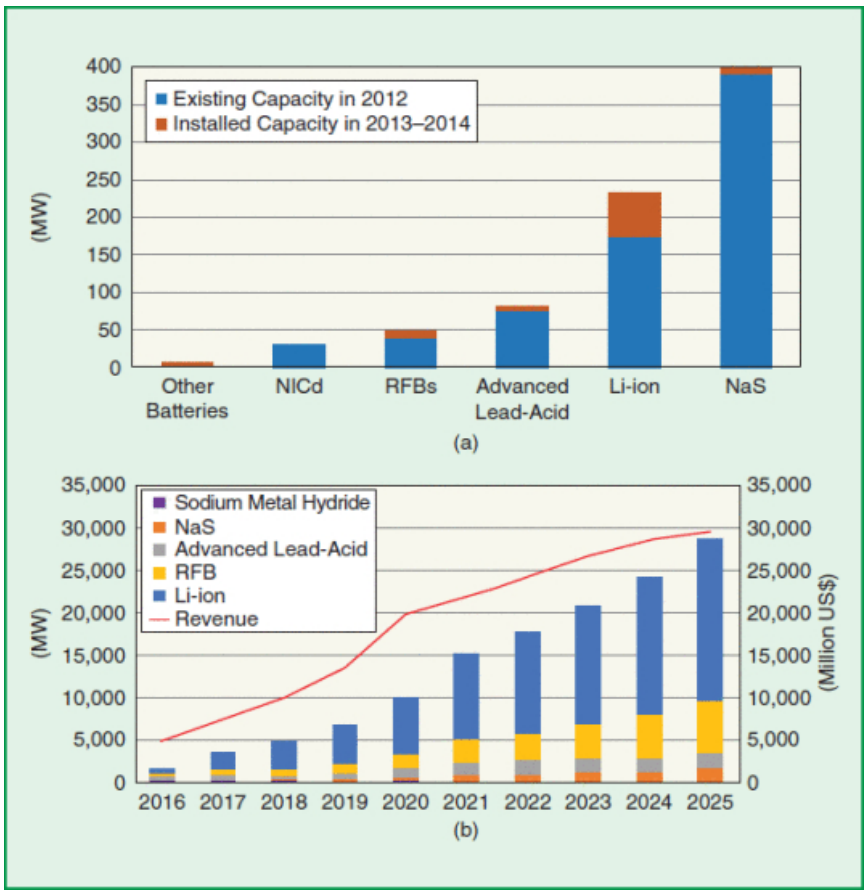


FIGURE 1.10: The (a) estimated installed battery capacity and (b) commissions ($MW$) in the worldwide power section [7].

## 1.4 Offshore Energy transmission

After studying different renewable energy systems related to the considered islanded site, mostly based on ocean energies (tidal turbines, offshore wind turbines and wave energy). One of the biggest problems faced is the offshore transmission of energy, which proved to be challenging and costly [9]. Three major transmission methods exist: Medium Voltage Alternative Current (MVAC), High Voltage Alternative Current (HVAC) and High Voltage Direct Current (HVDC). Each method has its own strength and weaknesses. In fact, higher the voltage is lower the losses are; but at the same time, higher the voltage is more complex and expensive the system's equipments are. Table 1.2 shows a comparison between the alternative current and the direct current systems [8, 49].

Most of offshore energy transmission studies relate the transmission method to two factors: the power transmitted and the transmission distance [8, 9]. In

TABLE 1.2: AC/DC comparison in offshore transmission.

| **AC** | **DC** |
|---|---|
| Possible to avoid offshore platform | Needs offshore platform |
| Possible to avoid switching losses (converters) | Switching losses at converters |
| Mature and reliable technology high power applications | Well proven technology in but in other applications |
| Less cost due to standard components | High cost |
| Need reactive power compensation | No need for reactive power compensation |
| Synchronous connection | Asynchronous connection |
| Considerable losses | Negligible losses |
| Highly effected by grid errors | Not very effected by grid error but needs stability control |

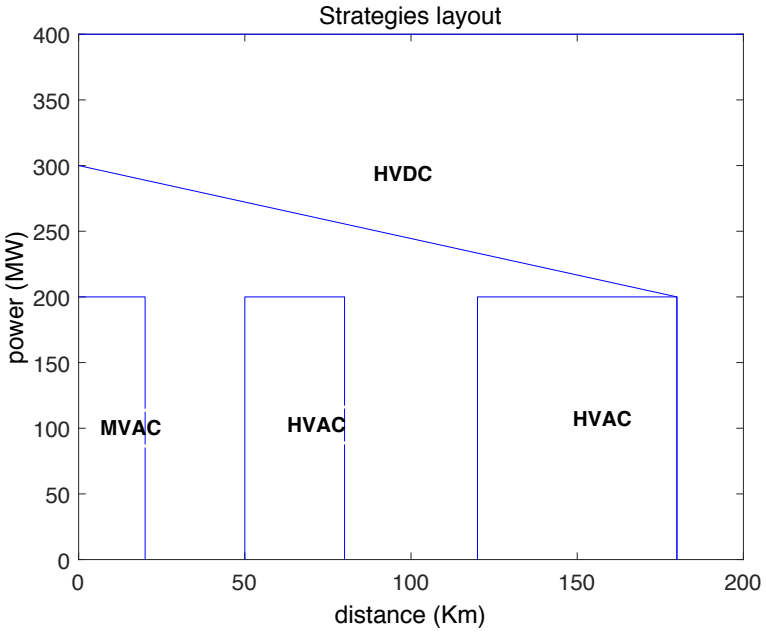


FIGURE 1.11: Offshore energy transmission strategy according to [8].

fact, as explained earlier, medium voltage needs less expensive and less complex systems but causes more losses on the lines. Therefore, when transmission distance is short and transmitted power is relatively low, using MVAC systems is the logical solution. HVAC and HVDC systems are more suitable for even longer distances and higher power [8,9]. Two different studies [8,9] illustrated in Fig.1.11 and Fig.1.12, present the boundaries at which different energy transmission methods in offshore projects are considered. Knowing that the considered site presents a power around $2\ MW$ and a relatively short

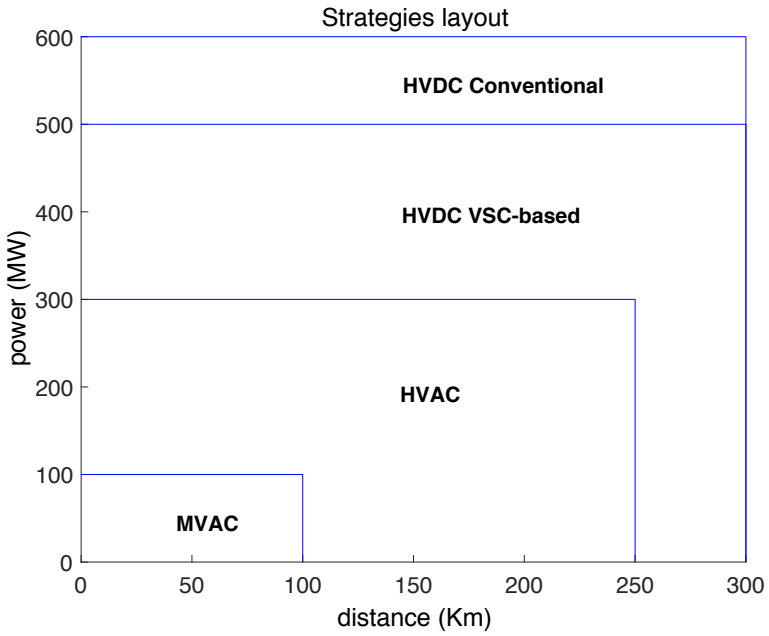


FIGURE 1.12: Offshore energy transmission strategy according to [9].

distance of offshore transmission (around $2\ km$), both references converge to the same solution of a MVAC transmission. Moreover, in low offshore power transmission ($< 5\ MW$), which includes the chosen site, a MVAC grid voltage lower than $10\ KV$ should be considered [50].

## 1.5 Renewable Energy Systems Regulation

Renewable energy sources started to appear in considerable capacity on the international grid since the beginning of the 21st century [10, 11, 51–53]. In fact, according to reference [52], in 1990, the total wind-power world capacity was around $1\ GW$, and the solar photo-voltaic one presented values even smaller than $1\ GW$. After 1990, the renewable energy world capacity started increasing at an accelerating rate. By the year 2007, always according to the reference [52], the wind-power world capacity reached more then $90\ GW$, and the solar one reached more then $11\ GW$. More recent references [10, 11] present the recent evolution of these technologies, Figures 1.13 and 1.14 illustrate the renewable energy growth. In fact, according to the 'Renewables 2015 Global Status Report', wind energy reached around $370\ GW$ in $2017$ and PV energy reached $177\ GW$ of installed rated power.

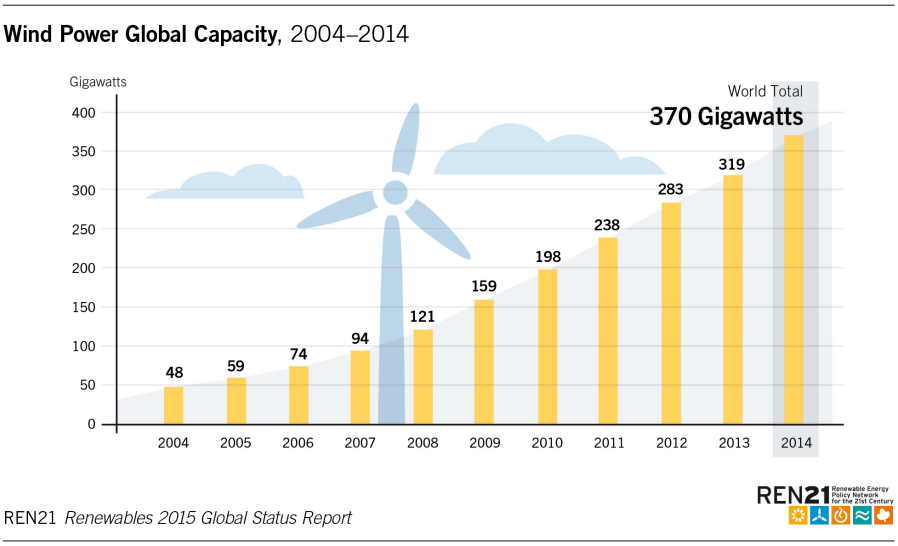


FIGURE 1.13: Wind power growth (2004-2014) [10, 11].

This recent increase in renewable energies on the grid is leading to new problems, particularly concerning the regulation and stability of the grid. In fact, renewable energies regulation and stability presents the following challenges:

- Most of renewable energy resources are not fully controllable. For example, when the load increases a diesel generator can increase the diesel combustion and produce more power; at the other hand, the wind can not be controlled at a faster value for a wind turbine to produce more power. Therefore, it is necessary to develop energy storage systems, in order to maintain the power stability on the grid [54].
- Many renewable energy resources are not yet fully mature. In fact, most renewable energy resources are still being researched and developed. Therefore, they can produce disturbances (counting voltage drop and frequency fluctuations) on the grid [55].
- Most renewable energy systems are connected to the grid via inverters. Knowing that inverters presents fast dynamics [56, 57], changes in the grid power can produce disturbances on the electrical signal.
- As presented earlier, large scale renewable energy systems are recently

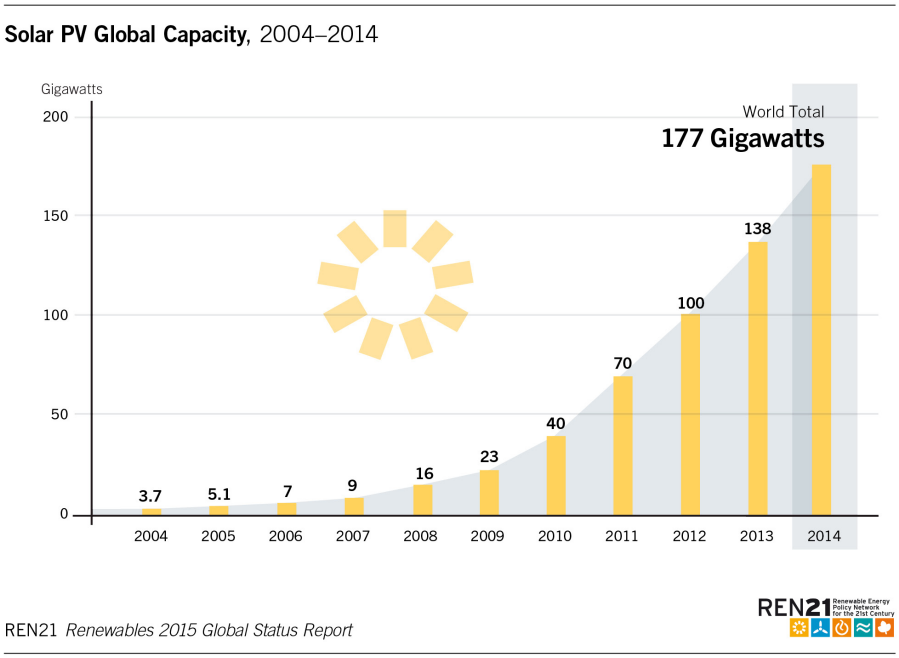


FIGURE 1.14: Solar power growth (2004-2014) [10, 12].

introduced to the grid. Therefore, regulation methods of such systems connected to the grid via inverters is a relatively new topic. Many traditional inverter control strategies already exist and are applied, for example the vector control strategy [58, 59]. But recently new generation of regulation methods are introduced, for example the virtual synchronous generator control strategy [60].

In the following, this last point will be investigated and different inverter control strategies will be presented.

### 1.5.1 Vector Control

The vector control strategy was first introduced for inverter driven electrical machines electromechanical control [61, 62]. It is used for different regulations of the machine, as speed regulation [63, 64] and torque regulation [62, 65].

Figure 1.15 illustrates a basic vector control strategy applied to an electrical machine [61–65]. The current of the machine is measured, and transformed to a $dq$ rotating frame. These currents are compared to reference values and

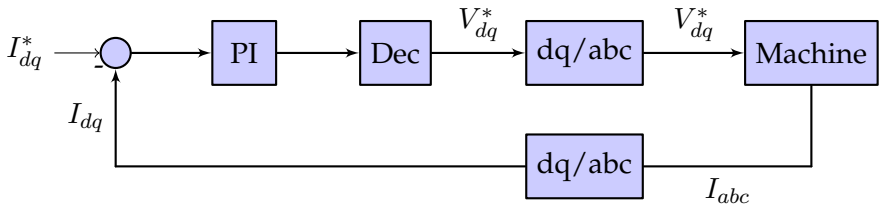


FIGURE 1.15: Control diagram of a vector control strategy.

regulated with a PI regulator. Then the resulting regulator output is corrected with decoupling equations, and becomes the reference value of the voltage in the $dq$ rotating frame. Finally, the reference voltage of the voltage source inverter (VSI) is recalculated using an inverse transformation of the $dq$ frame. This regulation diagram presents the basic vector regulation method, where the current is regulated. In order to build more elaborated regulation, for example the speed [63, 64] and torque [62, 65] regulations cited earlier, the reference current must be deduced from the reference speed and torque counter control loop respectively.

More recently, vector control strategy is used in renewable energy applications, where they are applied for inverter regulation [66, 67]. In fact, it is proven that the grid have similar behavior to a synchronous electrical machine but with a much faster response time [68–70]. Figure 1.16 illustrate a basic vector control diagram applied for grid connected inverters.

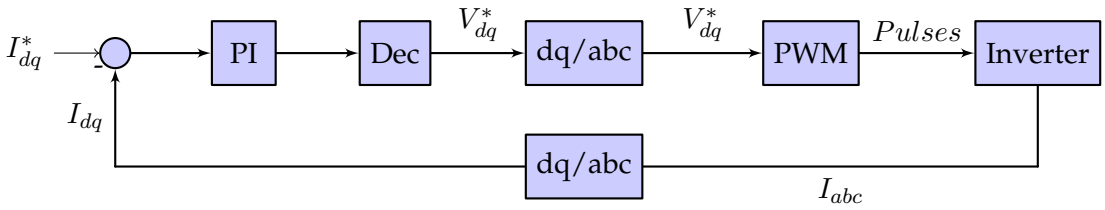


FIGURE 1.16: Control diagram of a vector control strategy applied to an inverter.

Similar to the case of machine control, the vector control strategy for grid inverters can be used in combination with higher level control strategy regulations, to connect renewable energy sources to the grid. The master-slave control strategy, adds a power regulation to the traditional vector control [71–73]. Therefore, the master-slave control strategy regulates the system to inject the maximum power to the grid. Such regulation presents a major disadvantage, since it does not regulate neither the voltage nor the frequency of the system, therefore it is highly dependent on the stability of the grid. For all these reasons, the master-slave control strategy is applied to relatively small

renewable energy systems connected to a highly stable and powerful master grid, and is often avoided in stand-alone sites and large renewable farms.

Another notable example is the voltage and frequency control strategy. This control strategy aims to regulate the voltage and the frequency of the grid [74–76]. In fact, with this control strategy a maximal power injection to the grid is forfeited, in order to maintain a stable signal (voltage and frequency). Moreover, this control strategy is known to be combined with a droop regulation, where it enables a multi-source connection on the grid, without a definition of a master source [75]. For all these reasons, the voltage control strategy is often applied to renewable energy systems in stand-alone sites and in large scale farms, but it is avoided in relatively small renewable energy systems connected to a powerful grid.

Islanded sites, like the studied island of Ouessant, are not connected to the continental gird, which makes their grid stability critical. Therefore a regulation of the voltage and frequency is essential. Furthermore, in such islanded sites, the resources are not stable. For example, in winter the wind can be strong enough to ensure the needed energy, but in summer such resource can drop to very low levels. Under such conditions, a master slave control strategy might not be well fitting since no master source can be chosen. As for the vector regulation with a voltage and frequency control strategy, it can present an interesting solution to such problem even tho it is more delicate to implement.

### 1.5.2 Observer-Based Control

Observer-based control strategies use mathematical approximations of the real system dynamics, in order to predict its different states, and therefore regulates them. Such control strategies are used in renewable energy systems [77–79]. Traditional observer based control strategies applied to renewable energy systems, try to build similar transfer functions as those governing the real system, by being very precise models [79] or by reducing their complexity [78].

Recently, a new observer based control strategy is introduced. The virtual synchronous generator uses the similarity between the VSI and electrical synchronous generator in order to build the observer. In fact, the built observer simulates the different states of a synchronous generator, but applies them

to the inverter fast dynamics, then uses them to regulate the inverter [80,81]. Furthermore, a droop control is added to the virtual synchronous generator regulation technique, in order to regulate large renewable energy farms [60,82].

The virtual synchronous generator is a relatively recent regulation method for renewable energy systems, the first application of this method is mentioned in articles in the year 2008 [83]. Therefore it is still being researched and studied, and it is not developed at its full potential yet. Still this regulation strategy can be interesting, view the actual tendencies for building hybrid systems. In fact, using the virtual synchronous generator technique, the dynamics of an inverter based system could be slowed, and therefore it would be easier to integrate them into more complex systems.

## 1.6 Conclusion

In this chapter, a state of the art was presented. Firstly, three different maritime renewable energy systems have been presented, and compared to the two most common renewable energy sources (wind turbines and solar panels). Maritime energy production system proved to be more expensive and less mature than their onshore counterparts. But at the same time, these offshore technologies present many advantages, such as free space for large scale farms installation, less constraints for noises, and high ocean power potential. Therefore such technologies are being heavily investigated. Considering the properties of the studied renewable energy systems, tidal turbines and offshore wind turbines appear to be an interesting choice for an islanded site like Ouessant island.

Secondly, suitable energy storage systems for stand-alone maritime sites were investigated. Starting with the most used PHS, that proved to be very effective; as well the SWPHS, which is less mature then normal PHS but can present advantages in such maritime islanded site. CAES technology has been also presented, including their underwater ocean-based application. These technologies are not as effective as the PHS but still interesting. Finally, different types of batteries were presented: vanadium redox batteries, Li-ion batteries, Lead-acid batteries, and sodium sulfur batteries. Such energy storage systems can be interesting for the studied site. In fact, for the

considered island of Ouessant, both batteries or SWPHS can be an interesting choice. But since the chosen island includes high cliffs ($60\ m$ - $70\ m$), a SWPHS was considered as an ESS for the island.

Thirdly, offshore energy transmission strategies where presented, where three major transmission methods were identified: MVAC, HVAC, and HVDC. The choice of the most suitable transmission strategy was proven to depend on two factors: the transmitted power and the transmitted distance. For the chosen site, a MVAC transmission appears to be the most suitable option.

Fourthly, renewable energy systems regulation methods were discussed. In fact two large families of control strategies were identified: the vector control and the observer-based strategies. Furthermore, interesting regulation methods were identified in these families. The master-slave control and the voltage and frequency control strategies for the vector control family, and the virtual synchronous generator for the observer-based family. For the chosen site properties, a master-slave control strategy can be problematic since it necessitates a primary power production source, which can not be determined for the considered study case. However, the voltage and frequency control and the virtual synchronous generator control strategies can be very interesting to apply for such sites.

This state of the art is essential for the rest of the study. In fact, the first two sections will allow to justify the work presented in chapters 2 and 3, where the different energies on the chosen site will be presented, and a rough optimization will be used in order to size the hybrid system. As for the third and forth sections of this state of the art, they will present the justification for chapter 4 studies, where the regulation of the previously sized hybrid system will be developed.

# 2. Methodology of Analysis of the Energy Resource and the Energy Storage System for the Studied Stand-Alone Site

## 2.1 Introduction

Ouessant is a French island, located in the Bretagne region west of the country ($48^o\ 28'\ N$, $5^o\ 5'\ W$) (Fig. 2.1). the island presents an area of $1541\ ha$ and an estimated population of $1000$ inhabitant [84]. Moreover, it is not connected to the French continental grid. Such an aspect is critical for an energetic analysis. In fact, in a stand-alone site, the energy must remain balanced on the local grid. Therefore an energy storage system (ESS) is essential to ensure such balance. Finally, for security reasons, and in order to complete the energy production when the ESS is empty and the renewable resources production is not sufficient, the use of a diesel power plant will be considered. It must be noted that such power plant already exists on the island.

This chapter focuses on an analysis of the different energy sources available on the site, the possibility of setting up an ESS, and the approximation of the island load curve. According to chapter 1, three energy sources present high maturity and promising production: wind, solar, and tidal energies.

Furthermore, the diesel production will be discussed in this chapter, where the existing generators and their corresponding diesel consumption will be analyzed. Finally, the energy storage system will be presented. In fact, according to chapter 1 and the site main characteristics, the pumped hydroelectric system presents a good solution view its key features: high maturity, low cost, and long discharge duration.

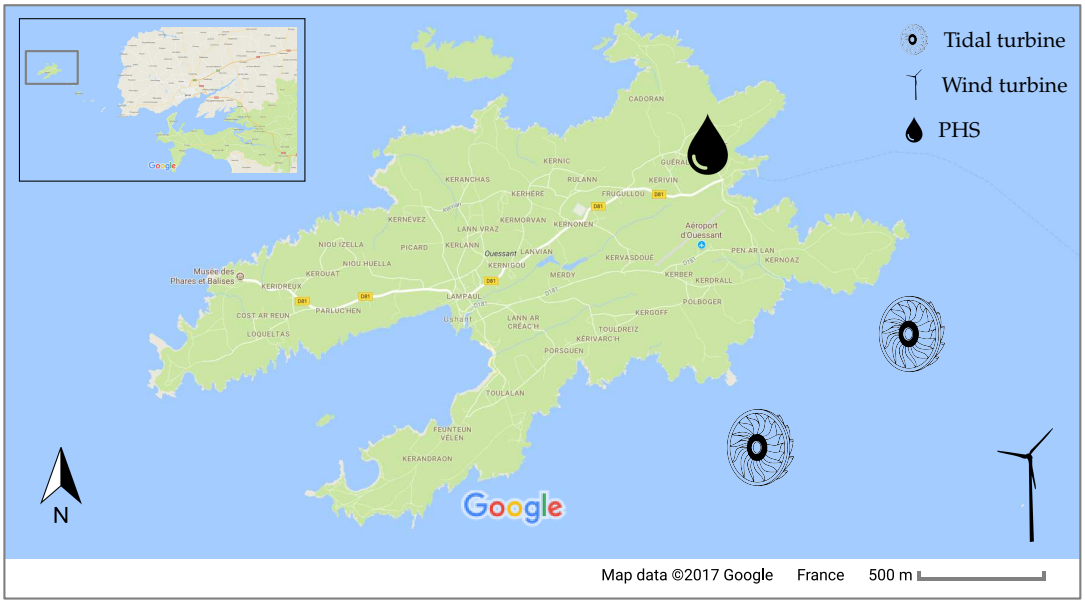


FIGURE 2.1: Ouessant island map, with the potential positions of the different farms and the energy storage system.

## 2.2 Ouessant Island Energy Consumption

As presented in the introduction, Ouessant is a French island located in the west of the Bretagne region. The island population can be approximated to 1000 person. The island also contains a port and a small airport. Considering the small number of the island inhabitance, for privacy reasons, the real

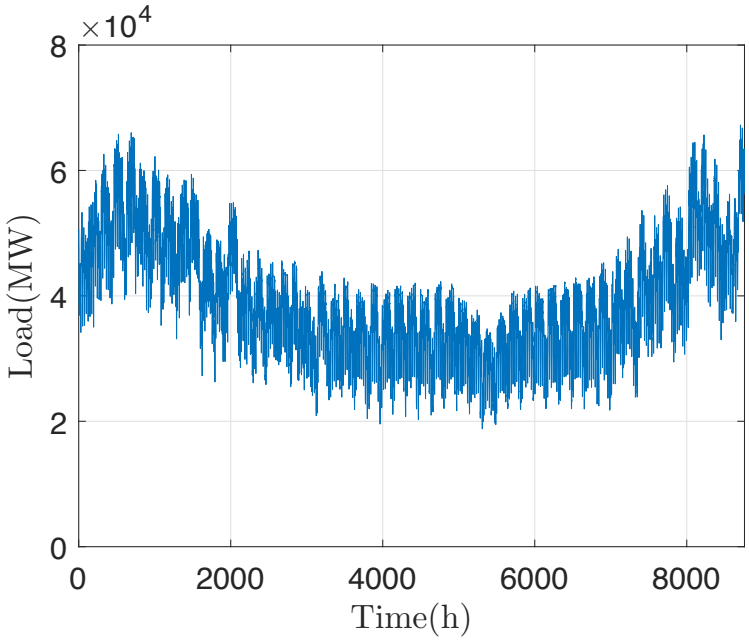


FIGURE 2.2: French national load variations for the year 2014.

load data could not be accessed. Therefore, the load variation of the studied site was deduced from the French national load curve for the year 2014 (Fig. 2.2). In fact, the national load variations were rescaled to fit the size of the island by applying a proportional relation between the two, as shown in equation (2.1). Even tho the island real load might be different, due to its local characteristics. The considered load curve is suitable for the study of a small islanded site.

$$Load_{Ouessant} = \alpha Load_{France} \tag{2.1}$$

$\alpha$ is a rescaling constant, and is determined by the ratio of the total energy consumed by the island over the total energy consumed at the national scale for the year 2014, as shown in equation (2.2).

$$\alpha = \frac{E_{Ouessant}}{E_{France}} \tag{2.2}$$

Figure 2.3 presents the considered load variations of Oussant island for the year 2014.

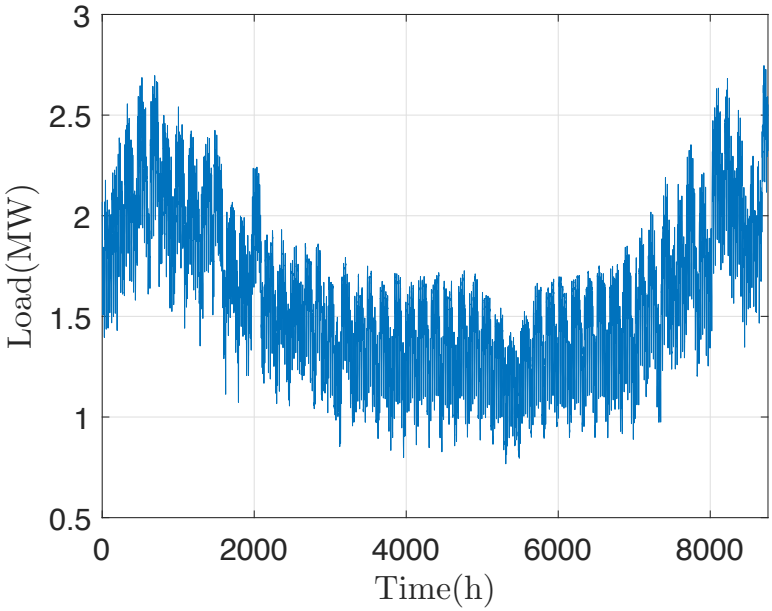


FIGURE 2.3: Ouessant approximated load variations for the year 2014.

## 2.3 Wind Characteristics on the Island

Wind turbines are characterized by one of the highest technology maturity level in all renewable energy systems [85]. But since offshore wind turbines will be considered, such technology is less mature then its onshore counterpart, still it presents hight maturity. In fact large offshore wind turbines models of 5 MW are available, and have been in the market for few years [86,87].

In contrast, wind energy presents several disadvantages. In fact, wind energy is an unpredictable energy source, which leads to high constraints on the stability of a stand-alone grid, where the power must be constantly sufficient to supply the totality of the load [88,89]. The same problem is faced with the seasonal aspect of the wind energy, where the winter presents a high energy potential and the summer presents low energy [90,91]. In the following section, the wind characteristics on the island will be studied, and the suitable wind turbine properties will be discussed.

### 2.3.1 Resource Characteristics

As discussed earlier, the wind energy is an unpredictable renewable energy resource with high daily and seasonal variations. To study the reliability of such resource, measurements of the wind speed were extracted from the database of "Météo Bretagne", at the Ouessant-Stiff station [92]. The year 2014 was considered as a reference for the extracted measurements. The data presents mean values of the wind speed for each hour.

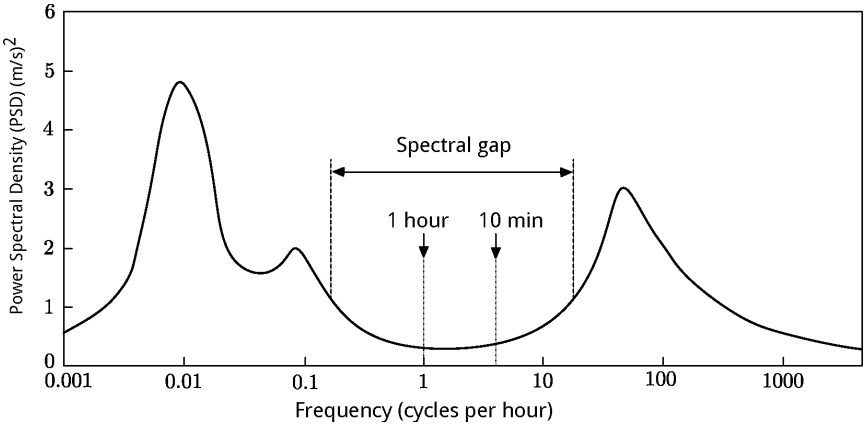


FIGURE 2.4: Van Der Hoven spectrum [13].

Figure 2.4 presents a typical Van Der Hoven spectrum [13,93–95]. This well known spectrum illustrates the wind speed variations frequency. In fact,

three variation peeks can be detected: The turbulence peek around $100$ cycles per hour, the diurnal peek around $0.1$ cycles per hour, and the synoptic peek around $0.01$ cycles per hour. This spectrum can confirm the choice of the measurements frequency. Indeed, the turbine inertia can highly filter the variations corresponding to the turbulence peek. As for the diurnal and synoptic ones, a one hour step is enough to take such variations into consideration.

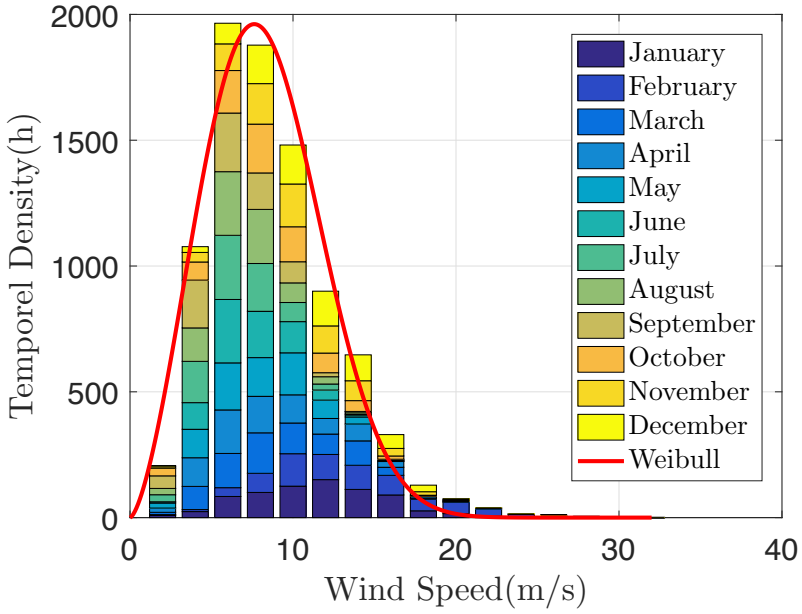


FIGURE 2.5: Wind speed distribution for the year 2014.

Figure 2.5 illustrates the wind speed distribution on the chosen site. Data shows a Weibull shaped distribution with a scale parameter ($\lambda_w$) of $283.45$ and a shape parameter $K_w$ of $2.53$ (the Weibull curve expression is presented in equation (2.3)) [96].

$$f(x; K_w, \lambda_w) = \begin{cases} \left(\frac{K_w}{\lambda_w}\right)\left(\frac{x}{\lambda_w}\right)^{(K_w-1)} e^{-(x/\lambda_w)^{K_w}} & \text{for } x \geq 0 \\ 0 & \text{for } x < 0 \end{cases} \tag{2.3}$$

Such distribution is typical for a favorable wind farming site [97]. In fact, The wind energy is a form of kinetic energy. The kinetic power of the wind at a given time ($t$) applied on a surface ($A$) is presented by equation (2.4) [98].

$$P_w(t) = \frac{1}{2}\rho_{air} A V(t)^3 \tag{2.4}$$

The energy production potential, can be therefore presented by equation (2.5)

$$E_w(t) = \int_t \frac{1}{2}\rho_{air} A V(t)^3 dt \tag{2.5}$$

Since the mean value of the wind speed is considered with a one hour step. The integral can be transformed to a sum, presented in equation (2.6)

$$E_w(t) = \sum_{t=1}^{8760} \frac{1}{2}\rho_{air} A V(t)^3 \Delta(t) \tag{2.6}$$

Finally, by considering a unitary area, and applying equation (2.6) to the data presented in fig. 2.5, the wind energy potential can be approximated to $4.4\ MWh/m^2$.

### 2.3.2 Turbine Properties

This section uses the previously analyzed wind speed data, to study the properties of a suitable wind turbine. In fact, this section focuses on three properties: the cut-in/cut-out speed of the turbine, its rated speed, and its rated power [20].

Figure 2.6 illustrates the cumulative extracted power of a wind turbine presented in a percentage of the total extracted energy, always on the chosen site. In fact, the energy power extracted by a wind turbine follow the same rules as presented in equation (2.5), and apply an additional turbine power coefficient ($C_p$), as show in equation (2.7).

$$E_{wt}(t) = \int_t \frac{1}{2} C_p \rho_{air} A V(t)^3 dt \tag{2.7}$$

using figure 2.6, less then $0.1\ \%$ of the extracted energy corresponds to a wind speed lower than $2\ m/s$, and more then $97.9\ \%$ of the extracted energy corresponds to a wind speed lower than $25\ m/s$. Using these cut-in and cut-out parameters, less than $2.5\ \%$ of the wind energy will be lost, such loss is largely acceptable. Furthermore, the cumulative extracted power presents an inflexion point at a speed of $15\ m/s$ corresponding to $75\ \%$ of the extracted power, such point presents a good choice for a rated speed. Finally, the rated power depends on the rated speed, the optimal value of $C_p$, and the turbine sizes (the sweeping area of the turbine). Since the studied site presents suitable conditions for a classical fixed offshore wind turbine, at a close distance to

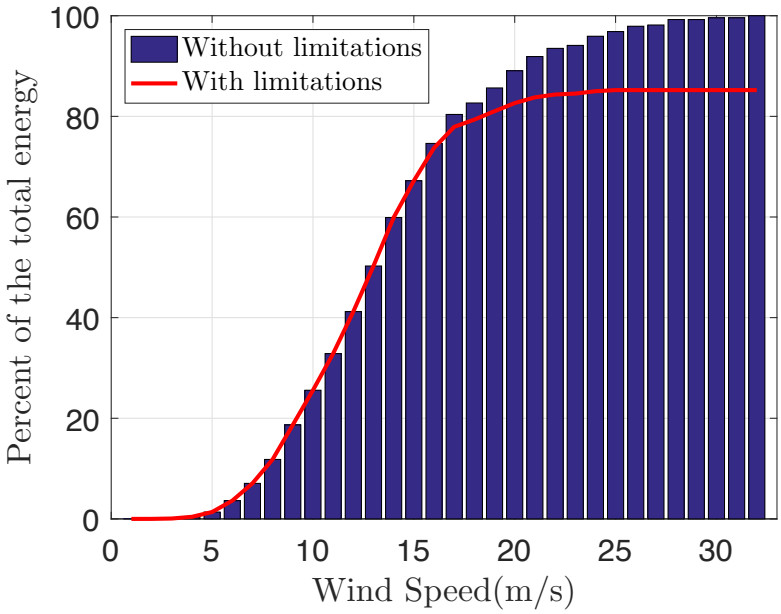


FIGURE 2.6: Wind cumulative extracted power using a Nordex N80 2500 wind turbine model.

TABLE 2.1: Nordex N80 2500 characteristics [16,17]

| | |
|---|---|
| Turbine diameter | 80 $m$ |
| Sweep area | 5026 $m^2$ |
| Cut-in wind speed | Approx. 3 $m/s$ |
| Cut-out wind speed | 25 $m/s$ |
| Rated speed | 15 $m/s$ |
| Rated power | 2.5 $MW$ |
| $C_{pmax}$ | 0.434 |

the shore, large turbines can be considered. Therefore a $2.5\ MW$ wind turbine properties can be considered for a first study of the system. The Nordex n80 2500 respects the presented conditions as shown in table 2.1 [16,17].

## 2.4 Tidal Characteristics in the Area Around the Island

### 2.4.1 Introduction

Tidal energy presents a high potential in numerous countries, counting: Canada, Argentina, United Kingdom, France, Ireland, Russia, Australia and China [99]. Furthermore, tidal energy presents high energy density, high level of

predictability, and low environmental impact [100, 101]. It presents an important energy source, the tidal energy potential worldwide is estimated to $450\ TWh/year$, where the European coast presents around $24\ TWh$ per year. The United Kingdom, France, and Ireland present $98\ \%$ of the European potential with $42\ \%$ on the French coast [102–104].

However, tidal turbine deployment faces a number of problems. These renewable energy systems are not as mature as wind turbines or PV systems [104, 105]. The biofouling can cause major problems on the system efficiency [38]. Another important problem is the identification of a suitable tidal system location, which is limited. Indeed, waves can cause a major disturbance on tidal turbines, when placed in shallow waters [106]. Moreover, deep water sites are unattractive since the current velocity decreases with depth and the cost of the project increases.

For theses reasons, and considering the critical context of such project, a specific tidal current energetic study for the positioning of tidal turbines is prerequisite for the project success. Such study will focus on the evaluation of the tidal energy variations with the position, and the implications of such tidal turbine design options (bidirectional fixed axis turbine or with a yaw [107, 108]).

All maps of this section respects the following characteristics:

- Geographical coordinates (latitude and longitude) are expressed in a RGF93 system (official French system).
- Geographical North is considered as a reference for the direction and counted from $0°$ (North) till $359°$.
- The maps are meshed in elementary spatial areas. The center of each of these areas is considered as a measurement node.

### 2.4.2 Existing measurements

The marine current velocity evaluation, and the corresponding tidal energy, depends on two parameters: the tidal coefficient and the spring and neap current velocities.

The tidal coefficient ($C$) characterizes the amplitude of a given tidal semi-diurnal cycle. $C$ is a non-dimensional coefficient varying between $20$ and

120. It can be calculated using equation (2.8) [109].

$$C = 100\frac{\Delta H}{\Delta H_{eq}} \tag{2.8}$$

Where $\Delta H$ is the tidal range (difference of water level between high and low tides) corresponding to the considered cycle at a reference location (reference harbor) of the considered area, $\Delta H_{eq}$ is the average value of this tidal range for equinox spring tides at this location (this average equinox tide corresponds to the reference coefficient of 100). Using astronomical observations, this coefficient is predicted many years in advance by oceanographic services as the French Navy Hydrographic and Oceanographic Service (SHOM) in France.

As shown in equation (2.8), $C$ is linearly related to $\Delta H$. Therefore the first needed measurement is the tidal range. In fact, the tidal range represents the difference in water level between high and low tides, it is measured in $m$. $\Delta H$ is constant for a cycle on a defined reference zone. By approximating the tidal period to $12\ h$, two values of $\Delta H$ are evaluated per day.

The spring and neap current velocities, $\mathbf{v}_{sw}$ and $\mathbf{v}_{nw}$ respectively, present the second needed measurement. In fact, $\mathbf{v}_{sw}$ and $\mathbf{v}_{nw}$ represent current velocities for tidal coefficients of $95$ and $45$ respectively at a specific location. These tidal current velocities are given by SHOM [110]. They are characterized by their hight sensitivity bathymetric features, even short distances can cause important current variations. Figs. 2.8 and 2.7 illustrate $\mathbf{v}_{sw}$ and $\mathbf{v}_{nw}$ maximal values for the studied area.

Finally, using the two hypothesis:

- All of the studied zone is covered by one tidal area (the reference harbor of Brest).
- the tidal speed is considered at $10\ m$ from the bottom of the ocean (most suitable for a tidal turbine application).

Corresponding measurements of $\mathbf{v}_{sw}$ and $\mathbf{v}_{nw}$ must cover the entire zone. Therefore, about $11000$ measurement points (spacial nodes) were placed. Furthermore, the year 2014 was considered as a reference for the study, and the tidal range of each cycle of the studied year must be measured.

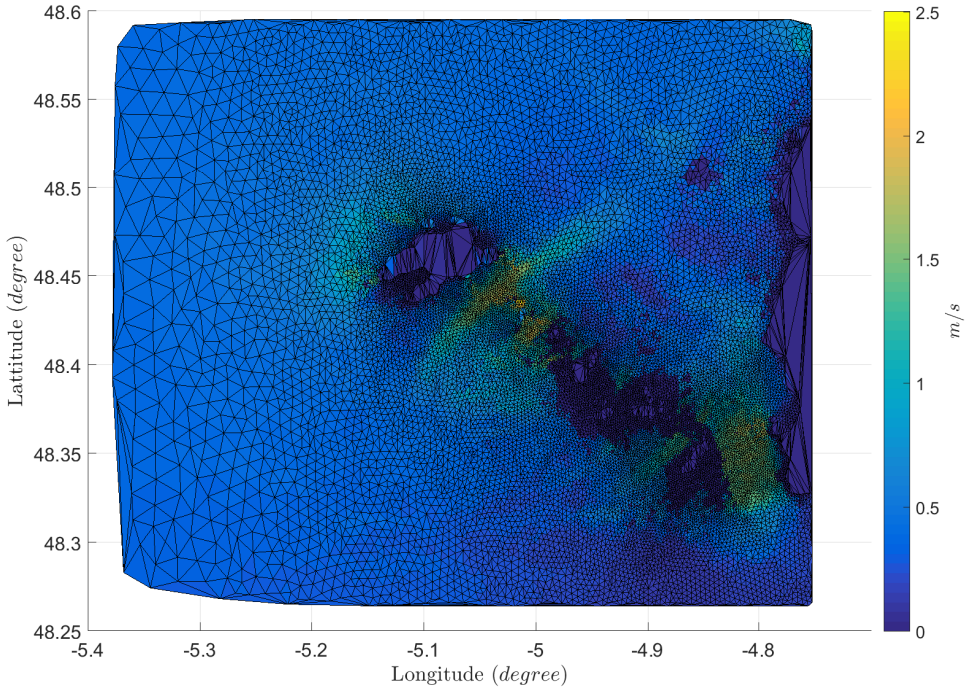


FIGURE 2.7: Maximal value of the neap current velocity (in m/s).

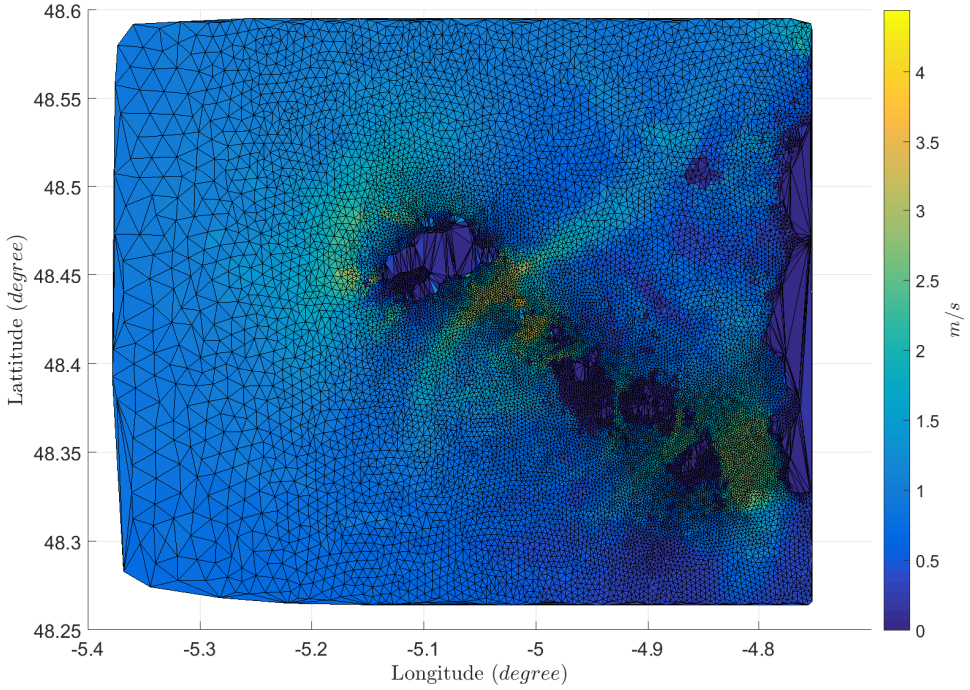


FIGURE 2.8: Maximal value of the spring current velocity (in m/s).

### 2.4.3 Marine current velocity

It is essential to present the characteristics and parameters of the tidal velocity, before presenting the different relations and mathematical equations that will help with its calculation. First, $\mathbf{v}_{sw}$ and $\mathbf{v}_{nw}$ are two essential parameters for the calculation of the marine current velocity ($\mathbf{v}_t$). The bathymetric features have a high effect on $\mathbf{v}_{sw}$ and $\mathbf{v}_{nw}$. Therefore $\mathbf{v}_t$ changes with the location, and all three current velocities ($\mathbf{v}_{sw}$, $\mathbf{v}_{nw}$, and $\mathbf{v}_t$) are dependent on the longitude and latitude (Figs. 2.8 and 2.7). Moreover, the tidal forcing is the main force affecting the tidal velocity. Such tidal forcing is a function of time, and presents a periodic variation. given that $\mathbf{v}_{sw}$ and $\mathbf{v}_{nw}$ are typical current velocities, they will have periodic variations too, and depend on a specific time ($t_n$), which refers to the coincident tide cycle time interval. Second, the tidal coefficient $C$ varies from one tidal cycle to another, while keeping a constant value during a given cycle, since it depends on $H$. As a result, $\mathbf{v}_t$ depends on position (longitude ($L$) and latitude ($l$)) and time ($t$). Moreover, $\mathbf{v}_t$ is defined as a vector, therefore it is composed from an amplitude and a direction.

Finally, $\mathbf{v}_t$ is evaluated for the reference year of 2014 with a step of one hour. It is also evaluated on the $11000$ points distributed on the studied zone. In fact, $\mathbf{v}_t$ follows the law presented in equation (2.9) [110].

$$\mathbf{v}_t = \mathbf{v}_{nw} + \frac{C - a_0}{b_0 - a0}(\mathbf{v}_{sw} - \mathbf{v}_{nw}) \tag{2.9}$$

where $a_0$ is the tidal coefficient for neap water (45) and $b_0$ is the tidal coefficient for the spring water (95). Using equation (2.8) to determine $C$ and placing its value in (2.9), a tidal velocity vector with a norm and a direction can be calculated for each time and location.

### 2.4.4 Tidal energy and turbine properties

The kinetic power of a tidal flow in a given location defined by a longitude ($L$) and a latitude ($l$), at a given time ($t$), and for a surface cross area ($A$) follows the law presented in equation (2.10) [101,107]. where $\rho_w$ is the density of the sea water.

$$P_t(L, l, t) = \frac{1}{2}\rho_w A|\mathbf{v}_t^3|(L, l, t) \tag{2.10}$$

The energy is the integral of the power, the tidal kinetic energy at a certain location ($L$,$l$), and for a given period time ($T$) is presented in equation (2.11).

$$\begin{aligned} E_{kT}(L,l) &= \int_{t\in T} P_t(L,l,t)dt \\ &= \int_{t\in T} \frac{1}{2}\rho_w A|\mathbf{v}_t^3|(L,l,t)dt \end{aligned} \tag{2.11}$$

(2.12) allows to estimate the energy extracted by a unitary cross area turbine in optimal conditions (maximal value of $C_p$), while considering the mean value of the tidal current with a one hour step. Where $C_p$ is the turbine power coefficient.

$$E_T(L,l) = \sum_{t_h\in T} \frac{1}{2}C_p\rho_w|\mathbf{v}_t^3|(L,l,t) \tag{2.12}$$

The direction of $\mathbf{v}_t$ changes in time, therefore two technological solutions are presented. The first solution considers a yaw driven-based tidal turbine [107]. And the second one considers a fixed axis, bi-directional tidal turbine [105].

#### Yaw drive-based tidal turbine

In a yaw drive-based tidal turbine, the turbine axis follows the current direction. The current speed projection on the axis ($v_{axis}$) of the turbine is the norm of the velocity vector ($\mathbf{v}_t$).

$$v_{axis} = norm(\mathbf{v}_t) \tag{2.13}$$

Using the values of the speed from equation (2.13), and replacing it at each point in equation (2.12), leads to energy distribution map 2.9.

#### Bi-directional fixed axis direction tidal turbine

A bi-directional fixed axis direction tidal turbine has a fixed axis direction with no possibility to follow the tidal current. The tidal current speed, to be considered in equation (2.12), is therefore the projection of the current velocity on the turbine fixed axis [36]. Figure 2.10 illustrates an example of an optimal axis direction for a certain chosen position. In this typical context, the tidal turbine axis direction ($\alpha_{axis}$) is an essential parameter for a better energy extraction [111, 112]. Equation (2.14) presents the velocity projection

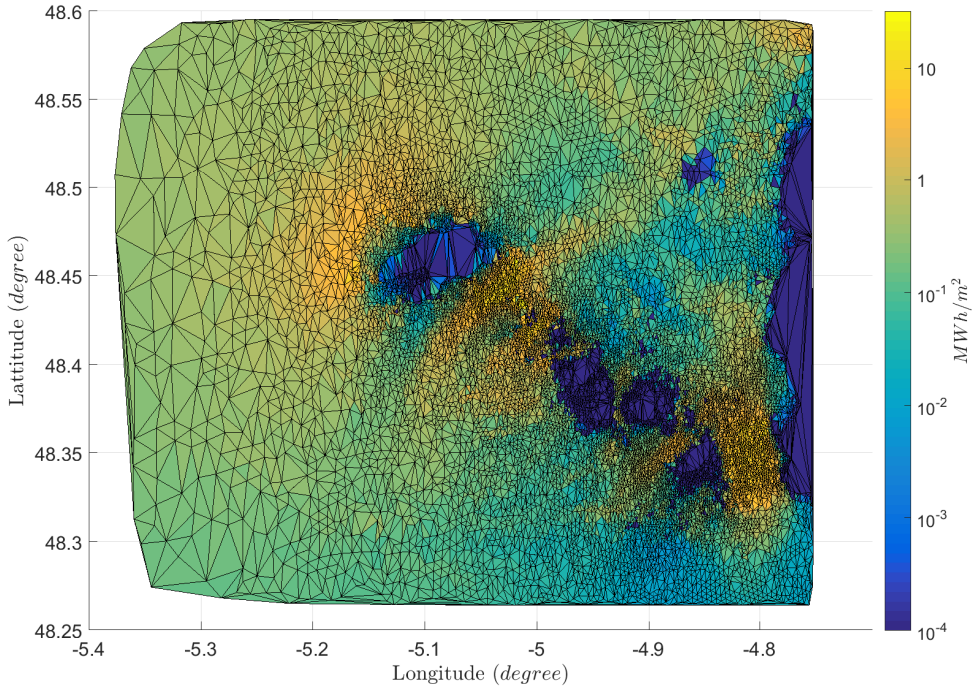


FIGURE 2.9: Energy distribution for one year (2014) in $MWh/m^2$ on a tidal turbine with a yaw presented in a logarithmic scale.

on the turbine axis.

$$v_{axis} = norm(\mathbf{v}_t)cos(\alpha_{axis} - \alpha_{current}) \tag{2.14}$$

In order to determine the optimal value of $\alpha_{axis}$, a tryout with a $1°$ step variation (from $0°$ till $179°$) was applied for each location. The result corresponding to the highest energy is considered as the optimal angle. Figure 2.11 illustrates the values of optimal $\alpha_{axis}$ for different locations in the studied area.

Using the values of the speed from equation (2.14), and replacing it at each point in equation (2.12), leads to energy distribution map 2.12.

**Results comparison and discussion**

The achieved results highlights an energetic zone at the northern entrance of the 'Passage du Fromveur' near the eastern cost of Ouessant island. furthermore, this zone presents short distance to the shore of the island, and a water depth between $30$ and $50$ $m$. All these conditions are optimal for the

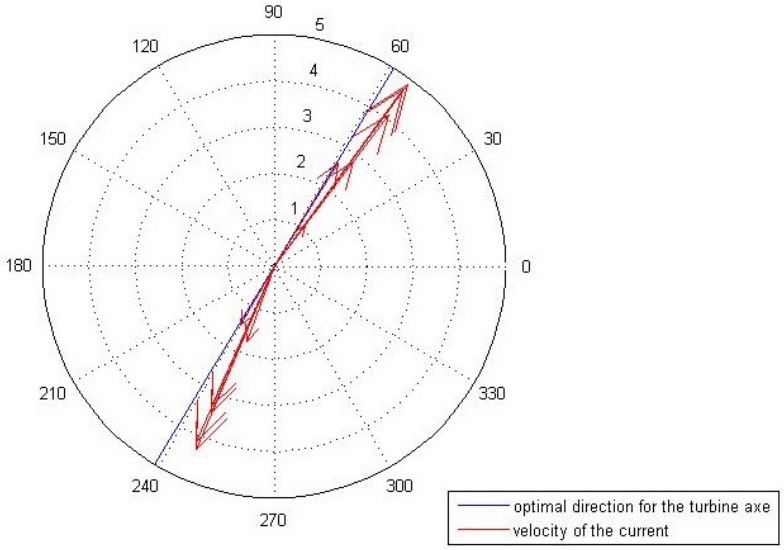


FIGURE 2.10: Tidal current speed (m/s) and direction (degree) for a given tidal cycle (1 value for each hour).

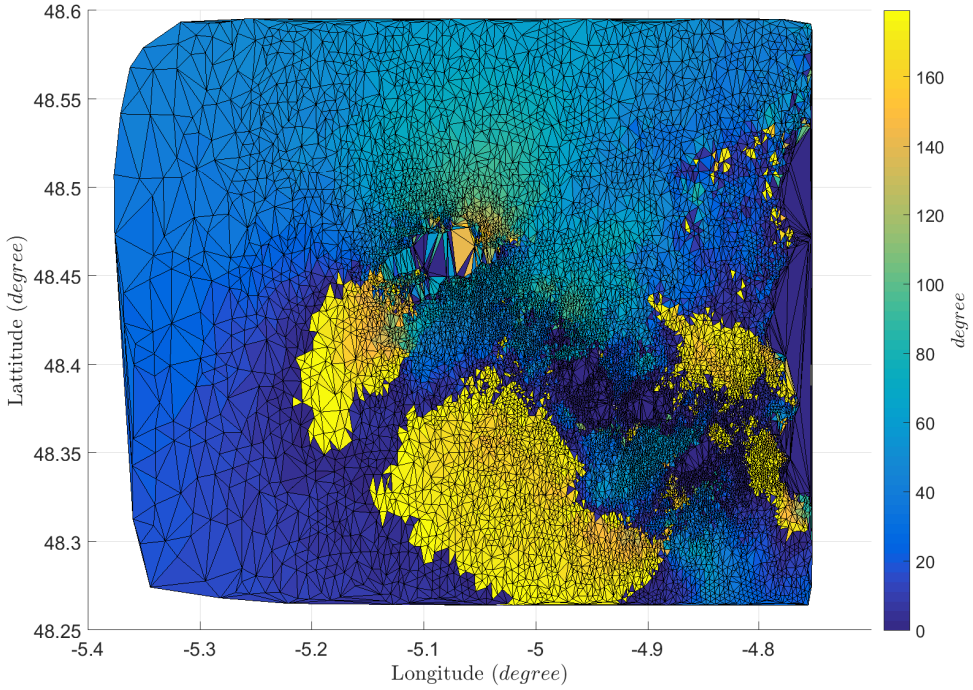


FIGURE 2.11: Optimal direction of the bidirectional tidal turbine axis.

insertion of tidal turbines. But the yaw drive system usefulness is still debatable in terms of energy extraction, and needs further evaluation. Therefore,

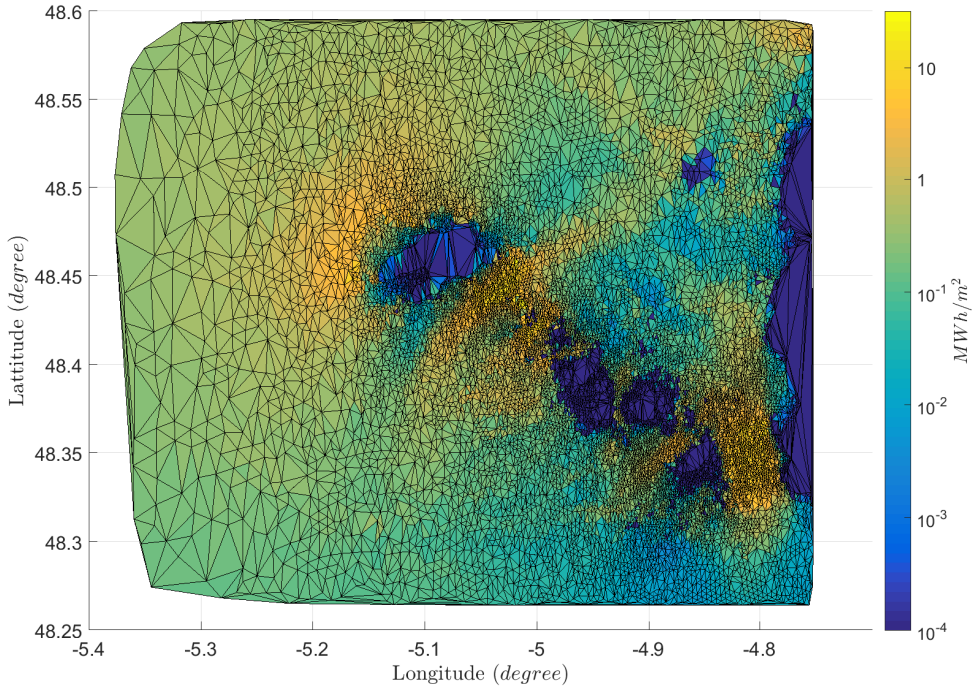


FIGURE 2.12: Energy distribution for one year (2014) in $MWh/m^2$ on a fixed axis turbine presented in a logarithmic scale.

a comparison of the two turbine types is essential. First, the energy extraction difference between the two system was calculated as shown in equation (2.15). Where $E_{multirectional}$ is the energy extracted with a yaw driven tidal turbine and $E_{bidirectional}$ is the energy extracted with a fixed axis tidal turbine.

$$e_{difference} = E_{multirectional} - E_{bidirectional} \tag{2.15}$$

Figure 2.13 illustrates the energy difference. In fact, the difference is greater where the energy is more important. Such distribution is not sufficient to evaluate the effectiveness of the yaw driven system. Therefore, the relative difference is evaluated as shown in equation (2.16).

$$e_{relative} = \frac{E_{multirectional} - E_{bidirectional}}{E_{multirectional}} \tag{2.16}$$

Figure 2.14 illustrates the relative energy difference between the two systems. The relative difference can change from one zone to another, and can reach considerably hight values ($50\%$) in particular areas of the map. However, in the earlier considered zones ('Passage du Fromveur' at the eastern coast of

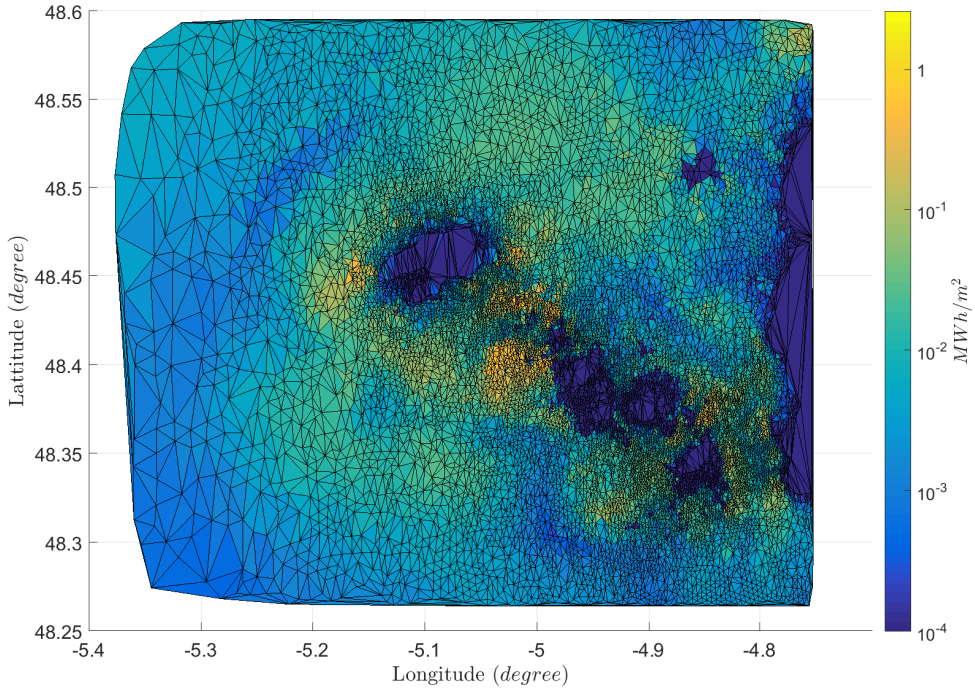


FIGURE 2.13: Multidirectional and bidirectional energy difference ($MWh$) presented in a logarithmic scale.

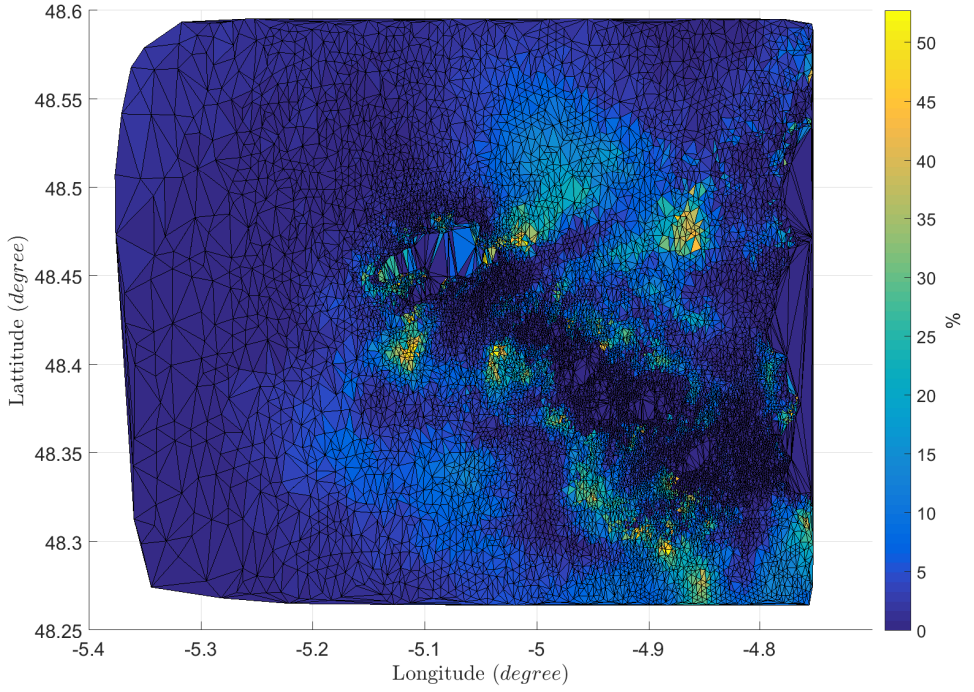


FIGURE 2.14: Bidirectional energy relative difference (percent).

TABLE 2.2: Tidal turbine characteristics [18]

| | |
|---|---|
| Turbine diameter | 16 $m$ |
| Sweep area | 201 $m^2$ |
| Cut-in tidal speed | Approx. 1 $m/s$ |
| Cut-out tidal speed | 4.5 $m/s$ |
| Rated speed | 3 $m/s$ |
| Rated power | 0.5 $MW$ |
| $C_{pmax}$ | 0.38 |

Ouessant island), the relative difference presents small values (lower than $5\%$). Such results highlights the advantage of a bi-directional fixed axis tidal turbine. In fact, the bi-directional fixed axis turbine presents simpler mechanic system and therefore lower maintenance cost. And since the energy extraction difference between the two systems is marginal, the usage of a bi-directional fixed axis tidal turbine seems a more interesting choice.

### 2.4.5 Turbine Properties

This section uses the previously analyzed tidal speed data. Previous study allows to choose a high energy point (fig. 2.11) in the northern part of the "Passage du Fromveur" (fig. 2.1). These data are used to study the properties of a suitable tidal turbine. However, tidal turbines are not as mature as wind turbines [113]. This section focuses on three properties: the cut-in/cut-out speed of the turbine, its rated speed, and its rated power [20].

Figure 2.15 illustrates the cumulative extracted power of a tidal turbine presented in a percentage of the total extracted energy for a period of one year (2014) in this point. In fact, the energy extracted by a tidal turbine follow the same rules as presented in equation (2.11), but in this case the turbine position is predefined and therefore the energy wont be a function of the position, as presented in equation (2.17).

$$E_{TT}(t) = \int_T \frac{1}{2} C_p \rho_{water} A V(t)^3 dt \tag{2.17}$$

Using figure 2.15, over $1.3$ % of the energy corresponds to a tidal speed less than $1\ m/s$, and around then $21.5$ % of the energy corresponds to a tidal speed higher than $4.5\ m/s$. Using these cut-in and cut-out parameters, less around $22.8$ % of the tidal energy will be lost. Furthermore, the cumulative extracted power presents an inflexion point at a speed of $3\ m/s$ corresponding to $40$ %

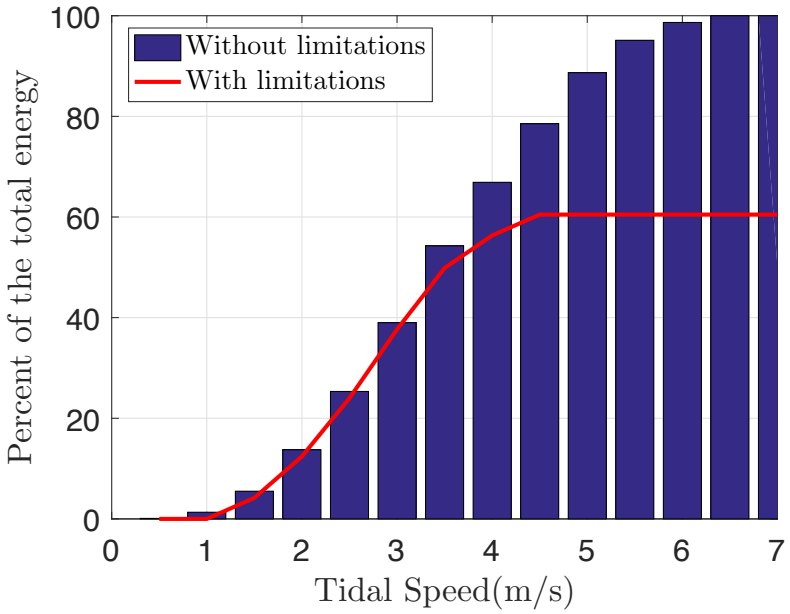


FIGURE 2.15: Tidal cumulative extracted power.

of the extracted power. Finally, concerning the rated power, it depends on the rated speed, and the turbine sizes notably the sweeping area of the turbine. Such properties can be further optimized by increasing the cut-out speed to $6$ $m/s$ and the rated speed to $4$ $m/s$. But tidal turbines are not fully mature yet, therefore such optimal properties are not considered. Finally, a reasonable choice of a $0.5$ $MW$ tidal turbine can be considered for a first study of the system. Table 2.2 presents the main turbine properties [18].

## 2.5 Solar Characteristics on the Island

In order to evaluate the solar energy potential on the island, the sunny hours of the region near the studied island for the year 2014 where obtained from 'Météo France' database [114]. Figure 2.16 evaluates the sunny hours of the region and compares them to the national mean value. The data highlights the lack in sunny hours at the studied site. In fact, the data shows a total of $1685$ sunny hours for studied region. The corresponding percentage of sunny hours is calculated as shown in equation (2.18). Where $Nb_{sh}$ is the number of sunny hours in the studied site and $Nb_{th}$ is the number of total hours in a year.

$$Per_{sh} = 100\frac{Nb_{sh}}{Nb_{th}} = 19.24\% \tag{2.18}$$

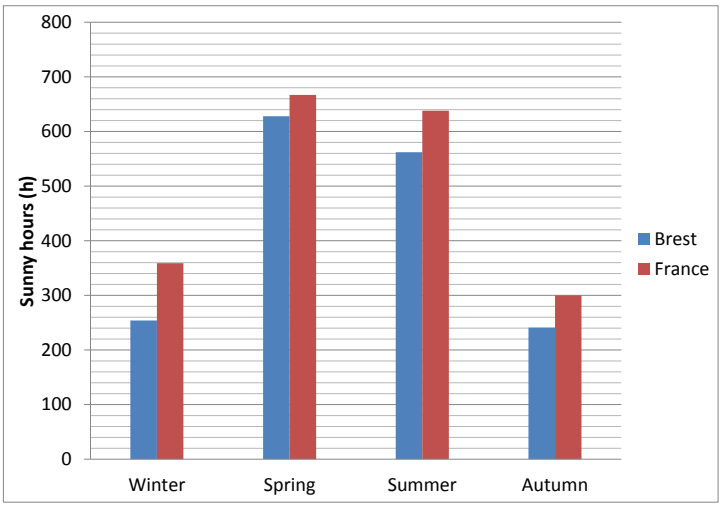


FIGURE 2.16: Sunny hours near Brest for the year 2014.

Furthermore, studies showed that the chosen site presents over half of the radiations in other sites worldwide known to having high solar potential (such as Huston Texas) [115]. Therefore, solar energy will not be considered in the study.

In this context, it is important to point that solar energy presents a major advantage. In fact, solar radiations are more important in summer time, when wind energy is lower. These two energies are both seasonal and opposite. In future studies, it will be interesting to combine solar energy systems with wind and tidal ones.

## 2.6 Diesel Generators

Diesel generators are well developed energy production systems used in traditional grids. In fact, they present more degrees of freedom in terms of energy production compared to renewable sources [116]. This section of the study focuses on three characteristics of these generators: the control strategy, the power production, and the fuel consumption estimation. Moreover, considering the particular case of Ouessant island, two electrical groups already exist, with two identical diesel generators in each group. The first group uses a $1\ MW$ system for both generators, while the second group uses $1.2\ MW$ ones. In this context, data of Wärtsilä diesel generators with the

same rated power are used. Fig. 2.17 shows the diesel generators manufacturer data sheet measurements and their estimated curves [14]. In fact, Fig. 2.17 illustrates the diesel consumption for a specific power production of the generator. The results clearly identify better diesel consumption efficiency of $1.2\ MW$ generator compared to the $1\ MW$ one. Therefore, the $1.2\ MW$ generators will be used first. Table 2.3 shows the power reference for each diesel generator for a given power demand ($P_{Dref}$). Where $P_{Dref}$ presents the power reference required to be produced the complete diesel system.

Finely, it is important to point at the maximal power production of the diesel system, which can go to a total of $4.4\ MW$. Compared to the maximal value of the load ($2.7\ MW$), this maximal value presents only $61.36\ \%$ of the diesel system power potential. Indeed, because such system does not depend on external parameters to produce power, it will be considered as the primary security system, and must have the potential to ensure the full power of the island in case of emergency or unexpected situations.

TABLE 2.3: Diesel generators control strategy.

| | $1.2MW$ generator | $1.2MW$ generator | $1MW$ generator | $1MW$ generator | total |
|---|---|---|---|---|---|
| $P_{Dref} < 0.6MW$ | 0.6 MW | 0 | 0 | 0 | $\geq P_{Dref}$ |
| $0.6MW < P_{Dref} \leq 1.2MW$ | 100% $P_{Dref}$ | 0 | 0 | 0 | $P_{Dref}$ |
| $1.2MW < P_{Dref} \leq 2.4MW$ | 50% $P_{Dref}$ | 50% $P_{Dref}$ | 0 | 0 | $P_{Dref}$ |
| $2.4MW < P_{Dref} \leq 3.4MW$ | 35.3% $P_{Dref}$ | 35.3% $P_{Dref}$ | 29.4% $P_{Dref}$ | 0 | $P_{Dref}$ |
| $3.4MW < P_{Dref} \leq 4.4MW$ | 27.27% $P_{Dref}$ | 27.27% $P_{Dref}$ | 22.73% $P_{Dref}$ | 22.73% $P_{Dref}$ | $P_{Dref}$ |

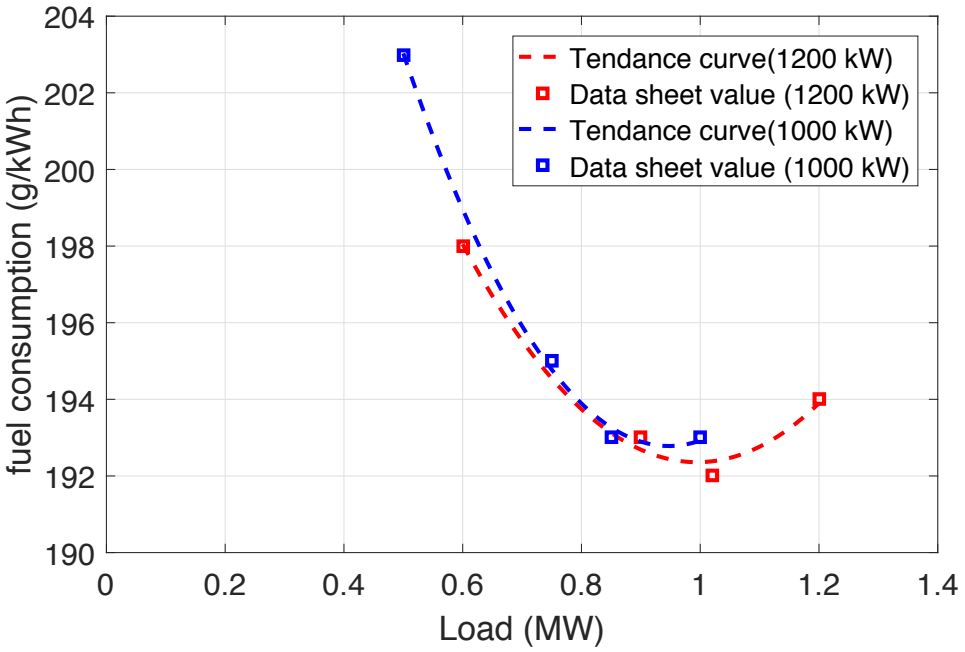


FIGURE 2.17: Diesel consumption vs power [14].

## 2.7 Pumped Hydroelectric System

The Pumped Hydroelectric System (PHS) is an energy storage system based on gravitational potential energy. In fact, when the system presents an excess of energy production, the PHS uses that excess to pump water from a lower reservoir to an upper one. When energy is needed, the water of the upper reservoir is lead to turbines at the level of the lower reservoir, and energy is produced [110, 117]. The studied island presents an interesting case, where coastal cliffs can be found at the northern side of the island. In this case, the lower reservoir will be discarded and the water can be pumped directly from the ocean. Such PHS is called Sea water Pumped Hydro Energy Storage (SPHES). SPHES are not commonly used and yet to be fully mature, but this technology is subject to numerous investigations and studies [45–48].

The stored energy in the SPHES, it respects a gravitational potential law (2.19)

$$E_{sto} = m_{wa} g h_{res} \eta_{sto} \tag{2.19}$$

where $E_{sto}$ is the stored energy, $m_{wa}$ is the mass of the stored water, $h_{res}$ is the altitude of the upper reservoir, and $\eta_{sto}$ is the efficiency of the system. Replacing the water mass by its equivalent volume in water ($Vol_{res}$) and the water density ($\rho_{wa}$). The storage capacity is given in equation (2.20).

$$E_{sto} = Vol_{res} \rho_{wa} g h_{res} \eta_{sto} \tag{2.20}$$

Considering equation (2.20), in addition to the gravitational constant $g$, four parameters characterize the energy rating of the SPHES: the upper reservoir volume, the density of the water, the altitude of the upper reservoir, and the efficiency of the system.

- The upper reservoir volume: the island topology and land use conflict limits strongly the reservoir sizing. Therefore, the upper reservoir volume presents a variable for the sizing of the SPHES.
- The density of the water: the variations of the water density with the temperature and the weather will not be considered, therefore $\rho_{wa}$ is considered as a constant.
- The altitude of the upper reservoir: the considered area for the SPHES

(Fig. 2.1), presents an altitude of $60\ m$. Which corresponds to the altitude of the cliffs near the Stiff lighthouse in the island.

- The efficiency of the system: PHS present hight efficiency compared to other storage systems, its efficiency is estimated between $65$ and $80\ \%$ [118]. But since the considered system is a SPHES and presents lower maturity levels then a normal PHS, the efficiency will be reduced to its lower limits ($64\ \%$) ($80\ \%$ of efficiency is considered in the charge half cycle and the discharge half cycle).

## 2.8 Conclusion

In this chapter, three promising renewable energy sources were evaluated. Wind and the tidal energies was proven to be more effective than the solar one. Indeed, wind and tidal energies on Ouessant island present very high production potential compared to solar energy. Therefore, only wind and tidal turbines were considered

The diesel power plant and the SPHES were analyzed from a cost/production point of view. In fact, the different diesel generators production curves were compared and priority was given to the highest efficiency. As for the SPHES, the reservoir sizes present the major constraint, where a detailed analysis was conducted in order to evaluate its value.

Finally, wind and tidal turbine properties, diesel generators production curves, and SPHES reservoir sizes, will be considered as critical constraints for the optimization in chapter 3.

# 3. Sizing Method of a Hybrid Renewable-based System for a Stand-Alone Site

## 3.1 Introduction

In this chapter, a sizing study of a hybrid renewable-based energy production system will be conducted. The chosen site is the French island of Ouessant. As presented in chapter 2, the Ouessant island is not connected to the continental grid. Therefore, the energy production is limited to the island and no power can be exchanged with the continental grid. In such case, security measures must be taken to ensure the continuous balance of the power on the local grid, where a diesel power plants, already existing on the island, will be considered. Furthermore, the studies in chapter 2 showed two main renewable energy sources, wind and tidal energies. Therefore, they will be considered in the sizing, as well as an ESS.

The sizing of the system is based on a rough optimization in order to ensure a good combination of a low cost and low $CO_2$ emission. First a basic power-exchange simulator of the system is developed. In fact, the simulation of the different elements of the system is based on the equations presented in chapter 2. Therefore, this chapter will focus on developing a system control strategy, as well as exploring the chosen objectives (cost and $CO_2$ emission evaluation) and analyzing the results.

## 3.2 Hybrid Renewable-based Farm Control Strategy

A first constraint in a stand alone system, is to balance the power on the grid, since a difference between the power production and the load can destabilize the grid. In fact, unbalanced power can cause fluctuations of the electrical signal voltage and frequency [119]. In respond to this constraint, a power management strategy must be established. Two strategies were proposed, a basic logic strategy and a fuzzy logic strategy. In both strategies the power management system (PWM) considers the powers produced by the wind and tidal turbines, the load, and the ESS state of charge (SOC); and determines the power stored in the ESS, the power produced by the ESS, the power produced from by the diesel power plant, and the limitation power of the renewable energy systems. View the complexity of such PWM, many steps were considered to simplify the approach:

- Summarizing the load and all renewable energy production potential (the power produced from the renewable energy source if the renewable energy systems are considered to extract the maximal possible power as a function of the resources (wind and tidal velocities). In other wards, with no power limitation applied on the resource) in one resulting signed power ($P_s$), where a positive sign is associated with the energy production and a negative sign to the load. $P_s$ is an uncontrollable power, it depends on the load and the wind and tidal velocities.

$$P_s = P_w + P_t - P_l \tag{3.1}$$

  where $P_w$ and $P_t$ are the maximal power which can be produced by the wind and tidal turbines farms respectively with no production limitation and $P_l$ is the load.

- Reducing the output of the PWM to a signed ESS power ($P_{ESS}$), where the positive sign is associated with a produced power and the negative sign to a stored one.

- The diesel power plant reference production ($P_d$) and the renewable energy sources power limitation ($P_{RElim}$) can be deduced from the the equation governing the energy balance on the grid [120]:

$$P_s + P_d + P_{ESS} + P_{RElim} = 0 \tag{3.2}$$

Furthermore, $P_{RElim}$ is negative at all time, since it represents the amount of power that must be reduced from the maximal renewable energy production potential, in order to maintain the power balance on the grid. And $P_d$ is positive at all time, since the diesel power plant can only inject power on the grid. Therefore two cases can be presented. A first case where the renewable energy production is greater then the load ($P_s > 0$). In this case, the diesel power plant will be shut down ($P_d = 0$), since there is no need for further production. A second case where the renewable energy production is lower then the load ($P_s < 0$). In this case, $P_{RElim}$ is reduced to zero, since the renewable system is needed to produce its full potential. Equations (3.3) and (3.4) presents the mathematical equations of $P_d$ and $P_{RElim}$ respectively.

$$P_d = \begin{cases} -(P_{ESS} + P_s) & if \quad P_s < 0 \\ 0 & if \quad P_s > 0 \end{cases} \tag{3.3}$$

$$P_{RElim} = \begin{cases} 0 & if \quad P_s < 0 \\ -(P_{ESS} + P_s) & if \quad P_s > 0 \end{cases} \tag{3.4}$$

- The output of the strategy can be reduced to the ratio between $P_{ESS}$ and $P_s$, using equation (3.5) the value of $P_{ESS}$ can be obtained, where $P_{reduced}$ is the output of the PWM

$$P_{reduced} = \frac{P_{ESS}}{P_s} \tag{3.5}$$

The resulting PWM considers two inputs ($P_s$ and SOC) and one output ($P_{reduced}$). As for the logic rules governing the PWM, they are based on the following hypothesis: The use of the diesel power plant must be minimized, and the use of the ESS as a power source increase with the value of its SOC. Therefore eighteen rules must be established for all possible states of the system (Table 3.1 presents those rules). Furthermore, the considered threshold of the SOC are $20\%$ for the low to medium SOC and $80\%$ for the medium to high SOC. The power demand presents two threshold values as well, the low to medium one is considered at the third of the maximal load value and the medium to high one at two thirds of the same value. Finally, the power production presents two threshold values, the low to medium one is considered at the third of the maximal total renewable power production value (maximal power production of the wind and tidal farms together) and the medium

to high one at two thirds of the same value.

TABLE 3.1: Fuzzy logic rules.

| | Low SOC | Medium SOC | High SOC |
|---|---|---|---|
| High demand | Low discharge | Medium discharge | High discharge |
| Medium demand | Low discharge | High discharge | High discharge |
| Low demand | Low discharge | High discharge | High discharge |
| Low production | High charge | High charge | Low charge |
| Medium production | High charge | High charge | Low charge |
| High production | High charge | High charge | Low charge |

**Basic logic strategy**

The basic logic strategy uses two sets of mathematical equations, one set is used when the production is higher than the load and the other set when the production is lower then the load.

First, in charging ESS conditions ($P_s > 0$), the goal is to minimize the energy losses and keep a safety zone. Therefore, a maximum amount of power is absorbed for low and medium SOC. But for a high SOC, only a part of the power is absorbed. The mathematical relations are presented in equation (3.6)

$$\begin{cases} P_{reduced} = 1 & if \;\; SOC < 80\% \\ P_{reduced} = -0.05SOC + 5 & if \;\; 80\% < SOC < 100\% \end{cases} \tag{3.6}$$

Second, in a discharging ESS conditions ($P_s < 0$), the goal is to smooth the energy storage output. Therefore the system produces its maximum when the SOC is high and shuts off when the SOC is low. In medium SOC conditions, the ESS production is limited with an exponential variation (using $tanh$) to keep the power output as smooth as possible. The mathematical relations are presented in equation (3.7)

$$\begin{cases} P_{reduced} = 0 & if \;\; SOC < 20\% \\ P_{reduced} = 0.2tanh(4(SOC - 50)) + 0.166 & if \;\; 20\% < SOC < 80\% \\ P_{reduced} = 1 & if \;\; SOC > 80\% \end{cases} \tag{3.7}$$

Figure 3.1 illustrates the presented law.

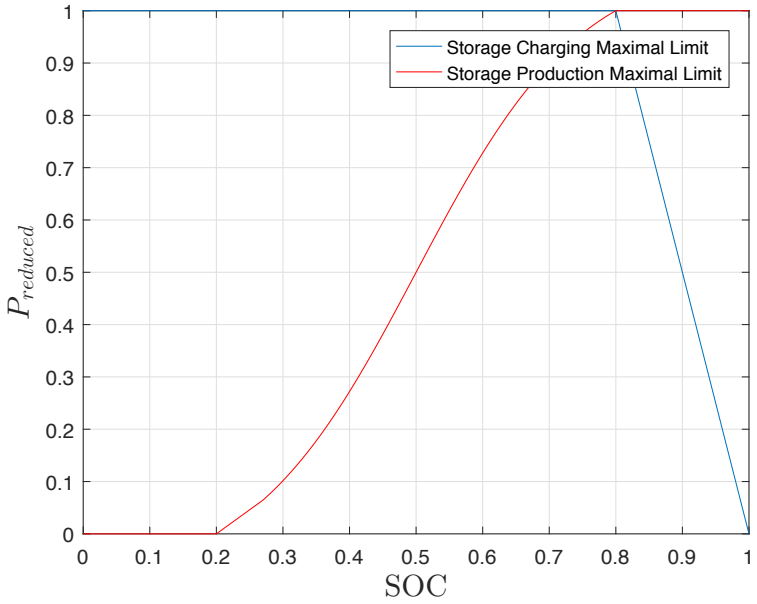


FIGURE 3.1: Storage charge and discharge law curves.

### Fuzzy logic

The fuzzy logic strategy considers two inputs ($P_s$ and SOC) and one output ($P_{reduced}$). The membership function of the input and output variables of the PWM were chosen in a similar way as the basic logic one. Where the SOC is divided between low SOC, medium SOC, and high SOC. $P_s$ is divided between high charge, medium charge, low charge, low discharge, medium discharge and high discharge. The output $P_{reduced}$ is divided between high charge, medium charge, low charge, low discharge, medium discharge and

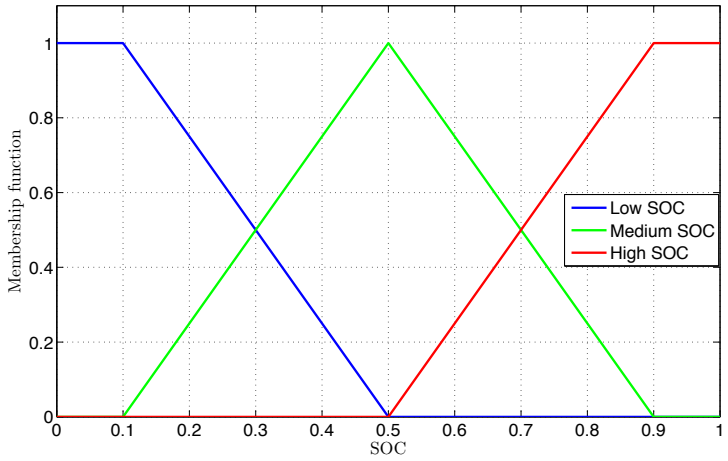


FIGURE 3.2: Membership function of the SOC.

high discharge as well. Figures 3.2, 3.3, and 3.4 illustrate the membership functions of the SOC, $P_s$, and $P_{reduced}$ respectively.

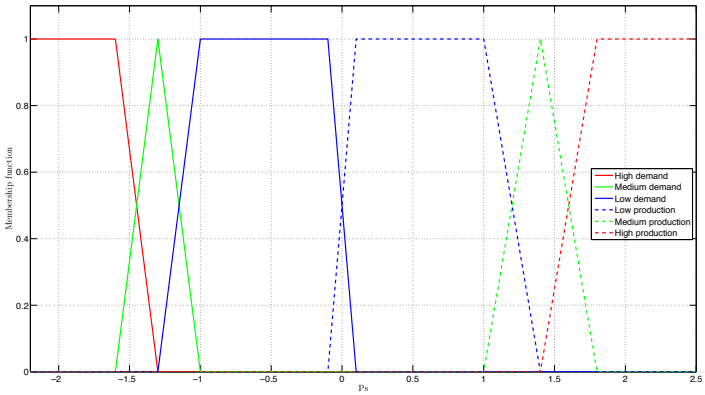


FIGURE 3.3: Membership function of $P_s$.

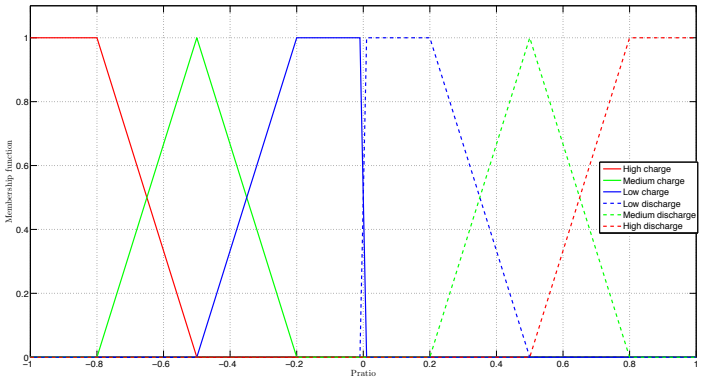


FIGURE 3.4: Membership function of $P_{reduced}$.

Both strategies were tested for a test period of two weeks, fig. 3.5 illustrates the response of these PWMs. Such response is highly satisfying, in fact table 3.1 is well respected. However, the fuzzy logic strategy is more limited in charge when the SOC is getting full or empty respectively. Therefore, the charge of the system is more efficient using the basic strategy. As for the discharge, the fuzzy logic presents faster response while the basic logic presents a more distributed one, such dynamics are very clearly represented in the ninth day in figure 3.5. Finally, tuning and refining the fuzzy logic strategy by applying changes on the membership functions of the different variables, will be interesting to explore in future works.

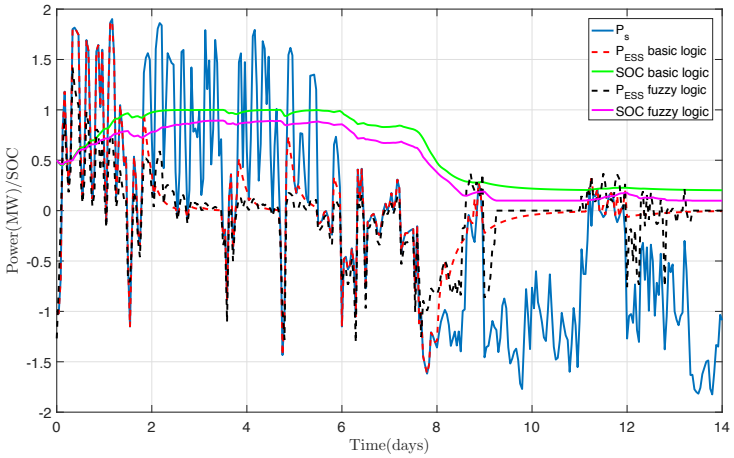


FIGURE 3.5: Test case for both control strategies.

## 3.3 Sizing and Optimization Objectives

In this part of the study, a power exchange network will be constructed with the fuzzy logic PWM linking the different elements together and keeping the power balance on the grid. Furthermore, the different subsystems (load, tidal and wind turbines, diesel generators, and PHS) modulation will be limited to their input and output power, and represented as explained in chapter 2. Furthermore, The simulation includes a cost estimation and the estimation of the $CO_2$ emission, which will present the objectives. A $15$ years system lifetime will be considered.

### $CO_2$ emission

The $CO_2$ emission related to the diesel consumption will be considered. All the $CO_2$ emission related to logistics and other situations will be discarded. Therefore, the $CO_2$ emission will be proportional to the diesel consumption, which is deduced from $P_d$, the consumption curves presented in chapter 2, and equation (3.8) [121]

$$\begin{aligned} M_{CO_2} &= \rho_D Per_C \frac{Ar_{CO_2}}{Ar_C} \\ &= 2.654 Kg/l \end{aligned} \tag{3.8}$$

where $M_{CO_2}$ is the mass of $CO_2$ produced, $\rho_D$ is the diesel density, $Per_C$ is the percentage of carbon in diesel, $Ar_{CO_2}$ is the molar mass of $CO_2$, and $Ar_C$ is the molar mass of carbon.

## Cost

The cost estimation of renewable energy systems is a hard and complex task due to its sensitivity to the site and the system properties. Therefore, basic economic models are used in this study and the results present a qualitative approach. To better estimate the cost, it is divided in two parts:

- The capital expenditure (CAPEX): This part sums all the capital costs of the project, which is the sum of all costs before the project exploitation. It is evaluated per installed MW ($M€/MW$).
- The levelized cost of energy (LCOE): This part presents the cost of energy production, which is the sum of all costs related to the operation of the system. The LCOE is evaluated per MWh ($€/MWh$) and is estimated by [26]

$$LCOE = \frac{\sum_{t=0}^{n} \frac{I_t + M_t}{(I_0+r)^t}}{\sum_{t=0}^{n} \frac{E_t}{(I_0+r)^t}} \tag{3.9}$$

where $t$ is the time of the investments ranging from zero to $n$, $I_t$ is the investments at time $t$, $M_t$ is the operation and maintenance costs at time $t$, $E_t$ is the energy generation at time $t$, and $r$ is the evaluation discount rate.

**Wind turbine:** The wind turbine cost estimation is studied and detailed in [26], where the CAPEX is evaluated taking into consideration the following key features:

- Development and consenting;
- Production and acquisition;
  - Substructure
  - Mooring
  - Grid connection
- Installation and commissioning;
  - Bottom fixed installation
  - Mooring system installation
  - Electrical infrastructure installation
- Decommissioning.

The estimation of the LCOE, is done by taking the following properties into consideration [26]:

- Operation and maintenance;
  - Personnel, accommodation, and port facilities
  - Vessel and equipment requirements
- Farm size;
- Offshore distance;
- Project life span;
- Water depth.

Finally, the considered values are compared to other references: [122] gives a CAPEX estimation of $3.1\ M€/MW$ and a LCOE estimation of $100\ €/MWh$. [123, 124] give a CAPEX estimation of $4\ M€/MW$ and a LCOE estimation of $180\ €/MWh$. Comparing different references, and applying the properties of the considered site, a CAPEX of $3.5\ M€/MW$ and a LCOE of $160\ €/MWh$ are considered based on [26].

**Tidal turbine:** The tidal turbine cost estimation is studied and detailed in [39], where the CAPEX is evaluated to $6\ M€/MW$ taking into consideration the following key features:

- Turbine cost;
- Foundation cost;
- Installation and dismounting.

For the estimation of the LCOE, the considered reference gave the value of $120\ €/MWh$ by studying the following project properties:

- Maintenance cost
  - Preventive maintenance
  - Corrective maintenance

**Diesel generators:** Concerning the diesel generators cost estimation, and since the diesel generators already exists in Ouessant island; the CAPEX will not be considered. As for the LCOE, different references [25, 125] give similar

cost estimation interval. But since the studied system is islanded, the diesel transportation is more expensive than normal sites, and the LCOE cost will be at the higher side of the interval, and will be estimated to $420$ €$/MWh$ [25, 125].

**Pumped hydroelectric system:** For the PHS, the cost estimation is complex because it is highly sensitive to the geological properties of the site. Moreover, a Sea water Pumped Hydroelectric Energy Storage (SPHES) system was considered. Such systems are rarely applied and no cost data were found. Therefore, the CAPEX and LCOE estimations were deduced from freshwater PHS projects, for rough optimization purposes.

Reference [39] shows existing hydro pumped storage system cost analysis. The study compares existing projects in different regions of the world (Europe, Japan, and the United States), and estimates the CAPEX to be between $1$ and $3$ $M$€$/MW$ and the LCOE to be $90$ €$/MWh$.

Other references [126, 127] studied the hydro pumped storage system cost taking into consideration the system sizes. For example, [126] considers for systems smaller than $10$ $MW$, a CAPEX of $4.4$ $M$€$/MW$ and a LCOE of $60$ €$/MWh$. [128] considers a CAPEX of $1$ $M$€$/MW$ and a LCOE of $150$ €$/MWh$.

However, in the considered island, the PHS contains just one reservoir since the ocean will be considered as the lower one. However, the system will have small sizes and should be salty water-tolerant. Therefore, the CAPEX will be estimated to $3M$€$/MW$ and the LCOE to $100$€$/MWh$.

**Cables cost:** Offshore cables cost depends on three key characteristics: the transmitted power, the transmission distance to the shore, and the transmission method [8, 9].

In this study case, the island load varies around 2 MW. The offshore wind and tidal farms are installed in a close range of the island without any link to the continental grid. Indeed, wind turbines are installed at a distance shorter than 3 km and the tidal ones at a distance shorter than 1 km. In this context and according to the above-cited works [8, 9], an MVAC transmission approach can be adopted.

Furthermore, the needs in terms of logistics for the installation and maintenance of the cables are largely similar to those of a tidal turbine (vessel, underwater operations, etc.). Their corresponding cost is already taken into consideration in the cost estimation of a tidal turbine. Finally, the cable cost is constant for all possible farm cases (since the farm is a small one in all these cases). The possible influence of taking into account cable cost will mainly result in a shift of the curves without affecting their shapes.

## 3.4 Simulation Results and Discussion

To better illustrate the system simulation and its respective outputs ($CO_2$ emission and cost), a simple simulation of two weeks (from January 1st to January 14th) will be presented. In this simulation, the already defined wind turbine in table II-2.1 and four tidal turbines presented in table II-2.2 are considered. As for the PHS, a $40\ MWh$ storage capacity is considered. Figure 3.6 shows the produced power of the different elements and figure 3.7 shows the PHS SOC variations.

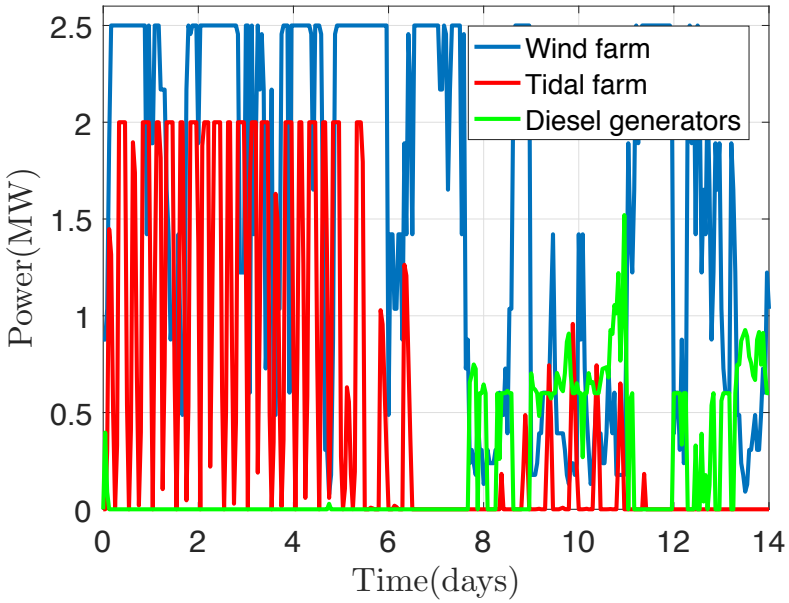


FIGURE 3.6: Wind farm, tidal farm, and diesel generators output power.

The simulation results show a charge of the PHS in the first week, where the energy production is high; and a discharge in the second week, where the

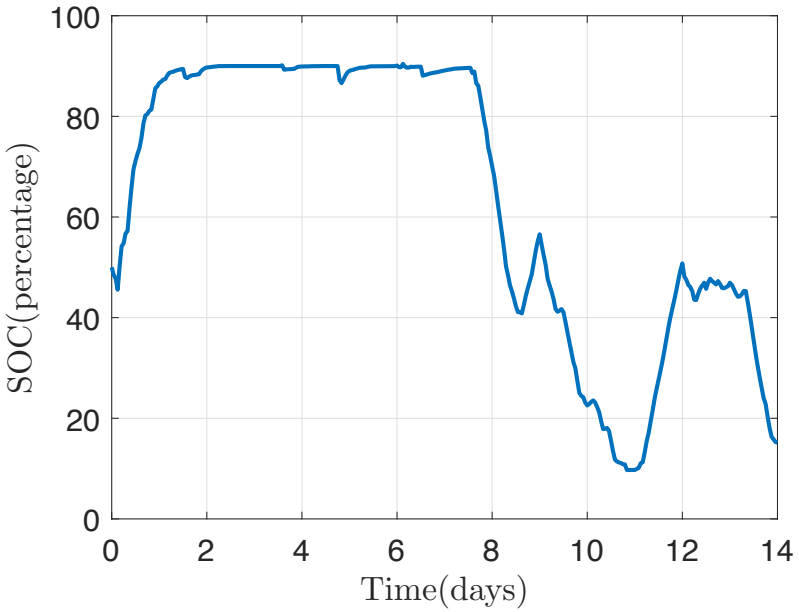


FIGURE 3.7: ESS state of charge variations.

energy production is low (Figs 3.6 and 3.7). Such response was expected, and the system responds to all laws established earlier.

### 3.4.1 Results using fixed ESS, wind turbine, and tidal turbine models sizes

For a clear analysis, the results will be represented in a bi-objective space, where the cost and the $CO_2$ emission will be represented on the horizontal and vertical axis respectively. For a better understanding of the different elements impact on the system, three different configurations will be studied, where specific parameters will be variating in each study. In this first one, the already presented wind and tidal turbine models will be used (tables II-2.1 and II-2.2). As for the PHS, reservoir sizes of $240000\ m^3$ is considered (corresponding to $40\ MWh$), such reservoir sizes are acceptable and similar to other constructed projects, for example the $380000\ m^3$ upper reservoir in the Spanish El Hierro island [129]. This PHS presents a suitable discharge time, in fact, considering the highest load peak on the island ($P_{lmax}$), equation (3.10) presents the minimal discharge time ($T_{min}$) of the system.

$$T_{min} = \frac{E_s to}{P_{l_{max}}} = \frac{40}{2.7} \approx 15h \tag{3.10}$$

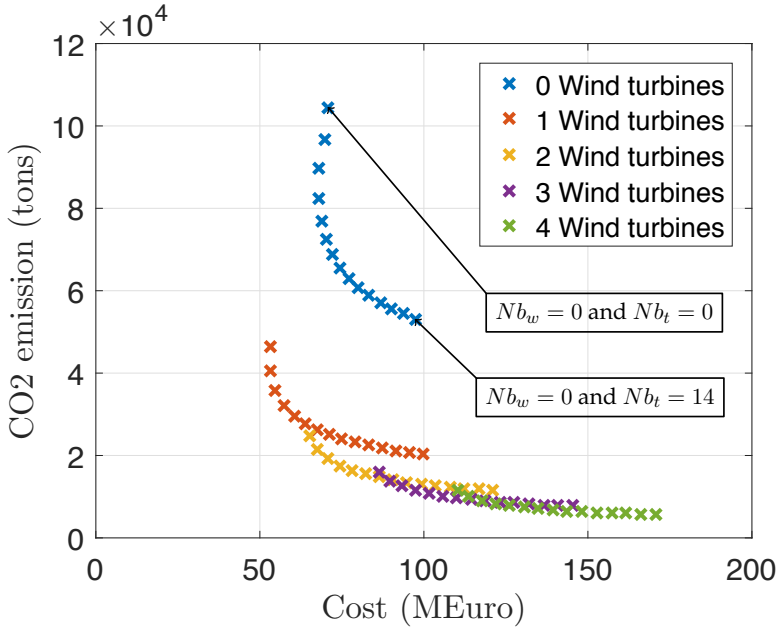


FIGURE 3.8: Bi-objective representation for the optimization results with prefixed 40 MWh ESS capacity, prefixed Nordex N80 2500 wind turbine model, and prefixed tidal turbine model.

With most of the system properties already prefixed, two variable will be used for the system sizing in this first study: the number of turbines in the wind farm ($Nb_w$) and the number of turbines in the tidal farm ($Nb_t$). Furthermore, and as presented in figure II-2.1, the wind turbine farm is expected to be placed east of the site, where a large zone of shallow water is present with a depth between $3$ and $9$ $m$. This large zone present suitable conditions for the placement of fixed bottom offshore wind turbines [26]. Furthermore, the studied area presents the underwater straight passage "Passage du Fromveur" which presents optimal condition for the placement of a tidal farm [130] (a depth between $30$ and $50$ $m$, and strong tidal currents). Therefore a large number of wind and tidal turbines can be placed around the island (eq. (3.11)).

$$\begin{cases} Nb_t = \{0, 1, ..., 14\} \\ Nb_w = \{0, 1, 2, 3, 4\} \end{cases} \tag{3.11}$$

Results given in Fig.3.8 show a starting point (for a $Nb_w = Nb_t = 0$) of $70.9$ $M€$ cost and $105$ $ktons$ of $CO_2$ emission, a minimal cost point (for $Nb_w = 1$ and $Nb_t = 1$) of $53.1$ $M€$ cost ($25.1\%$ reduction) and $40.5$ $ktons$ of $CO_2$ emission ($61.4\%$ reduction), and a minimal $CO_2$ emission point (for$Nb_w = 4$ and $Nb_t = 14$) of $170.6$ $M€$ cost ($240.6\%$ increase) and $5.67$ $ktons$ of $CO_2$

emission ($94.6\%$ reduction).

The first objective ($CO_2$ emission) presents a monotonous variation, where it decreases when either one of the variables ($Nb_t$ and $Nb_w$) increases. However, the cost presents two phased variations: the first phase is a decreasing cost for the increase of the wind and tidal turbines number, this can be explained by the decrease of the diesel consumption. The second phase is an increasing cost for the increase of the wind and tidal turbines number when they surpass a certain value. By mixing both objectives, the global variations in the bi-objective space, can be separated into two parts. A first part, where both objectives decrease with the increase of the turbines number, and the curve presents an evolution to the left-bottom direction. And a second part, where the cost increases and the $CO_2$ emission decreases with the increase of the turbines number, and the curve presents an evolution to the right-bottom direction. Such variations can be explained by the stand-alone aspect of the studied site. In fact, under such conditions, the produced energy can not be extended nor exchanged to a larger grid with a higher capacity. Therefore, when the SOC of the PHS is high, the extra power will not be extracted. Other studies for stand-alone sites showed similar results, for example, in [131] a hybrid system of wind turbines and photo-voltaic solar panels has been applied in a different site. The achieved results presents similar variations.

### 3.4.2 ESS sizes variation

In this second configuration, all system properties were kept same as the first configuration. Furthermore, the PHS capacity is presented as a variable. In this study, not all points are presented. in fact, the minimal cost and $CO_2$ emission limit curves will be drawn for each storage capacity case. The results are shown in figure 3.9. These results show a decrease in the both objectives with the increase of the PHS capacity.

For a deeper analysis, the difference for both $CO_2$ emission and cost are introduced (eq. (3.12))

$$\begin{cases} \Delta Em_{m/n} = Em_m - Em_n \\ \Delta C_{m/n} = Cost_m - Cost_n \end{cases} \tag{3.12}$$

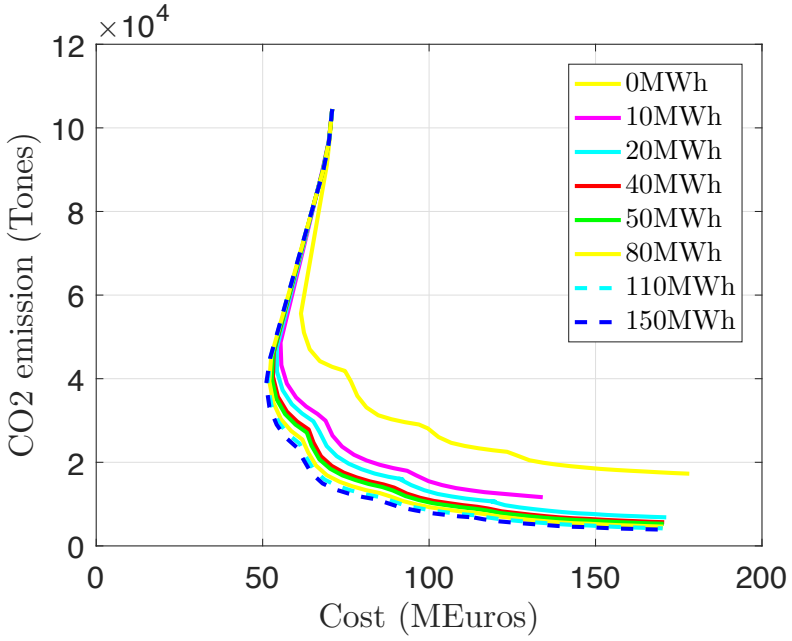


FIGURE 3.9: Bi-objective representation for the optimization results with storage capacity variation.

where $\Delta Em_{m/n}$ is the $CO_2$ emission difference between systems with storage capacities of m $MWh$ and n $MWh$, $Em_m$ is the $CO_2$ emission for a system with a storage capacity of m $MWh$, $\Delta C_{m/n}$ is the cost difference between systems with storage capacities of m $MWh$ and n $MWh$, and $Cost_m$ is the cost for a system with a storage capacity of m $MWh$. It is obvious that for a constant value of $(m - n)$, $\Delta Em_{m/n}$ and $\Delta C_{m/n}$ decrease with the storage capacity evolution. However, as the increase of the storage capacity will result in an increase of the water reservoir volume, a careful choice should be made. In the case of Ouessant island, a storage capacity between $10$ and $20MWh$ seems reasonable.

### 3.4.3 Reducing wind turbine sizes

In a third studied configuration, the wind turbine sizes are reduced to match the rated power of the tidal turbine. As table 3.2 shows, only the turbine diameter was changed, all other changes are resulting of such variation. Furthermore, the maximal number of wind turbines to be considered is increased from $4$ to $10$. Such configuration is established in order to compare the impact of the different renewable energy sources. Finally, an energy storage system capacity of $40$ $MWh$ is considered.

TABLE 3.2: Reduced wind turbine parameters.

| | |
|---|---|
| Turbine diameter | 17.8 $m$ |
| Sweep area | 1005 $m^2$ |
| Cut-in wind speed | Approx. 3 $m/s$ |
| Cut-out wind speed | 25 $m/s$ |
| Rated speed | 15 $m/s$ |
| Rated power | 0.5 $MW$ |
| $C_{pmax}$ | 0.434 |

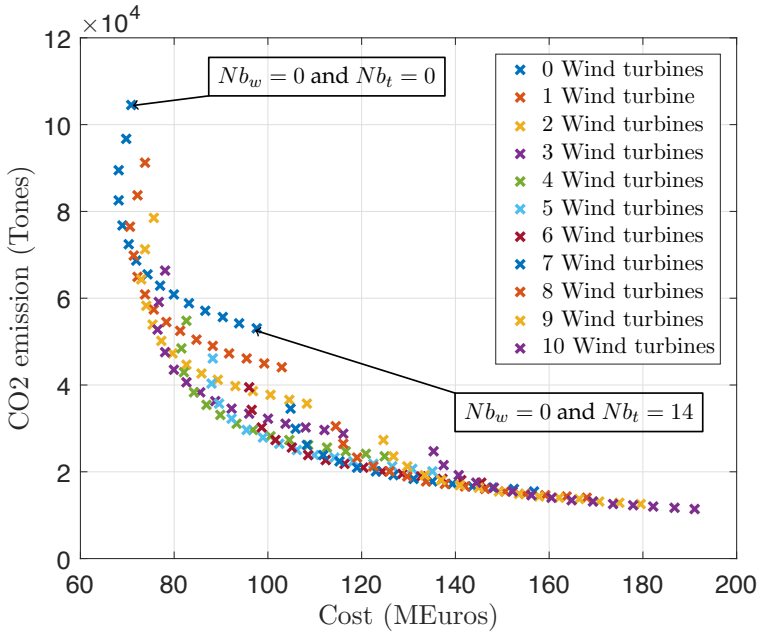


FIGURE 3.10: Bi-objective representation for the optimization results with a reduced wind turbine.

The results shown in fig. 3.10 shows the same variations as the first configuration. A first part, where both objectives decrease with the increase of the turbines number, and the curve presents an evolution to the left-bottom direction. And a second part, where the cost increases and the $CO_2$ emission decreases with the increase of the turbines number, and the curve presents an evolution to the right-bottom direction. But in this case, the results show a larger impact of the wind energy, compared to the tidal one. Indeed, for a given number of wind and tidal turbines ($Nb_w$ and $Nb_t$), the variation of the $CO_2$ emission and the cost for an increase of the wind turbines number ($Nb_w$+1) is more important than the ones caused by an increase of the tidal turbines number ($Nb_t$+1). Such behavior is expected, and can be explained by three major points:

- The difference between the power related to the cut-in speed of the 2 hybrid systems shows a smaller cut-in power for the wind turbine:

$$\begin{cases} P_{win} = \frac{1}{2} N b_w C_p \rho_{air} \pi R^2 V_{win}^3 = 7.3KW \\ P_{tin} = \frac{1}{2} N b_t C_p \rho_{wa} \pi R^2 V_{tin}^3 = 46.3KW \end{cases} \tag{3.13}$$

- For the chosen turbines of the same power limits, a wind turbine produces a total energy of $1488.5MWh$, while a tidal turbine produces $1325.6MWh$. This energy production difference is related to the site characteristics and to the turbines power limitations.

- The global cost of a wind turbine is lower than a tidal turbine with the same rated power.

One final simulation, using the same wind and tidal turbines and ESS configurations is proposed. But in this case, the basic logic was considered for the system control strategy. Figure 3.11 presents the achieved results.

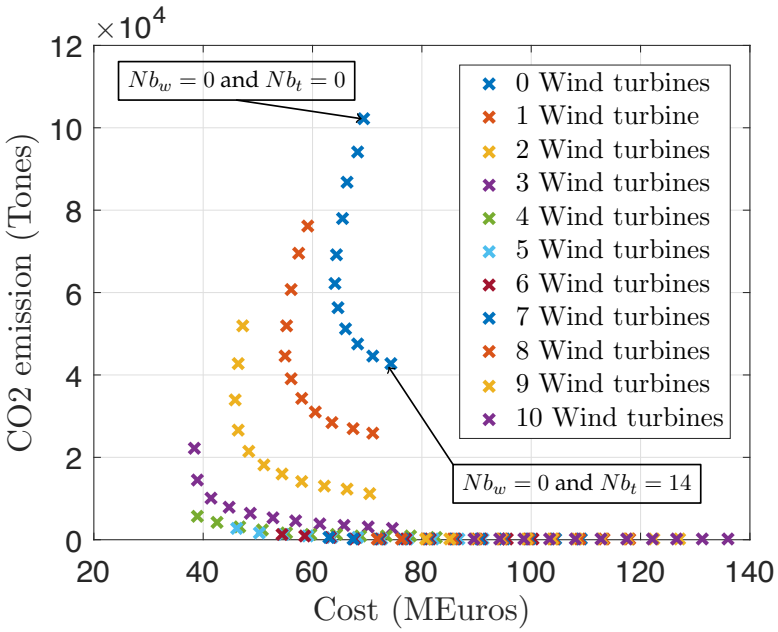


FIGURE 3.11: Bi-objective representation for the optimization results with a reduced wind turbine.

The results show a better response, when the basic control is used. However, the fuzzy logic is not optimally tuned in this study. In fact, tuning the fuzzy logic PWM needs many tryouts. Furthermore, the power network considered in all the simulations, presents a long simulation time. Due to the lack of time, the optimal fuzzy logic low is yet to be determined. However, a fuzzy logic PWM can be adapted easier when the system changes. As discussed

in the introduction, hybrid grids present the capability of evolution and including more renewable with time. Therefore Fuzzy logic PWM present an advantage on such level.

## 3.5 Conclusion

In this chapter, a power exchange network between the different elements of the system was established, to simulate the system performance for a long time period. Two power management strategies have been proposed. The first one is based on basic logic rules and the second one on fuzzy logic rules. These two strategies are able to control the power sources, the ESS, and the diesel power plant, while respecting the needed power balance, in order to minimize both system cost and $CO_2$ emission.

TABLE 3.3: Nordic N-1000 turbine characteristics [19]

| | |
|---|---|
| Turbine diameter | 54 $m$ |
| Sweep area | 2291 $m^2$ |
| Cut-in wind speed | 5 $m/s$ |
| Cut-out wind speed | 25 $m/s$ |
| Rated speed | 16.5 $m/s$ |
| Rated power | 1 $MW$ |

The system was simulated for these two strategies and the results in terms of cost and $CO_2$ emission were analyzed. The achieved results show that including renewable energy sources to the grid can decrease both cost and $CO_2$ emission, when the sources are well chosen. For example, in the third study case results (Reducing wind turbine sizes), figure 3.10 present an interesting point ($Nb_w$=4 and $Nb_t$=1) where the cost is around 38 $M€$ and the $CO_2$ emission is around 1.8 $kTones$ (the basic logic results considered). Therefore, a a hybrid system with two wind turbines of 1 $MW$ each (for example the Nordic N-1000 of table 3.3 [19]), a tidal turbine of 0.5 $MW$, and a PHS of 40 $MWh$ will be considered in chapter 4 for the study of the different elements regulations.

# 4. Design and Analysis of Inverter Control Methods for Micro-grid Applications in a Stand-Alone Site

## 4.1 Introduction

The renewable energy sources, which are progressively installed in the grid, are connected via inverters. These inverters present small output impedance and therefore fast dynamics [132, 133]. Such systems could have substantial influence on the grid stability, by causing voltage and frequency fluctuations [134, 135]. To deal with this issue, different control strategies were developed. First, a PMS, for example fuzzy logic and basic logic control strategies, presented in chapter 3, deals with the hybrid system at a macro level and ensures the power equilibrium on the grid level. Second, a regulation strategy, which will be studied in details in this chapter, deals with the hybrid system at a micro level and ensures the inverter regulation.

In a first part of this study, three inverter control strategies are considered. The power control strategy ($P/Q$) is developed for inverters connected to a powerful grid and focuses on the regulation of the power injected to the grid [136]. The voltage and frequency control strategy ($V/f$) is developed for stand-alone systems and focus on the regulation of the voltage and frequency of the grid [137]. Finally the inverter virtual synchronous generator control strategy ($IVSG$) is a more recent regulation method and can be used in both grid-connected and stand-alone systems [138].

In a second part, multi-source control strategies will be developed. First, the Master-Slave ($M/S$) control strategy is a well known traditional regulation method, in which all inverters are regulated using a $P/Q$ control strategy [139, 140]. This regulation method will be discarded since it is used for a grid connected system. It is therefore not very effective in a stand-alone site

like the island of Ouessant [141–143]. Second, the traditional droop control strategy is a method in which all inverters are regulated using a $V/f$ control strategy [80]. This regulation can be effective for the studied island, since it can be applied for stand-alone systems. Third, the virtual synchronous generator ($VSG$) control strategy is a more recent method in which all inverters are regulated using an $IVSG$ control strategy [80]. This regulation can be effective for the studied island as well, since it can be applied for stand-alone systems.

In a final part, chapter 3 achieved results will be considered and the full system will be simulated. In this context, chapter 3 concluding case with two wind turbines of $1\ MW$ each, a tidal turbine of $0.5\ MW$, and a $40\ MWh$ ESS are considered. Afterwards, a $VSG$ regulation associated to a fuzzy logic control strategy will be applied to the system.

## 4.2 Design and Analysis of Single Inverter Regulation for Renewable Energy-based Systems

This section of the study focuses on the regulation of a single grid side inverter. Figure 4.1 describes briefly an inverter-based energy production system. In the presented diagram, the control strategy is implemented in the control block.

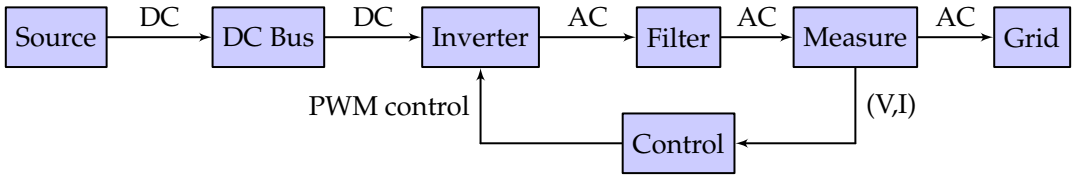


FIGURE 4.1: Control diagram of a single inverter system.

### 4.2.1 System Elements Description

The different elements of the considered system are presented in the control diagram 4.1: The source, the DC bus, The inverter, The filter, and the grid.

### Source

In this study, the source and its corresponding inverter will be considered as fully controlled, and the details of this control are not addressed. Other studies have already addressed this problem, for example, reference [98] discussed the case of a tidal turbine. Therefore, the source will be considered as a DC current source connected to the inverter DC bus, and will follow the law presented in equation (4.1).

$$I_S = \frac{P_S}{V_{DC}} \tag{4.1}$$

Where $P_S$ is the power produced by the source, $I_S$ is the current produced by the source, and $V_{DC}$ is the voltage of the grid side converter DC bus.

### DC bus

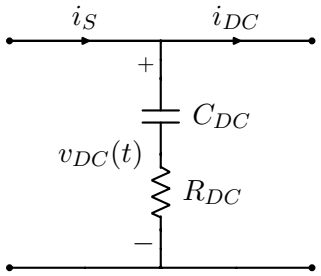


FIGURE 4.2: DC bus model.

The DC bus is represented by a capacitor $C_{DC}$ and a small resistance $R_{DC}$ (fig. 4.2). The DC bus voltage ($V_{DC}$) can be approximated by equation (4.2), where the resistance is neglected since it is small compared to the effect of the capacitor.

$$V_{DC} = \frac{1}{C_{DC}} \int (I_S - I_{DC}) dt \tag{4.2}$$

Where $I_{DC}$ is the current produced by the DC bus. Or, under quasi-continuous conditions, the power can be approximated as the product of the voltage and the current. Equation (4.2) highlights the DC bus voltage variation possibilities. In fact, if the source production is higher than the load $V_{DC}$ will increase, and if the source production is lower than the load $V_{DC}$ will drop. Therefore a regulation of the DC bus voltage is essential. Reference [18] presents a solution by adding a second control loop for $V_{DC}$ regulation, where the regulated error on the DC bus voltage presents the active power reference

production. However, in a stand-alone system, a voltage and frequency regulation is indispensable, therefore such solution can not be adapted, and the DC bus must be regulated using another method. In this work, a small energy storage system with a fast reaction time is proposed. Some previous works [144–146] present batteries as a possibility, and some others [146, 147] present super-capacitors. Furthermore, renewable energy sources are connected to the grid via inverters. Such systems presents negligible energy storage capacity compared to the inertia of classical generator. Such low energy capacity makes the system sensitive to power fluctuations. This clearly point out the ESS importance [148, 149]. Figure 4.3 illustrates the proposed DC bus regulation, where CS refer to current source.

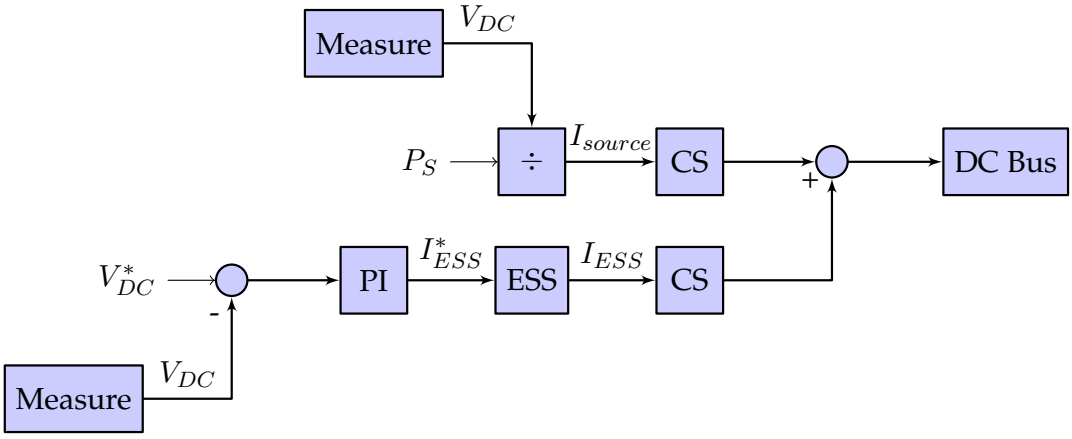


FIGURE 4.3: Control diagram of the source and the DC bus.

### Inverter

The considered inverter for this study is a three-phase IGBT-based one, controlled by a PWM (fig 4.4).

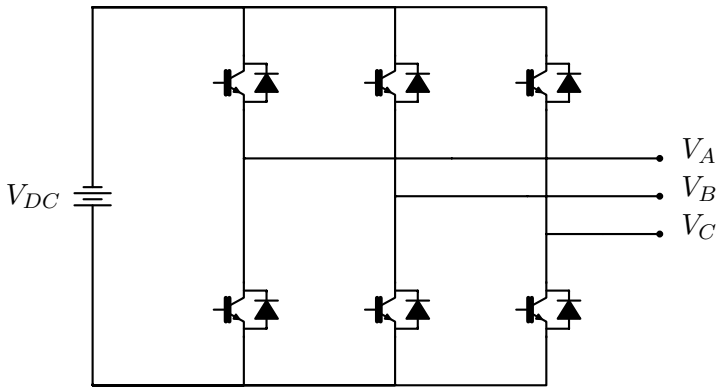


FIGURE 4.4: Inverter electric circuit.

### Filter

Filtering the inverter output signal is essential. Therefore a filter was added to the system, with a cut-off frequency $f_C$ between $100$ and $200$ $Hz$. The considered filter is a series LC one, where the capacitor $C_f$ and the inductance $L_f$ are related to the frequency as shown in equation (4.3). Finally, the grid related inductance is included in the filter.

$$f_C = \frac{1}{2\pi\sqrt{C_f L_f}} \tag{4.3}$$

### Grid

In this study, the grid is considered as a three phase balanced system. Moreover, two grid models are are used in the following studies. The first grid type represents an isolated site and considers only the load. The second grid type represents a system connected to a powerful main grid and considers the load and a main grid power source.

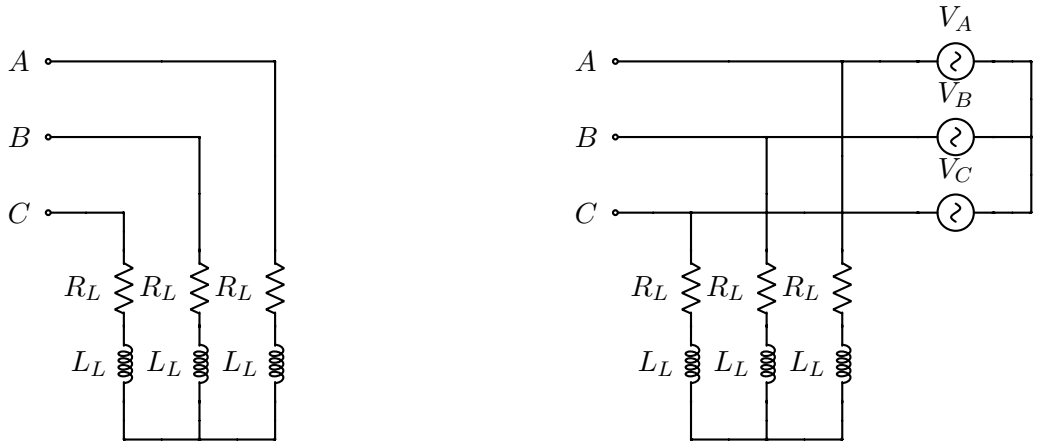


FIGURE 4.5: Grid electrical model for stand-alone case (left) and grid-connected case (right).

- Isolated site: In this case, the load is considered in his two forms, active and reactive. In order to represent such load, a three-phase RL load was introduced.
- Grid-connected site: In this case, the grid is formed of a load and a power source. The load is modeled the same as the isolated site load. Concerning the power source, since the main grid is considered having

a much higher power then the renewable energy source, its power capacity will be considered infinite. Therefore it will be represented by an ideal three-phased voltage source.

### 4.2.2 P/Q Control Strategy

This inverter control strategy regulates the active and reactive power output of the inverter [150]. This control strategy us used in grid-connected systems. It can be also used in master-slave control strategy for multi-source systems in stand-alone sites, where the voltage and frequency are regulated by the master source, and the slave source regulates the power injected to the grid [139, 140]. However in the second case, the master source must be a highly stable one that wont be shut down at any given time.

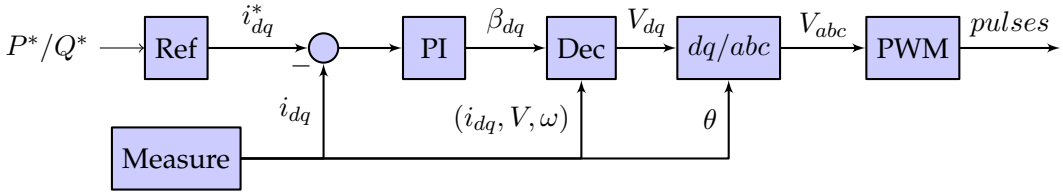


FIGURE 4.6: Control diagram of the $P/Q$ control strategy.

The $P/Q$ control strategy is based on a vector control strategy, where the projections of the current on the $dq$ rotating frame ($i_d$ and $i_q$) are used as regulation variables [151]. In fact, in the $dq$ frame, the active and reactive powers respects the law shown in equation (4.4).

$$\begin{cases} P = v_d i_d + v_q i_q \\ Q = v_d i_q - v_q i_d \end{cases} \tag{4.4}$$

where $v_d$ and $v_q$ are the projections of grid voltage on the $dq$ rotating frame.

As discussed above, the voltage and frequency are not regulated in the $P/Q$ control strategy and they are predetermined by the grid interaction. Therefor, $v_q$ can be considered as the reference of the $dq$ frame. Furthermore, the load is considered perfectly balanced. Under these conditions, $v_d$ can be neglected, and the reference value of the power follow the relation presented in equation (4.5)

$$\begin{cases} P_{ref} = v_q i^*_q \\ Q_{ref} = -v_q i^*_d \end{cases} \tag{4.5}$$

where $i^*_d$ and $i^*_q$ are the current reference values.

Afterwards, the reference values of the current are compared to the measured values and the errors are regulated with traditional PI regulators, where ($\beta_d$ and $\beta_q$) are the output of the regulators. The inverter reference voltages ($v_d^*$ and $v_q^*$) are therefore deduced by decoupling the $dq$ axis as shown in equation (4.6)

$$\begin{cases} v_d^* = \beta_d - L_f \omega i_q \\ v_q^* = \beta_q + L_f \omega i_d + v_q \end{cases} \tag{4.6}$$

where $L_f$ is the filter inductance value.

Figure 4.6 illustrates the $P/Q$ control strategy diagram.

### 4.2.3 V/f Control Strategy

This inverter control strategy regulates the voltage and frequency of the electrical signal [152,153]. It is used in stand-alone site condition, where it can be associated with a droop control or a master-slave control [139,140].

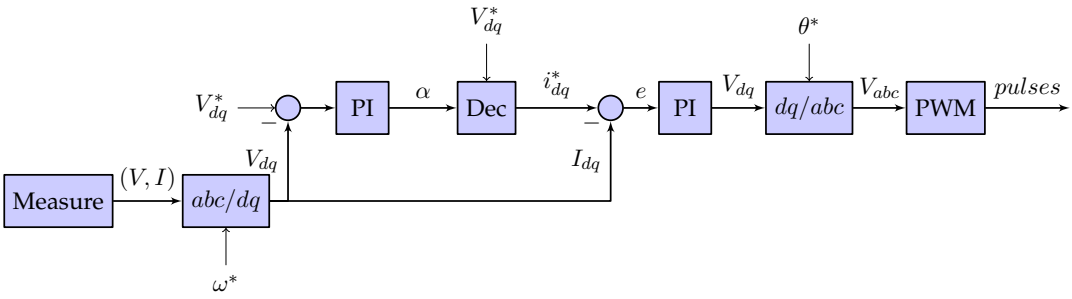


FIGURE 4.7: Control diagram of The $V/f$ control strategy.

Similar to the $P/Q$ control strategy, the $V/f$ strategy is based on a vector control strategy. but in this case a double control loop is used. In the inner loop, the current projection on the $dq$ frame is regulated and in the outer loop, the voltage projection on the $dq$ frame is regulated. Therefore, the current regulation, in the $V/f$ case, is not decoupled in the same way as the $P/Q$ case. In fact, in this case, the decoupling follows the law presented in equation (4.7)

$$\begin{cases} i_d^* = \alpha_d - C_f \omega v_q \\ i_q^* = \alpha_q + C_f \omega v_d \end{cases} \tag{4.7}$$

where $\alpha_d$ and $\alpha_q$ are the output of the voltage regulation, and $C_f$ is the filter capacitor value.

Figure 4.7 illustrates the $V/f$ control strategy diagram.

### 4.2.4 IVSG Control Strategy

This inverter control strategy regulates all four parameter: voltage, frequency, active power, and reactive power. Furthermore, this control strategy can be used in both stand-alone and grid-connected sites. In this study, a stand-alone condition will be considered for this regulation case. In fact the $IVSG$ does not use vector control strategy. instead, the reference voltage of the PWM is considered as a voltage of a virtual synchronous generator [60, 82]. In this context, a droop control relation is established between the voltage and the reactive power as shown in equation (4.8), (Fig. 4.8).

$$U_{ref} = U^* + K_v(Q^* - Q) \tag{4.8}$$

Where $U_{ref}$ is the reference value of the voltage regulation loop (affected by the droop regulation), $U^*$ is the voltage reference, $Q^*$ is the reactive power reference, $Q$ is the reactive power value, and $K_V$ is the voltage droop constant.

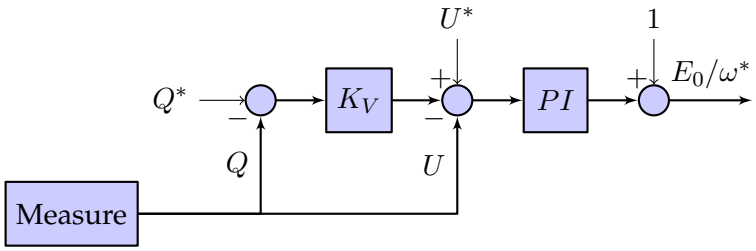


FIGURE 4.8: Control diagram of the $IVSG$ control strategy excitation regulator.

The virtual excitation regulator is the part where the voltage is regulated (Fig. 4.8). It is defined by equation (4.9)

$$\begin{cases} E_0 = \omega M_f i_f \\ i_f = i_f^* + \Delta i_f \end{cases} \tag{4.9}$$

where $\omega$ is the virtual electrical angular velocity, $E_0$ is the virtual excitation of the electromotive force (and it forms the output of the voltage regulation), $M_f$ is the virtual mutual inductance of the stator winding and $i_f$ is the virtual excitation current.

Similar to earlier, a droop relation is established between the frequency and the active power (Fig. 4.9). This relation is included in the virtual speed

regulator (4.10).

$$P_{ref} = P^* + K_f(f^* - f) \tag{4.10}$$

where $P_{ref}$ is the reference value of the active power regulation loop, $P^*$ is the active power reference, $f^*$ is the frequency reference, $f$ is the frequency value, and $K_f$ is the frequency droop constant.

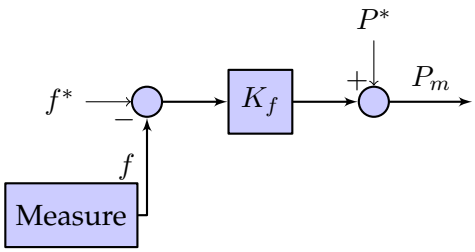


FIGURE 4.9: Control diagram of the $IVSG$ control strategy speed regulator.

The third and final part of the $IVSG$ strategy is the main algorithm (fig. 4.10). This part can be divided into a mechanical module and an electrical one. Equation (4.11) presents the laws of the mechanical module.

$$\begin{cases} \frac{P_m}{\omega} - \frac{P_e}{\omega} - D\Delta\omega = J\frac{d\Delta\omega}{dt} \\ D\Delta\omega = \omega - \omega_B \\ \omega = \frac{d\theta}{dt} \end{cases} \tag{4.11}$$

Where $P_m$ is the mechanical virtual power, $P_e$ is the electrical power, $D$ is the virtual damping coefficient, $J$ the virtual rotational inertia, $\omega_B$ the rated angular velocity, and $\theta$ the electrical angle.

The electrical module is presented by the following equation (4.12)

$$E_0 = U + ZI \tag{4.12}$$

Where $U$ is the stator voltage, $Z$ is the equivalent inductance and $I$ is the stator current. As the virtual generator stator is connected to the grid and the electromotive force to the inverter output voltage, $Z$ will be the equivalent impedance of the filter.

Appendix B shows the full control diagram of the $IVSG$ regulation.

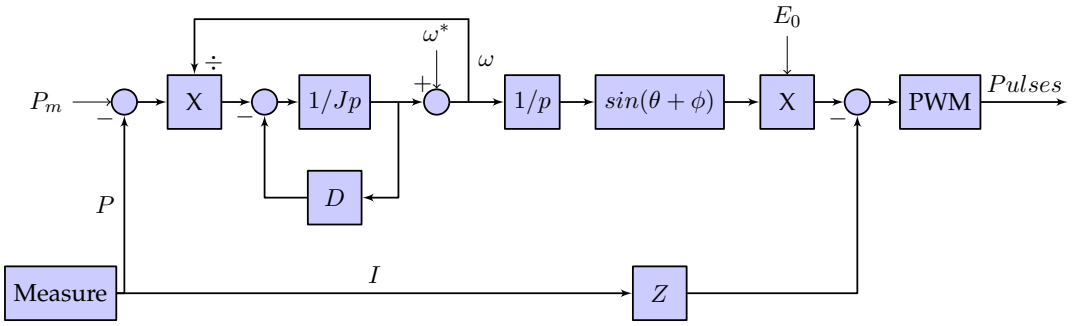


FIGURE 4.10: Control diagram of the $IVSG$ control strategy algorithm.

### 4.2.5 Simulation Results

In order to test the stability and evaluate the above-discussed control strategies, a simulation of the system presented in control diagram 4.1 was conducted using Matlab/Simulink PowerSim toolbox. Table 4.1 lists the simulated system parameters values.

Table 4.2 gives the regulators values of each control method: PI regulator parameters for the $P/Q$ control strategy (Fig. 4.6), both voltage and current PI regulators parameters for the $V/f$ control strategy (Fig. 4.7), parameters of the $IVSG$ control strategy, including both voltage and frequency droop parameters (Fig. 4.7), excitation regulator PI parameters (Fig. 4.8), and the $IVSG$ algorithm mechanical and electrical modules different parameters.

The three systems were simulated under the same conditions:

- At initial state $t = 0$, a $0.5MVA$ total load is applied to the system with a power factor of $0.95$.

TABLE 4.1: System parameters.

| Parameter | Value |
|---|---|
| $V_N$ (V) | 6900 |
| $f$ (Hz) | 50 |
| $P_s$ (MW) | 0.5 |
| $V_{DC}$ (V) | 720 |
| $C_{DC}$ (mf) | 5 |
| $R_{DC}$ ($\omega$) | 0.008 |
| $\tau_{Bat}$ (s) | 1 |
| $K_{Bat}$ (SI) | $10^6$ |
| $E_{Bat}$ (MWh) | 0.1 |
| $C_f$ ($\mu$f) | 47 |
| $L_f$ (mH) | 46.25 |

TABLE 4.2: Inverter regulator parameters.

| | Parameter | Value |
|---|---|---|
| P/Q | $K_{Pi}$ (SI) | 16.5 |
| | $K_{Ii}$ (SI) | 5000 |
| V/f | $K_{Pi}$ (SI) | 0.5 |
| | $K_{Ii}$ (SI) | 20 |
| | $K_{Pv}$ (SI) | 5 |
| | $K_{Iv}$ (SI) | 5 |
| IVSG | $J$ $(Kg.m^2)$ | 0.2 |
| | $D$ (SI) | 4 |
| | $R_a$ $(\Omega)$ | 0.02 |
| | $L_a$ (mh) | 0.5 |
| | $K_{PE}$ (SI) | $10^{-4}$ |
| | $K_{IE}$ (SI) | $5.10^{-3}$ |
| | $K_f$ (SI) | $10^{-6}$ |
| | $K_v$ (SI) | $10^{-5}$ |

- At $t = 0.3s$, a step load of $50\%$ of the initial value is added.
- At $t = 0.6s$, the step load is removed.

The produced active and reactive powers and their references in the case of the $P/Q$ control strategy are shown in figure 4.11. For the $V/f$ control strategy, figures 4.12, 4.13, and 4.14 show the load variations, the voltage RMS value, and the frequency, respectively. Finely, for the $IVSG$ control strategy, figures 4.15, 4.16, and 4.17 show the power variation, the voltage RMS value, and the frequency, respectively. The simulation results clearly highlight the stability and convergence of all three control strategies, therefore they can be included into more complex multi-source control strategy.

Comparing the different strategies, the $P/Q$ control strategy is used in grid-connected systems and presents fast dynamics but large error margins. The $V/f$ control strategy is used in stand-alone systems and presents fast dynamics but large voltage error. Finely the $IVSG$ control strategy is used in stand-alone systems and presents slower dynamics and important voltage and frequency errors.

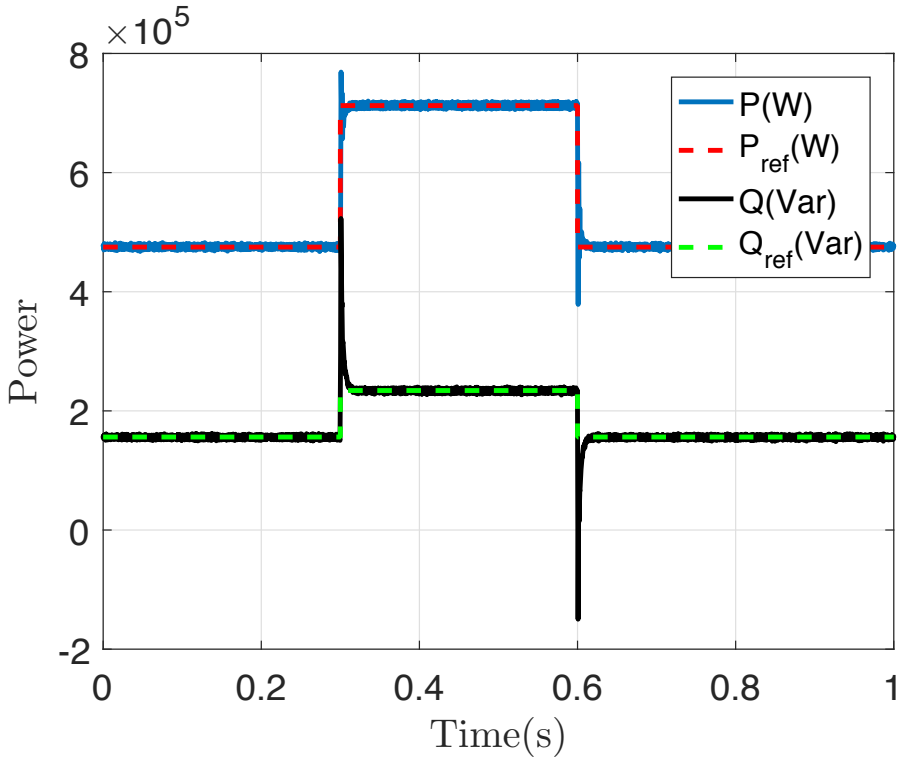


FIGURE 4.11: The power produced by the renewable energy system in the $P/Q$ control case.

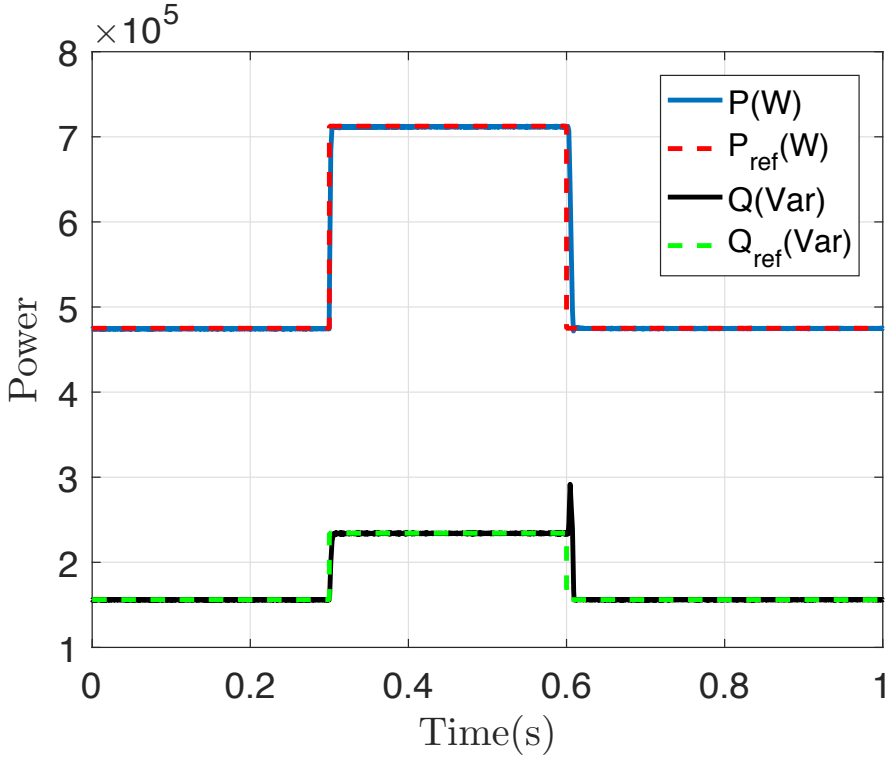


FIGURE 4.12: The power produced by the renewable energy system in the $V/f$ control case.

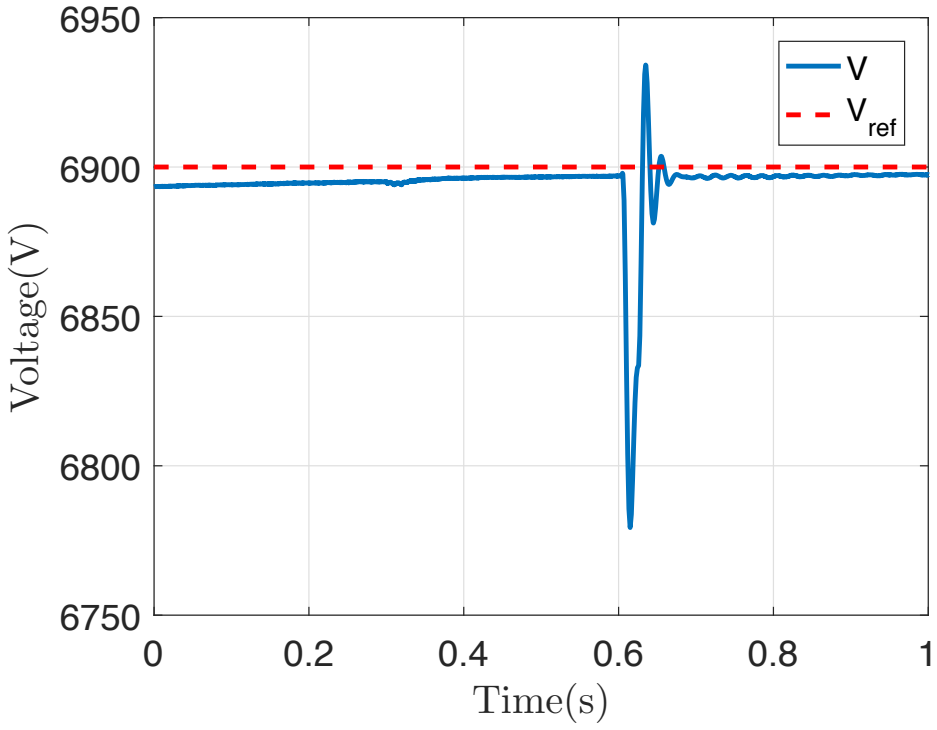


FIGURE 4.13: The variations of the voltage RMS value in the $V/f$ control case.

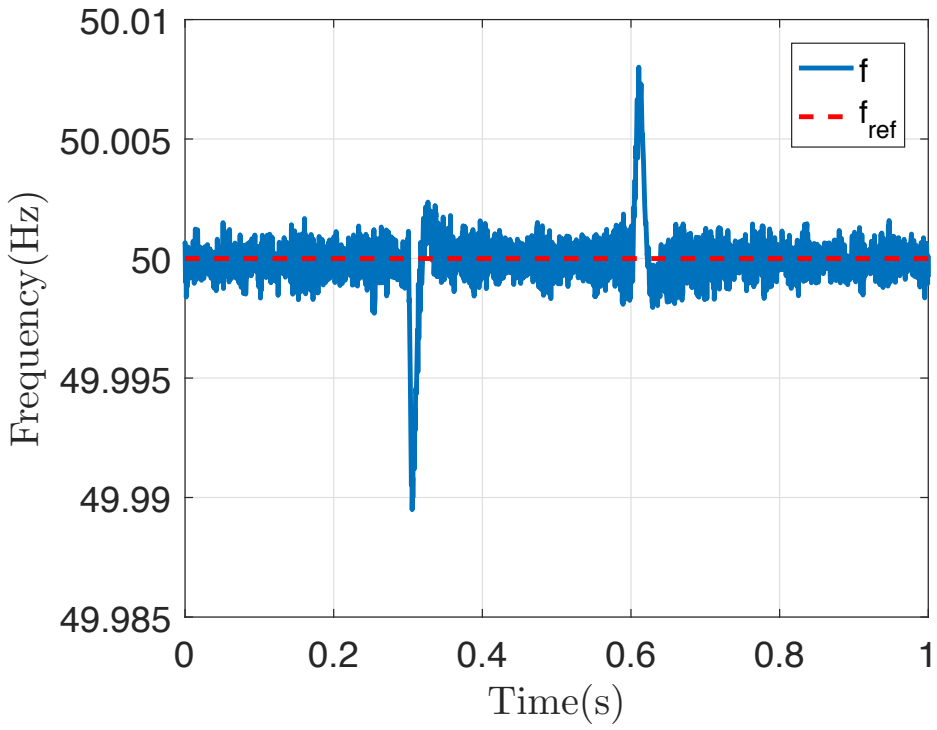


FIGURE 4.14: The frequency variations in the $V/f$ control case.

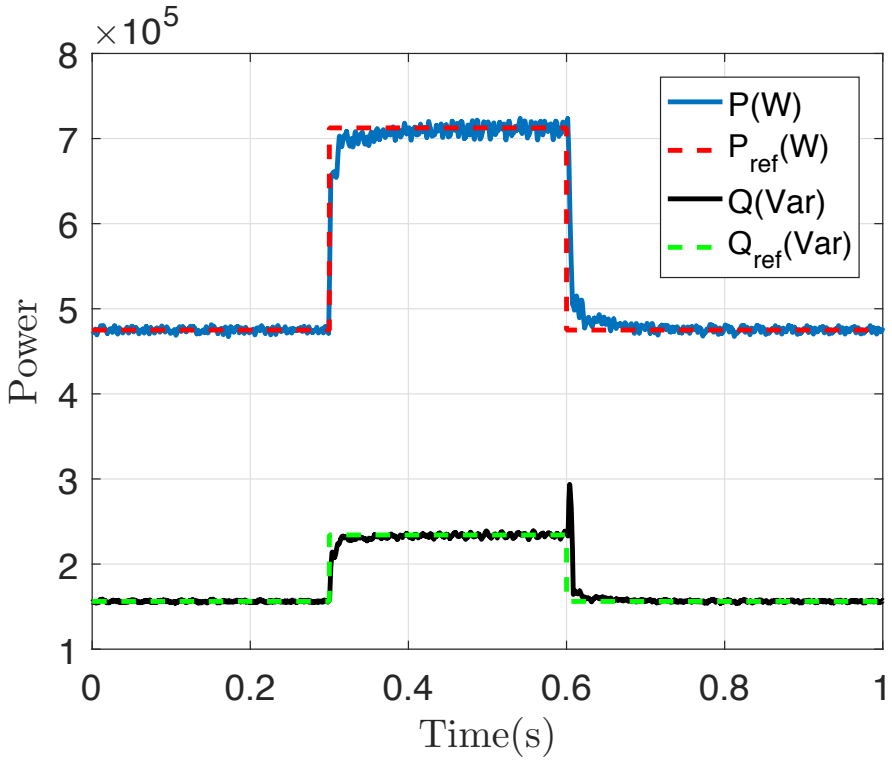


FIGURE 4.15: The power produced by the renewable energy system in the *IVSG* control case.

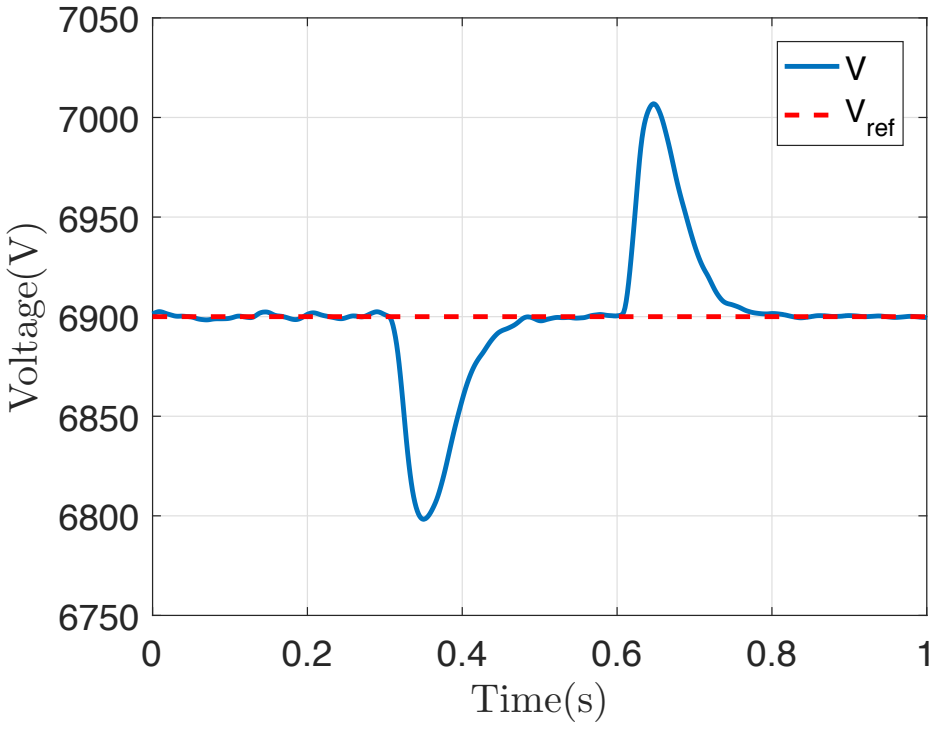


FIGURE 4.16: The variations of RMS value of the voltage in the *IVSG* control case.

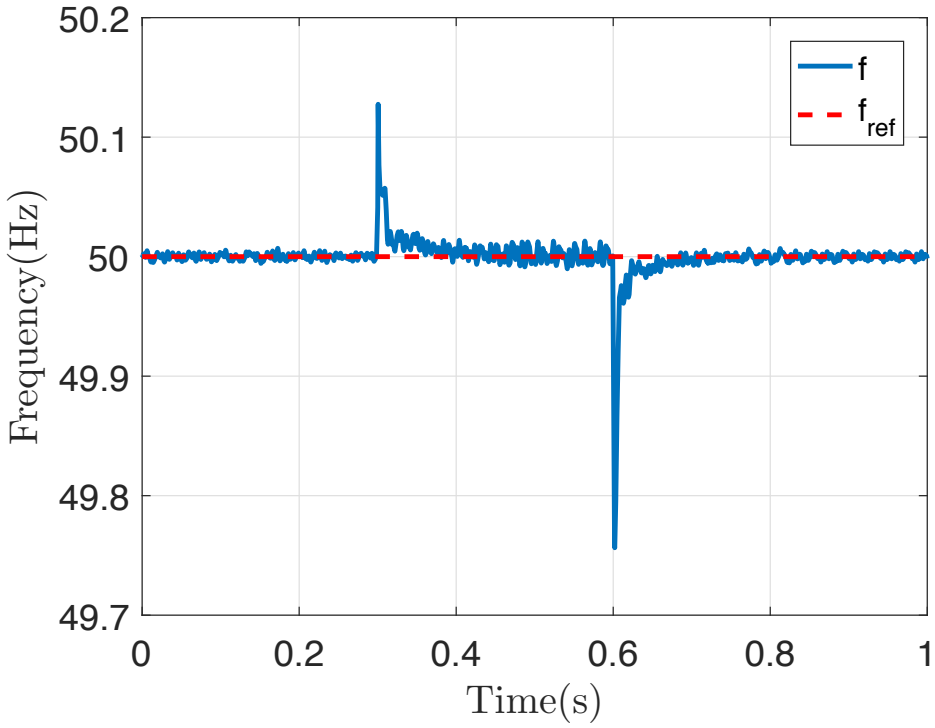


FIGURE 4.17: The frequency variations in the $IVSG$ control case.

## 4.3 Design and Analysis of Inverter Control Methods in a Multi-Source Case

In this part, two different renewable farm control strategies will be investigated in a stand-alone condition. The traditional droop control strategy is used for systems in stand-alone context and is based on the $V/f$ control strategy, where multiple $V/f$ controlled sources are linked together with a droop control strategy [154, 155]. The virtual synchronous generator ($VSG$) is used for systems in stand-alone context and is based on the $IVSG$ control strategy, where multiple $IVSG$ controlled sources are linked in a droop control strategy [156, 157]. However, the mater-slave control strategy ($M/S$) is a well known renewable farm control strategy based on the $P/Q$ inverter regulation, where multiple $P/Q$ controlled sources are considered as slave sources and connected to the powerful grid that is considered the master source [141–143]. Such regulation will be discarded, since the considered site is a stand-alone one, and no master source can be chosen.

Diagram 4.18 describes briefly a 2-sources system, where the control strategies are implemented in the control blocks of the diagram. Furthermore,

the considered elements in the system (Sources, DC buses, Inverters, Filters, and Grid) have the same properties and parameters as presented in the single inverter case (paragraph 4.2.1, table 4.1). As for regulators parameters, the values presented in table 4.2 are considered for all parameters except the droop related ones.

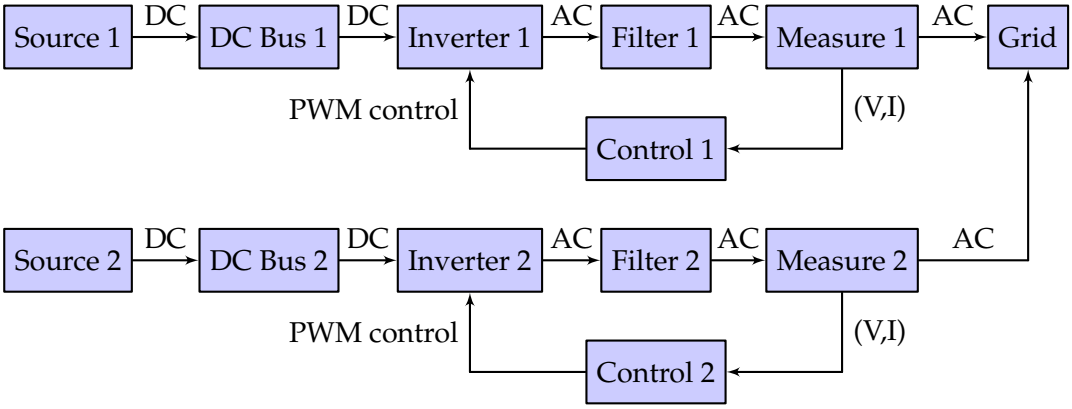


FIGURE 4.18: Control diagram of a multi-source system.

### 4.3.1 Traditional Droop Control Strategy

The traditional droop control strategy is used in a stand-alone context, where the regulation of the voltage and frequency is the main objective. This control strategy consists of multiple $V/f$ controlled inverters [154, 155]. In fact, the reference value of both the active and reactive power are compared to the feedback measured ones, and the difference is afterwards multiplied by the droop constant. The resulting values are added to the frequency and voltage references of the $V/f$ control strategy [158]. Figures 4.19 and 4.20 show the voltage and frequency droop control diagrams. Here it is important to discuss the role of the droop parameters, in fact the droop parameters not only rescale the error value and therefore affect the response time of the system; but in this case these parameters can help with the determination of the

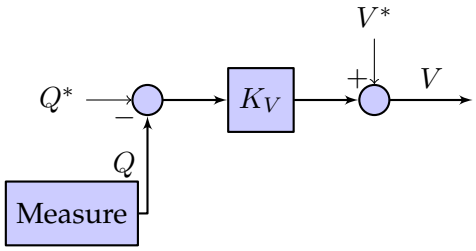


FIGURE 4.19: Control diagram of the voltage droop control.

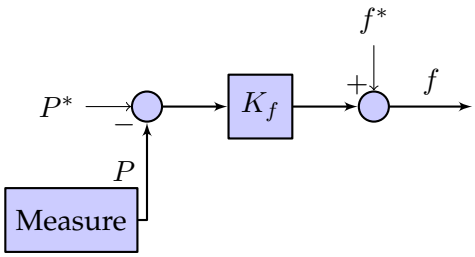


FIGURE 4.20: Control diagram of the frequency droop control.

dependency on the corresponding source. In other wards, the source with the higher droop parameter, will be reacting faster to the load and will be therefore insuring more stability to the grid.

### 4.3.2 VSG Control Strategy

The $VSG$ control strategy can be used in both stand-alone and grid-connected sites. In this control strategy, the inverter is controlled in the same way as a synchronous generator with a low inertia [156, 157]. Therefore, using this strategy, all four parameters can be regulated (active and reactive, voltage, and frequency). Furthermore, the $VSG$ control strategy is composed from multiple $IVSG$ control strategies.

### 4.3.3 Simulation Results

In order to evaluate the performance of the above-discussed strategies, a simulation of the system presented in control diagram 4.18 was conducted using Matlab/Simulink PowerSim toolbox. The system elements parameters will be considered the same as earlier presented in table 4.1, except the source power that will be changing from one case to another. As for the regulators parameters, the considered values are the same as those presented in table 4.2 for the following: The parameters of both voltage and current PI regulators for the $V/f$ control strategy used in the traditional droop case, the PI parameters of the excitation regulator used for the $IVSG$ control strategy in the $VSG$ case, and the different parameters of the $IVSG$ algorithm mechanical and electrical modules also used in the $VSG$ case. The droop parameter values of both traditional droop and $VSG$ control strategies will be changed. In fact, as explained earlier, the droop parameters can affect the grid stability, therefore each source will have its own droop value.

The three systems were simulated under the same conditions:

- Three sources are considered: a $750kW$ source, and a couple of $375kW$ sources.
- At initial state $t = 0$, a $1\ MVA$ total load is applied to the system with a power factor of $0.95$.
- At $t = 0.4s$, a step load of $50\%$ of the initial value is added and conserved till the end of the simulation.

For the traditional droop control strategy, figures 4.22, 4.23, and 4.24 show the load variations, the voltage RMS value, and the frequency, respectively. For the $VSG$ control strategy, figures 4.25, 4.26, and 4.27 show the power variation, the voltage RMS value, and the frequency, respectively. The simulation results clearly highlight the stability and convergence of both control strategies, even under harsh conditions where a $50\%$ load increase is considered. Therefore these control strategies can be included in more complex systems. For example, the full system considered at the end of chapter 3.

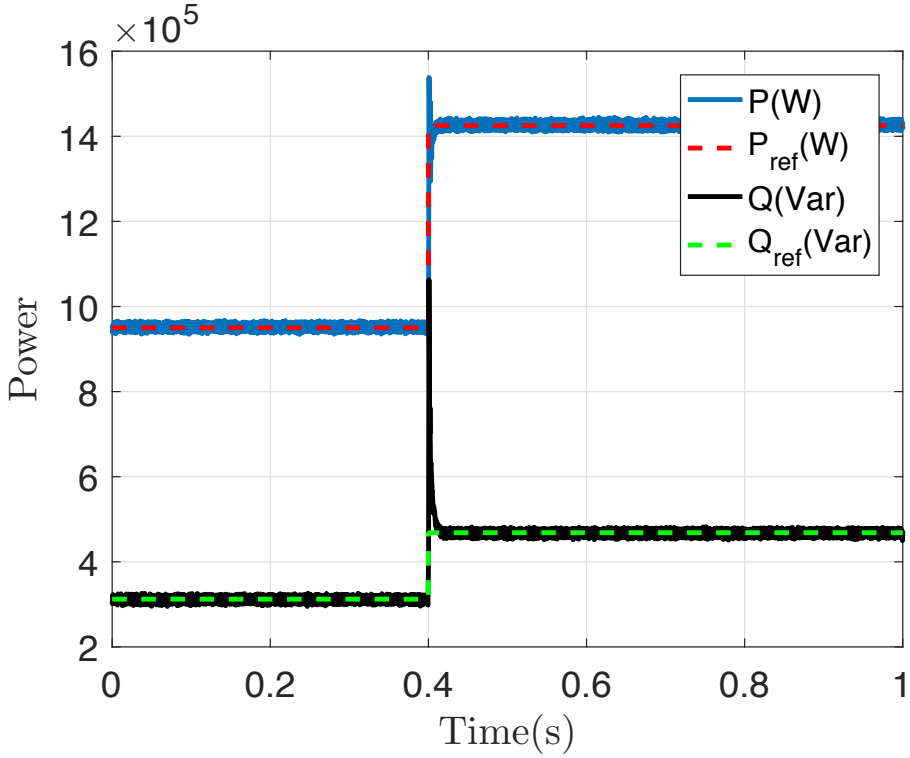


FIGURE 4.21: Power variations for the Master-Slave control case.

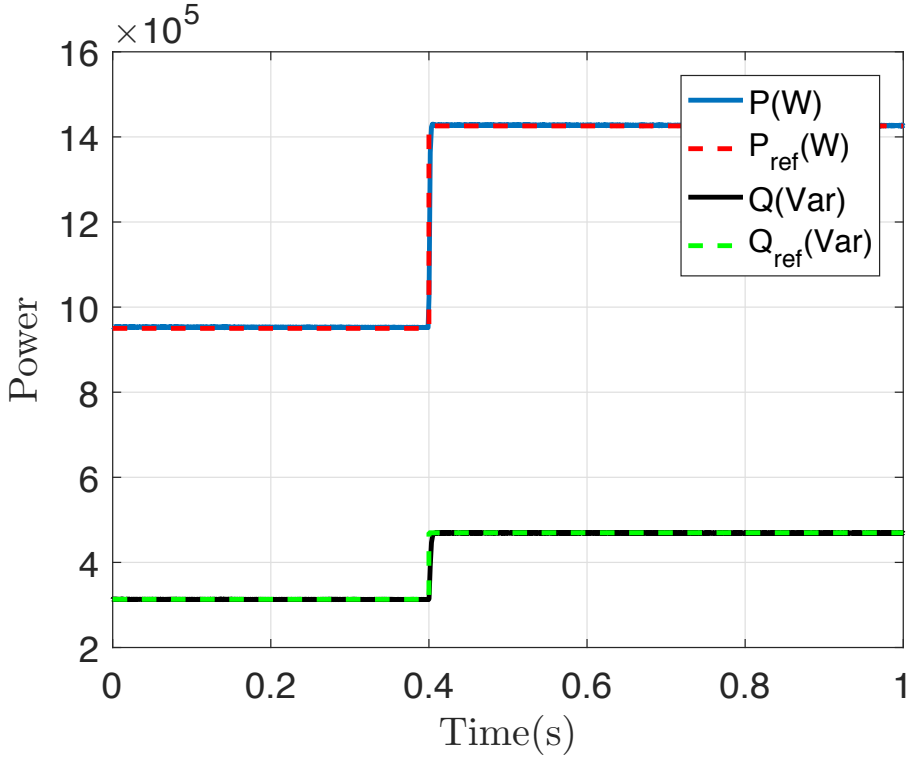


FIGURE 4.22: Power variations for the droop control case.

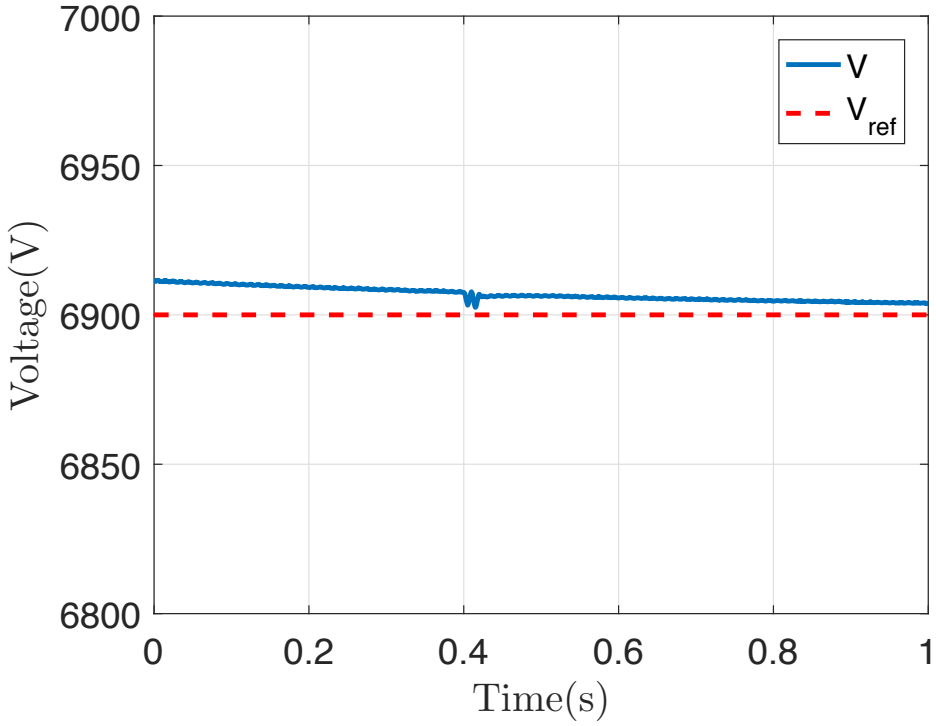


FIGURE 4.23: Voltage variations for the droop control case.

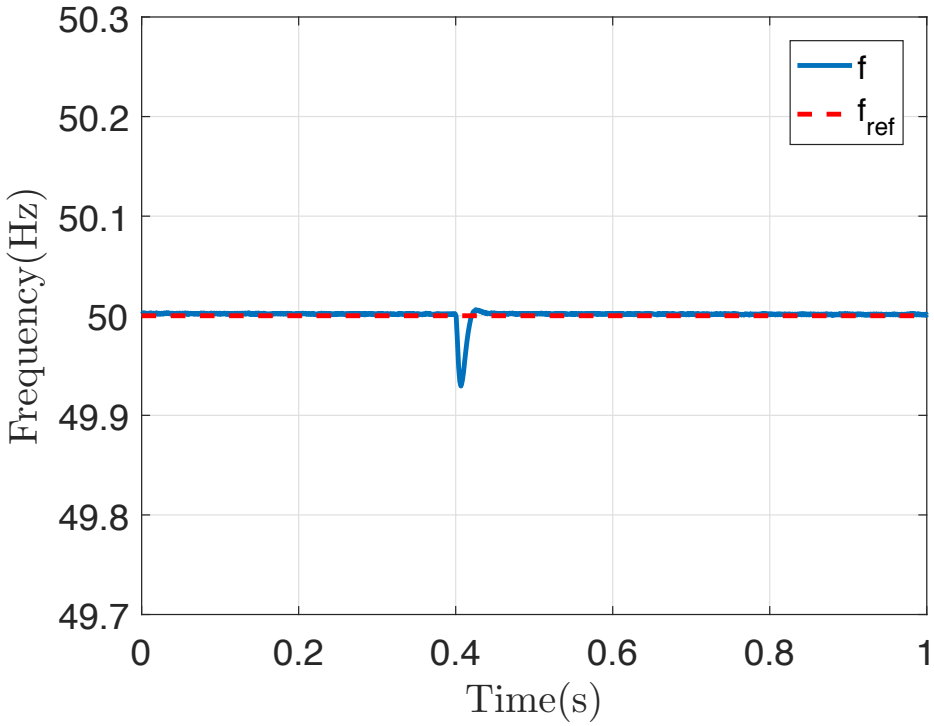


FIGURE 4.24: Frequency variations for the droop control case.

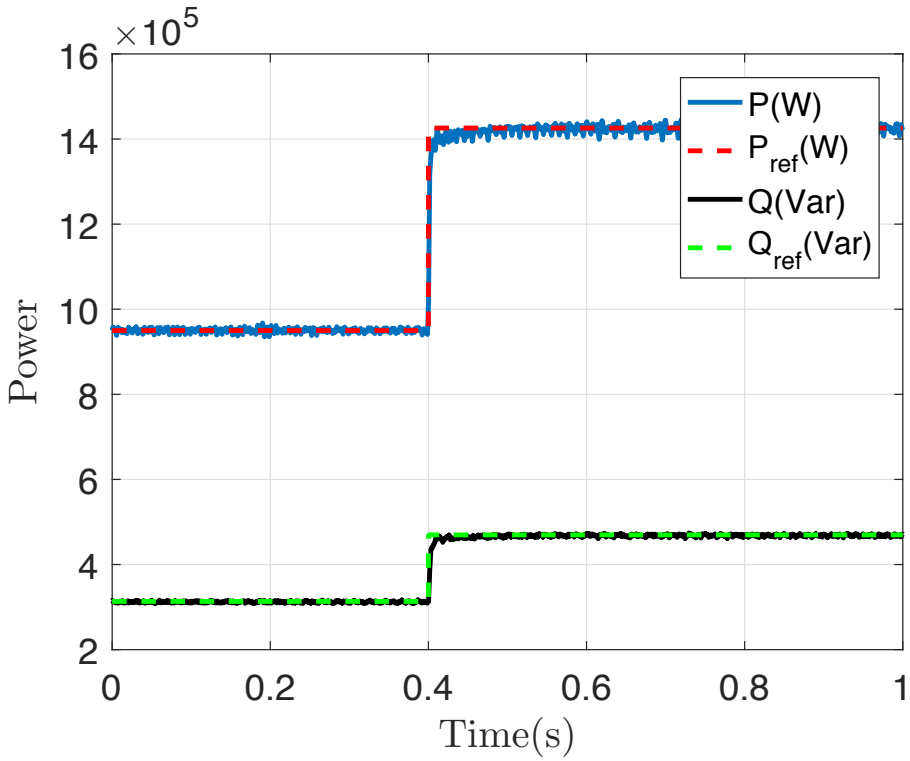


FIGURE 4.25: Power variations for the VSG control case.

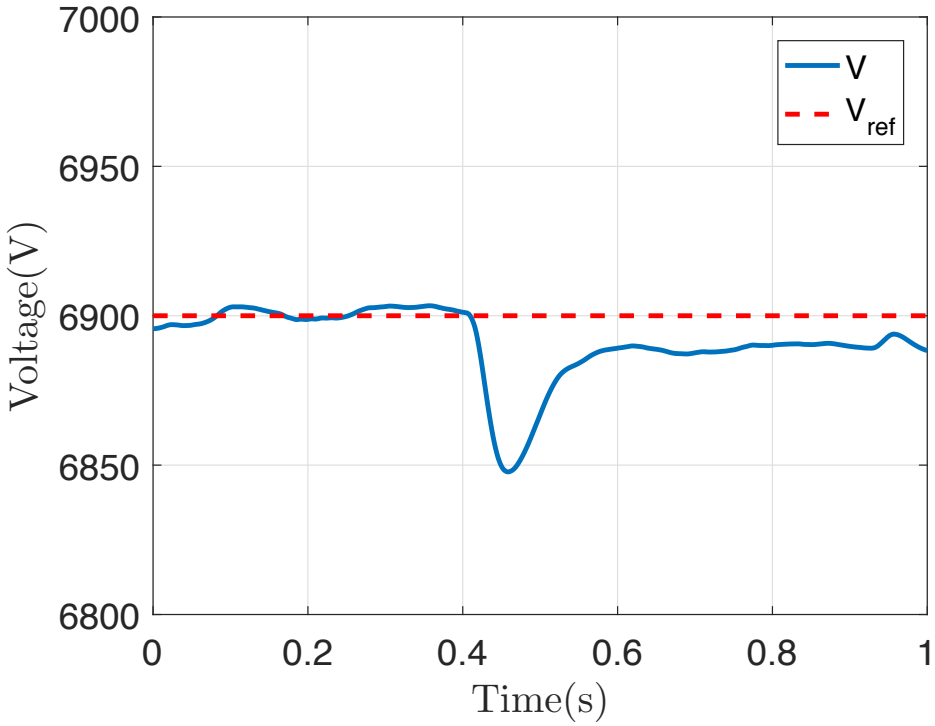


FIGURE 4.26: Voltage variations for the VSG control case.

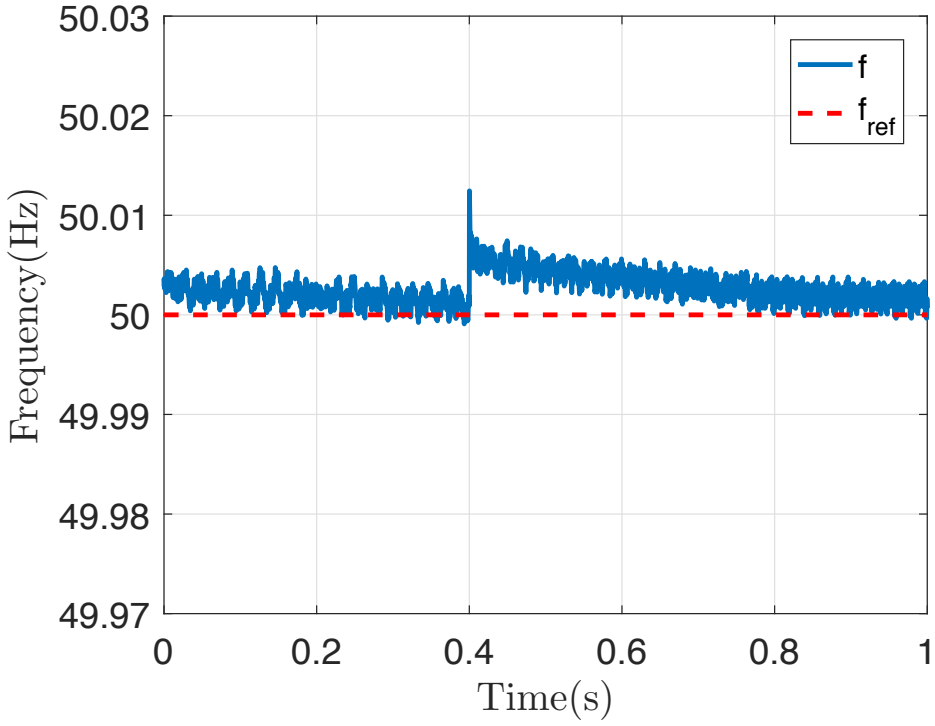


FIGURE 4.27: Frequency variations for the VSG control case.

### 4.3.4 Comparison and Discussion

The traditional droop simulation presented in Figure 4.22 shows an accurate and quick response to the power demand variation. In fact, the response of the system is of the first order with no ripples around the reference value and a response time of $0.002\ s$ for the active power and $0.004\ s$ for the reactive one. The voltage variations are illustrated in Figure 4.23. The results show a small voltage error of less then $0.1\ \%$ with a response time of $0.02\ s$. Finally, figure 4.24 illustrates the frequency variations of the system. The results show an error of $0.14\ \%$ and a response time of $0.04\ s$. These results clearly highlight a good system stability with a quick response time.

The $VSG$ simulation presented in Figure 4.25 show an accurate response to the power demand variation but slower than the traditional droop control. In fact, the system presents a response time of $0.02\ s$ for the active power and $0.03\ s$ for the reactive one. The voltage variations are illustrated in figure 4.26. The results show a voltage error of $0.73\ \%$ and a response time of $0.1\ s$. Finally, figure 4.27 illustrates the frequency variations of the system. The results show an error of $0.04\ \%$ and a response time of $0.1\ s$. These results present a high frequency stability of the system, with a lower voltage stability and a slower response time compared to the traditional droop control.

Table 4.3 summarize the achieved results for the traditional droop and $VSG$ strategies, which makes the comparison easier, where $T_{5\%}(s)$ is the response time for a $5\%$ accuracy. The dynamics of the systems that were detailed earlier, can be explained by the virtual inertia added by the $VSG$ strategy. Such a method can slow down the overall dynamics of the system but increases the stability. In fact, the results prove the proposed explanation since the inertia is added to the mechanical mode of the virtual generator, which is in turn

TABLE 4.3: Multi-source control strategies performances.

| | | Droop | VSG |
|---|---|---|---|
| Active power | $T_{5\%}(s)$ | 0.002 | 0.02 |
| | error(%) | - | - |
| Reactive power | $T_{5\%}(s)$ | 0.004 | 0.03 |
| | error(%) | - | - |
| Voltage | $T_{5\%}(s)$ | 0.02 | 0.1 |
| | error(%) | 0.1 | 0.73 |
| Frequency | $T_{5\%}(s)$ | 0.04 | 0.1 |
| | error(%) | 0.14 | 0.04 |

associated to the frequency. Therefore the $VSG$ control presents a higher frequency stability. For this reason, the $VSG$ control strategy will be used in the next part of this study.

## 4.4 Application to the Renewable Sources-based System for Ouessant Island

### 4.4.1 Introduction

Using the different control strategies that were studied, built, and discussed earlier, and since a hybrid power supply system was already deployed in chapter 3, the next step is to apply the different regulations on the chosen system. The chosen hybrid system is depending on the results of the sizing in chapter 3. Therefore, the hybrid system will includes: two identical wind turbines of $1\ MW$ each, one tidal turbine of $0.5\ MW$, two pairs of identical diesel generators of $1.2\ MW$ for the first group and $1\ MW$ for the second group, one PHS of $40\ MWh$, and the load as described in the conclusion of chapter 3. A model of each element of the system must be built first. Therefore an in-depth study of each subsystem will be presented. Furthermore, knowing that the global system will be controlled using a fuzzy logic strategy [159–161], a link will be established between the different elements and the regulation strategies will be implemented accordingly.

Appendix A presents the detailed power exchange network of the considered hybrid system.

### 4.4.2 System Elements Description

Diagram 4.28 presents the elements of the system. First, a description of the system different elements will be carried out, so a simulation model can be derived.

#### Wind Turbine

Both wind turbines are considered identical to the model Nordic N-1000 presented in chapter 3 table 3.3. A VSG regulation will be applied to both wind

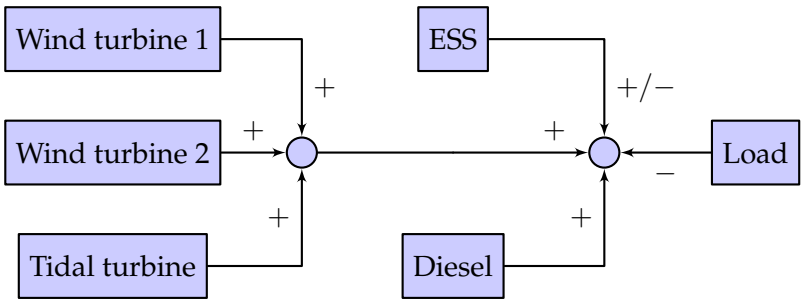


FIGURE 4.28: Considered hybrid system elements.

turbines grid side inverter. Therefore, the model already presented in paragraph 4.3.3. will be used (section 4.3.).

### Tidal Turbine

The considered tidal turbine is presented in chapter 2 (Table 2.2). A VSG regulation will be applied to the tidal turbine grid side inverter as well. Therefore, the model already presented in paragraph 4.3.3. will be used (section 4.3.).

### Load

The load is simulated using the block "Three-Phase Dynamic Load" of Matlab, which is already defined in the "Simscape Power Systems" library of "Matlab/Simulink". In fact, this block simulates a three phased balanced load, with a time depending user defined active/reactive power functions.

### Diesel System

The diesel system is composed of four diesel generators, two identical generators of $1.2\ MW$ and two others of $1\ MW$. In order to reduce the complexity of the system, a global diesel generator simulator was built, and the different models were represented by different parameters. Furthermore, the consumption of the diesel system is calculated in parallel to the simulator, using the practical curves presented in chapter 2 figure 2.17. As well, the inner control strategy of the diesel system follows the laws presented in chapter 2 table 2.3.

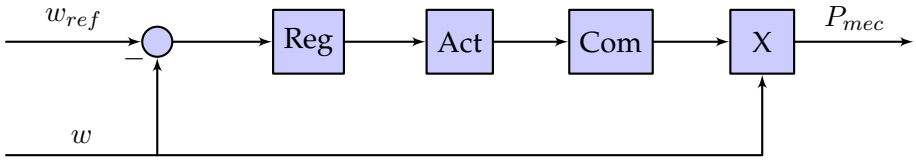


FIGURE 4.29: Diesel engine governor block diagram.

The diesel generator simulator is divided into three subsystems: a diesel engine governor, an excitation regulator, and a synchronous generator. The diesel engine governor is formed of a speed control system presented by a second order regulator. The regulator is followed by an actuator formed of a gain, two first order equations, and an integrator. The combustion is represented with a pure time delay [162–164] (Fig.4.29).

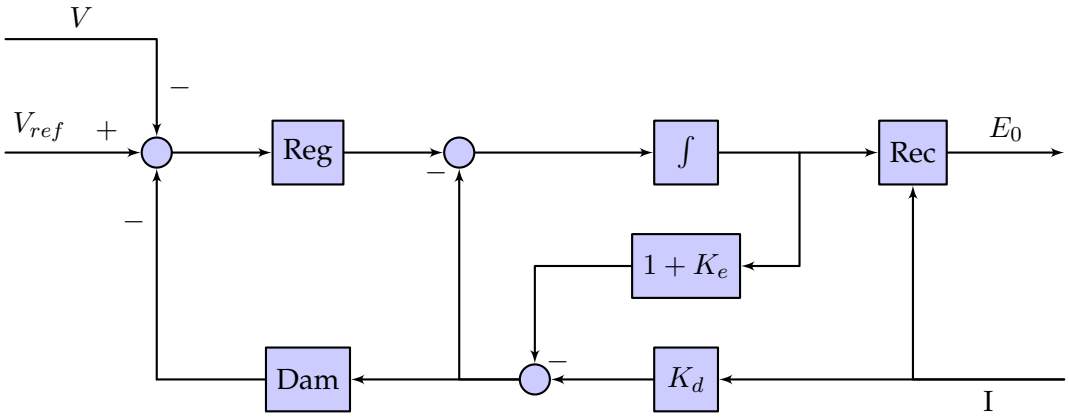


FIGURE 4.30: Excitation regulator block diagram.

The considered excitation regulator is an IEEE-AC1A standard. The excitation regulator aims for maintaining the voltage of the diesel generator. In fact, it contains a first order voltage regulator. The corrected signal passes throw a rectifier, to form the excitation voltage of the generator. To improve the dynamics of the excitation regulator, a damping feedback is added. The block diagram in figure 4.30 illustrates the different components of the excitation regulator [165–167].

A three-phase round-rotor synchronous machine was considered. Such model is already defined in the "Simscape Power Systems" library of "Matlab/Simulink". the electrical model of the machine is presented in figure 4.31.

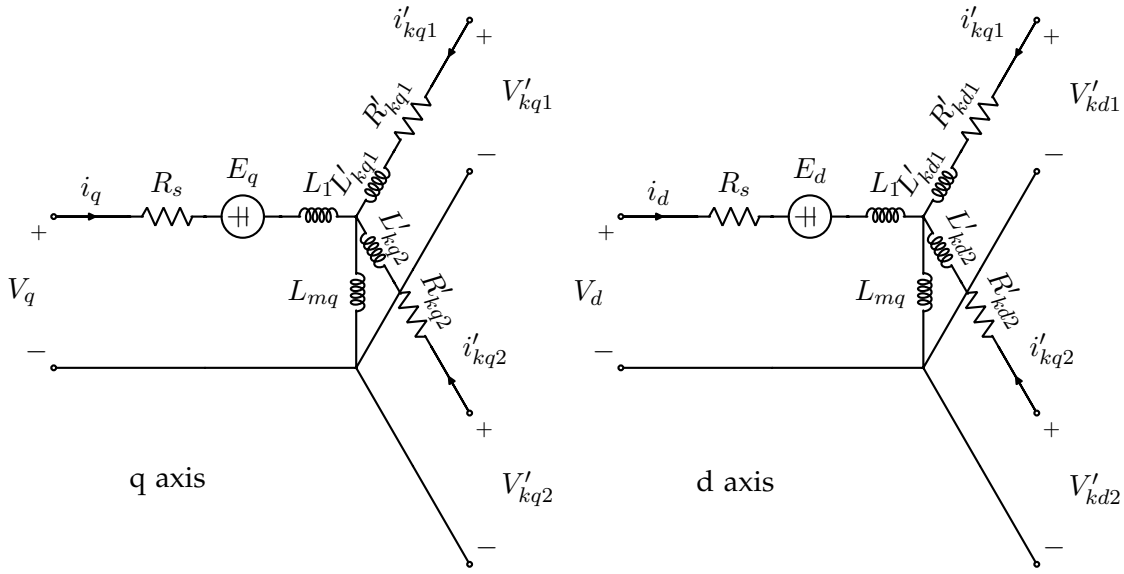


FIGURE 4.31: Synchronous generator electrical model.

**PHS**

The PHS is composed of three essential parts: a hydraulic turbine, a pump, and a reservoir. Each of theses elements will be discussed for a simulator building.

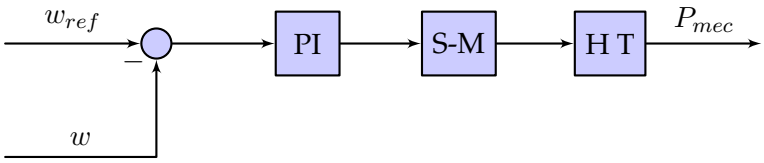


FIGURE 4.32: Hydraulic turbine block diagram.

The hydraulic turbine is responsible of the energy production in a PHS. It presents a mechanical system, an electrical generator, and an excitation system. The electrical generator and the excitation system are the same as already presented previously in the case of a diesel generator. The mechanical system is responsible of regulating the rotational speed of the electrical generator. It is composed of a PI regulator, a servo-motor, and a hydraulic turbine as shown in the block diagram 4.32 [168]. Where the servo-motor is represented with a first order transfer function, followed by an integrator and a feedback (with a saturation for the speed limit) as shown in the block diagram 4.33 [169–171].

Finally, the hydraulic turbine considered in this work, is a turbine with a pen stock, unrestricted head and tail, and with either very large or no surge

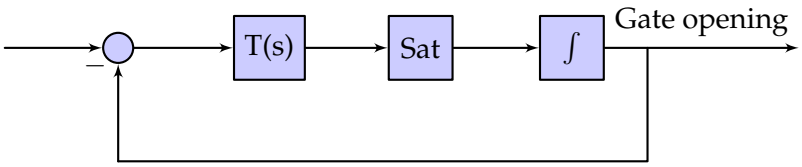


FIGURE 4.33: Servo-motor block diagram.

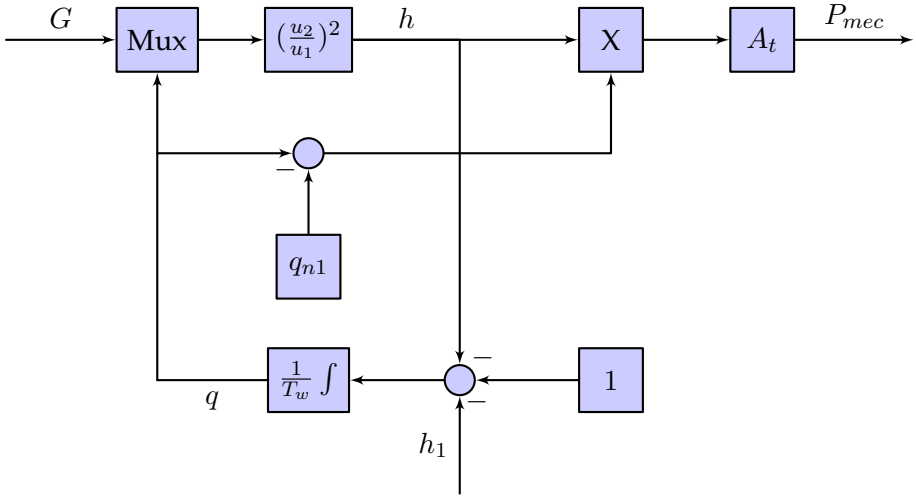


FIGURE 4.34: Hydraulic turbine mechanical block diagram.

tank [168, 171]. Such turbine presents highly nonlinear dynamics:

$$\frac{dq}{dt} = \frac{1-h-h_1}{T_w} \tag{4.13}$$

$$h = \frac{q^2}{G^2} \tag{4.14}$$

where $q$ is the flow in the conduit, $h$ is the head of the turbine, $h_1$ is the head losses, $G$ is the gate opening, and $T_w$ is the water time constant. The friction losses in the pen stock are neglected, therefore the mechanical power of the turbine can be expressed as:

$$\begin{aligned} P_{mec} &= T_m\omega = A_t h(q-q_{n1}) \\ &= A_t\frac{q^3}{G^2} \end{aligned} \tag{4.15}$$

where $A_t$ is a constant proportionality factor (calculated using the turbine and the electrical generator power ratings) and $q_{n1}$ is the per-unit no load flow. The block diagram 4.34 illustrate the dynamics of the hydraulic turbine.

The pump and the reservoir of the PHS are represented in a reduced and highly simplified manner, view their limited effect on the energy production

and the electrical signal. Therefore, the reservoir is represented by an integrator and a saturation and the pump is represented by a dynamic load.

### 4.4.3 Simulation Results and System Performances Analysis

In the following, a simulation of the full system is proposed. However, a detailed system of such complexity can not be simulated for a long period of time. Therefore only two critical scenarios will be investigated:

- The first scenario concentrates on the steady-state of the system. In fact, a large load variation will be applied to the system (between $1.5$ $MW$ and $3.5$ $MW$). Such load variation is not possible in a matter of seconds, therefore the transient state will be discarded, and studied in the second case. Finally, this scenario will be tested for high, medium, and low SOC.
- The second scenario considers a step load variation of $0.5$ $MW$. Such variation is considered as a harsh dynamics, but still possible. Therefore it can be considered as a critical test for the dynamics of the system. This scenario will be tested in two cases. In the first case a high SOC will be considered so that the combination of renewables and ESS can be tested. In the second case a low SOC will be considered so that the combination to renewables and diesel generator can be tested.

#### Steady-State Analysis

In this part, a load variation between $1.5$ $MW$ and $3.5$ $MW$ will be simulated. The renewable power potential production will be considered constant and equal to $2.5$ $MW$. Therefore the system will switch from a positive $P_{renewables} - P_{load}$ to a negative $P_{renewables} - P_{load}$, and reacts differently depending on the SOC of the ESS. Three cases will be considered: a SOC of $100\%$, a SOC of $50\%$, and a SOC of $0\%$.

- For a SOC of $100\%$, figures 4.35, 4.36, and 4.37 illustrate the power of the different elements of the system, the grid voltage and frequency respectively.

  The results clearly show that the system presents stable steady-state phase, from voltage and frequency perspectives, and the power reaction of the system follows the power references, since in this case the

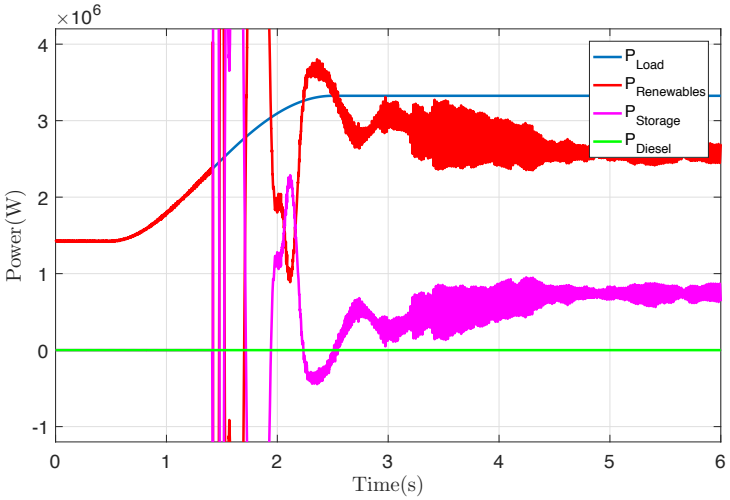


FIGURE 4.35: Power variations for the full system steady-state test, with a SOC of 100%.

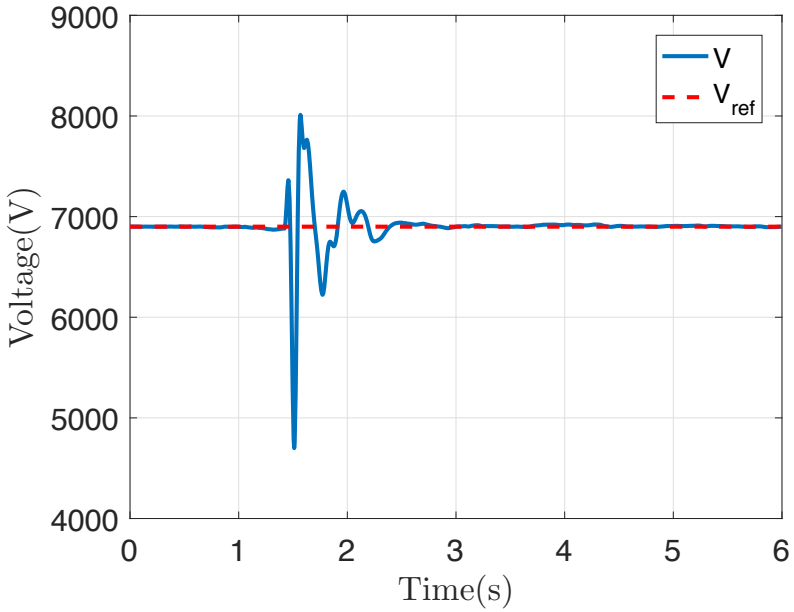


FIGURE 4.36: Voltage variations for the full system steady-state test, with a SOC of 100%.

ESS is full, therefore the diesel will be kept turned off and the ESS will react when a power deficit is present. Furthermore, figure 4.35 presents more details concerning the power exchange in the system. First, the power limitations on the renewable energy production in the first 1.5 $s$ of the simulation is very clear. Second, the renewable energy system presents a faster reaction compared to the ESS, which is explained by the inverter dynamics. Then after few seconds, the ESS stabilize at its reference value, as well as the renewable energy system.

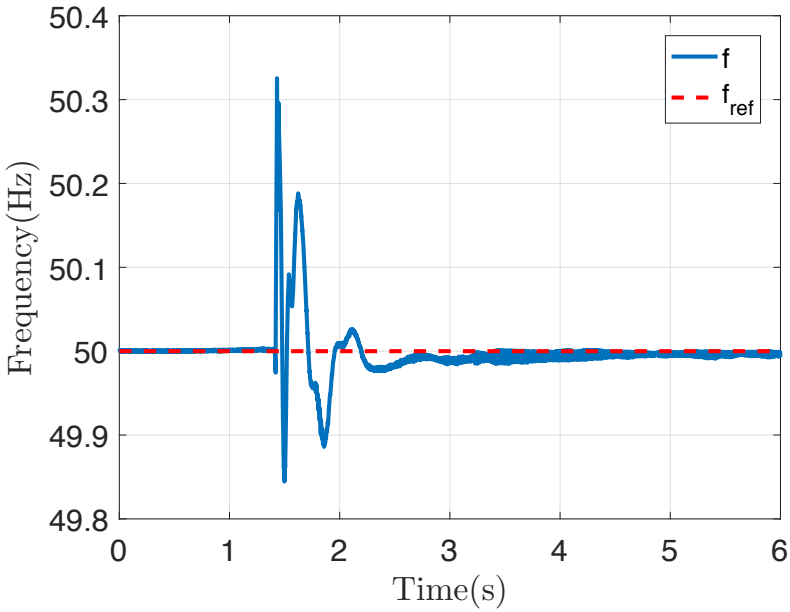


FIGURE 4.37: Frequency variations for the full system steady-state test, with a SOC of 100%.

- For a SOC of 50%, figures 4.38, 4.39, and 4.40 illustrate the power of the different elements of the system, the grid voltage and frequency respectively.

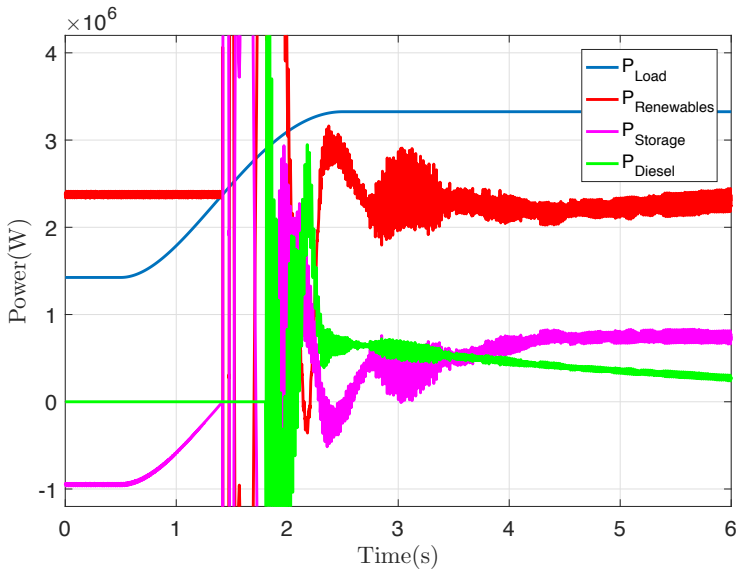


FIGURE 4.38: Power variations for the full system steady-state test, with a SOC of 50%.

The results clearly show that the system presents stable steady-state phase, from voltage and frequency perspectives, and the power reaction of the system follows the power references, since in this case the

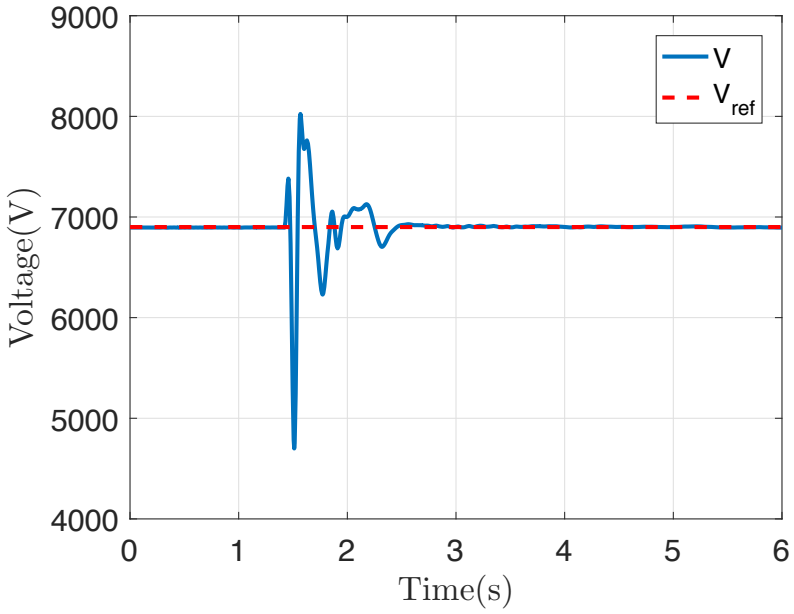


FIGURE 4.39: Voltage variations for the full system steady-state test, with a SOC of 50%.

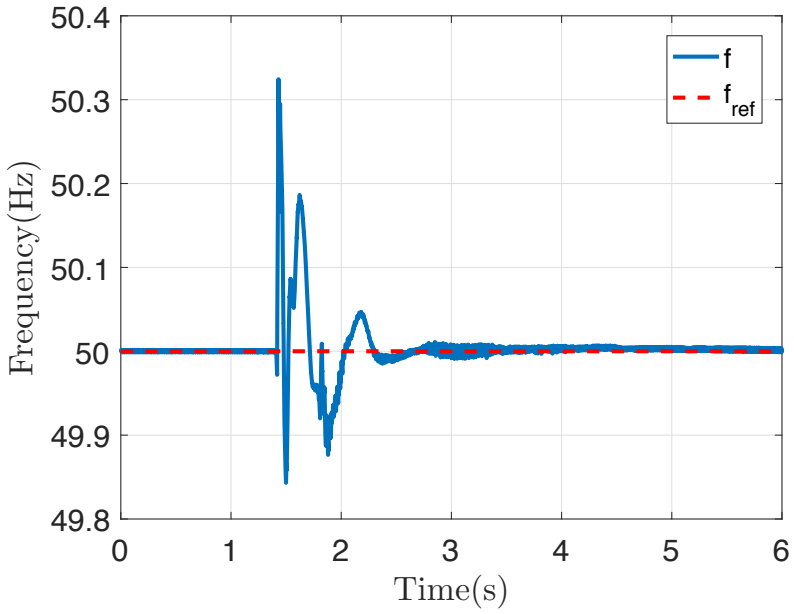


FIGURE 4.40: Frequency variations for the full system steady-state test, with a SOC of 50%.

ESS is half-full, therefore both the diesel and the ESS will react when a power deficit is present. Furthermore, figure 4.38 presents more details concerning the power exchange in the system. In fact, in the first $1.5\ s$ of the simulation the ESS is charging, since the storage power is negative. In this case, the renewable sources stay around their reference value,

and the exchange between the diesel and the storage systems will occur, where the diesel presents faster dynamics compared to the ESS, so the ESS power will increase slowly and the diesel power will decrease till reaching their corresponding reference values.

- For a SOC of $0\%$, figures 4.41, 4.42, and 4.43 illustrate the power of the different elements of the system, the grid voltage and frequency, respectively.

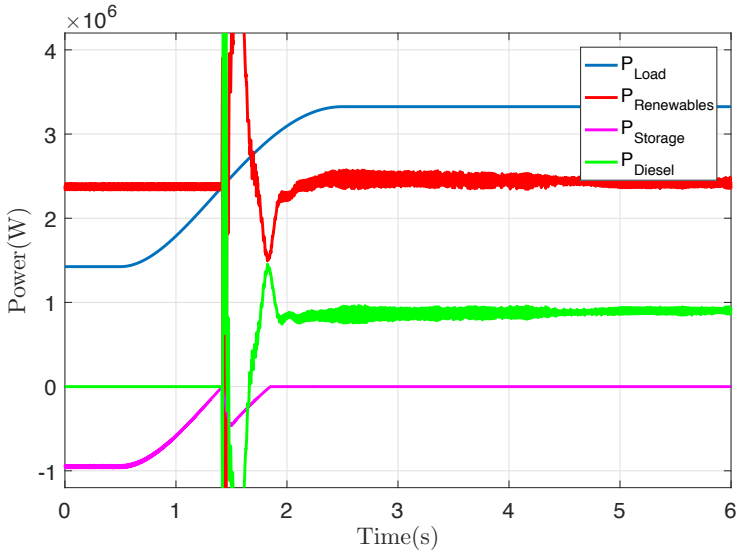


FIGURE 4.41: Power variations for the full system steady-state test, with a SOC of $0\%$.

The results clearly show that the system presents stable steady-state phase, from voltage and frequency perspectives, and the power reaction of the system follows the power references, since in this case the ESS is empty, therefore the ESS will charge and the diesel system will react when a power deficit is present. Furthermore, figure 4.41 presents more details concerning the power exchange in the system. In fact, in the first $1.5\ s$ of the simulation the ESS is charging, since the storage power is negative. Second, this case presents a power exchange between the renewable sources and the diesel system. In this case, the renewable sources stay around their maximal possible value, since the diesel system reaction time is relatively fast.

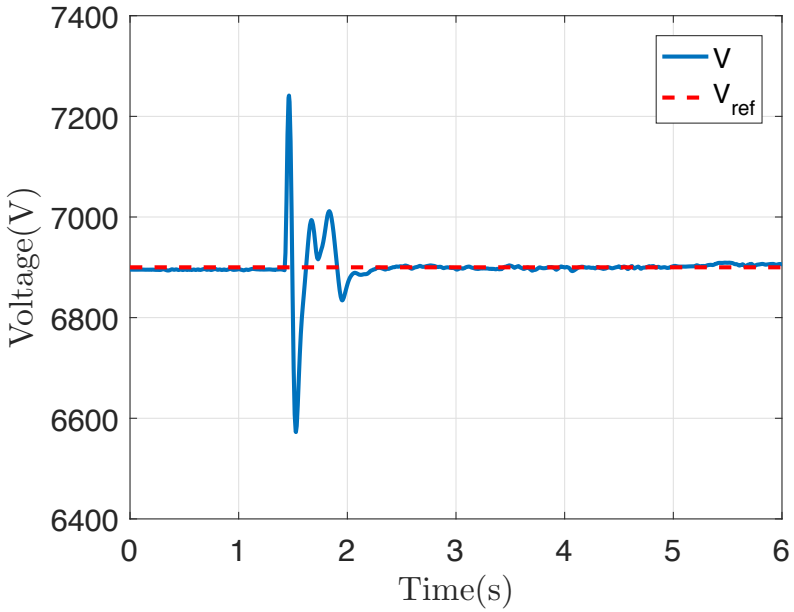


FIGURE 4.42: Voltage variations for the full system steady-state test, with a SOC of $0\%$.

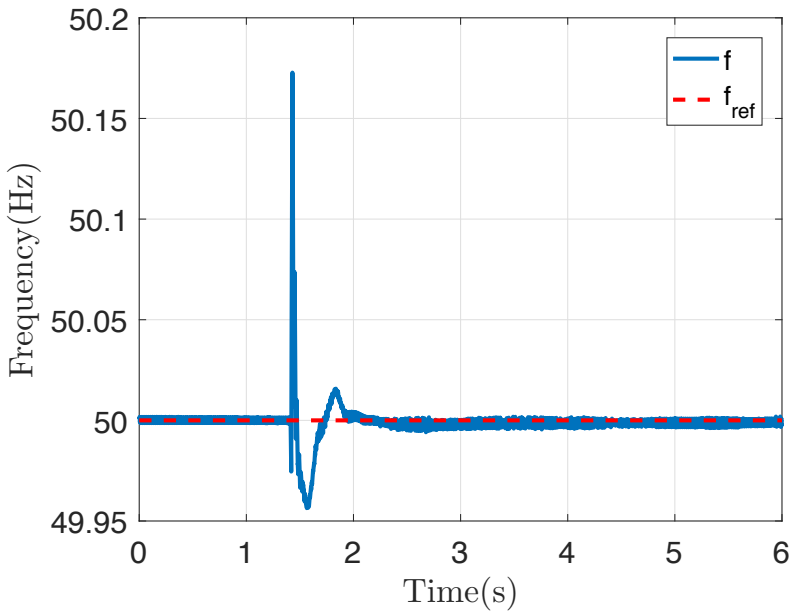


FIGURE 4.43: Frequency variations for the full system steady-state test, with a SOC of $0\%$.

**Transient-State Analysis**

In this part, a step load variation between $3\ MW$ and $3.5\ MW$ will be simulated. The renewable power production will be considered constant and corresponds to $2.5\ MW$. Furthermore, since the renewable power production is

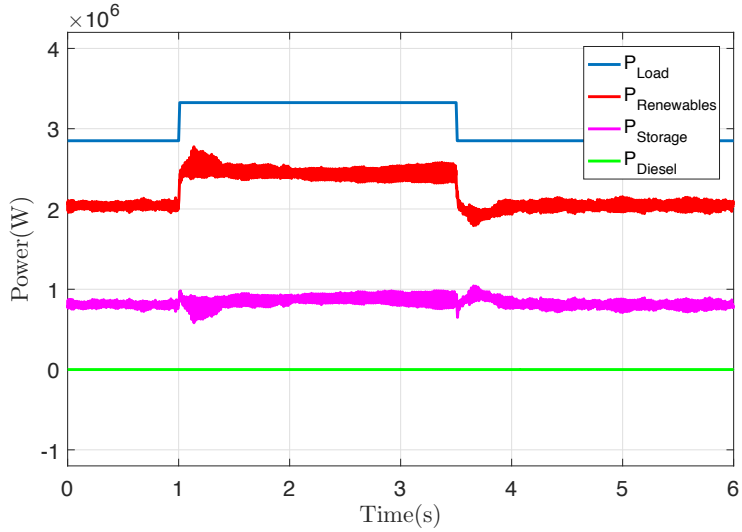


FIGURE 4.44: Power variations for the full system transient state test, with a SOC of 100%.

lower than the load, the system will use different configurations depending on the SOC. Therefore, two cases will be considered: a SOC of 100% and a SOC of 0%.

- For a SOC of 100%, figures 4.44, 4.45, and 4.46 illustrate the power of the different elements of the system, the grid voltage and frequency respectively.

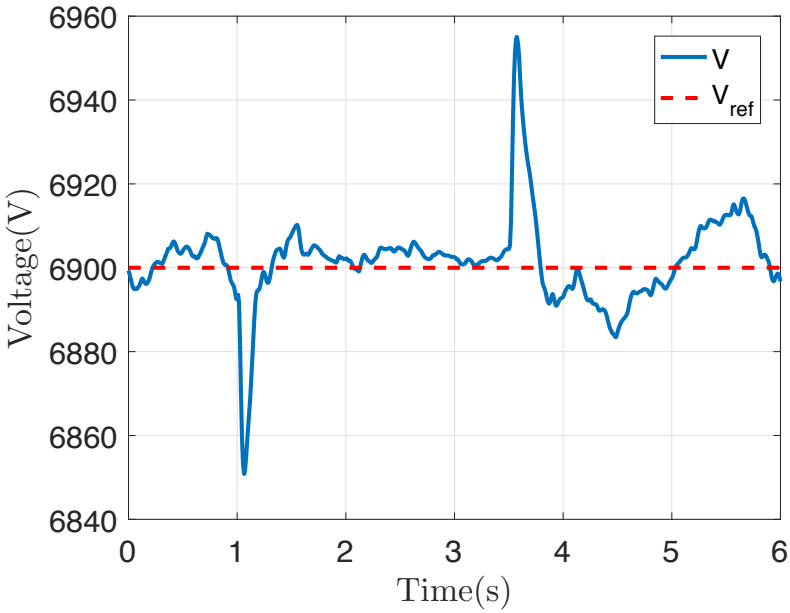


FIGURE 4.45: Voltage variations for the full system transient state test, with a SOC of 100%.

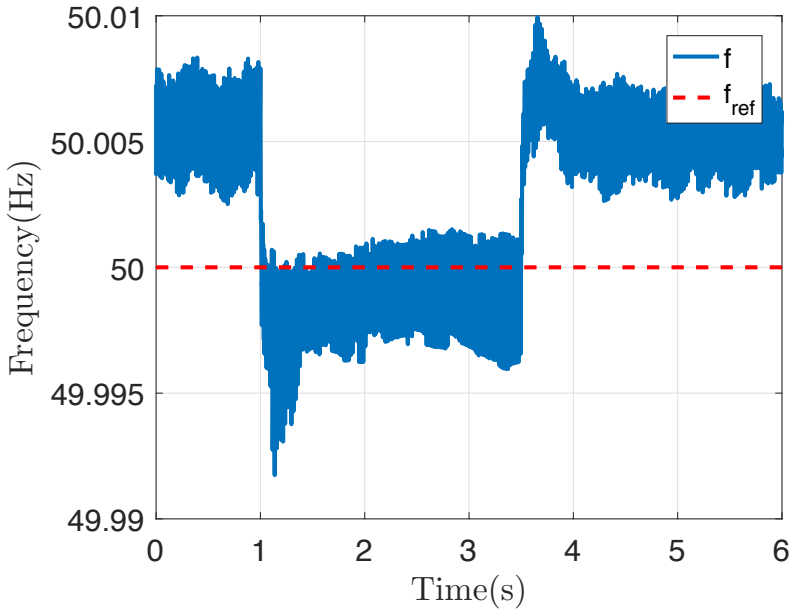


FIGURE 4.46: Frequency variations for the full system transient state test, with a SOC of 100%.

In fact, with a 100% SOC, the diesel will be turned off, and the system will present a renewable/storage state. The results present a high stability. First, the figure 4.46 shows frequency variation margin smaller then 0.1%. As for the voltage, figure 4.45 shows a voltage variation margin around 1%. Such variations are largely acceptable, and illustrates a high system stability, even under severe variation of the load.

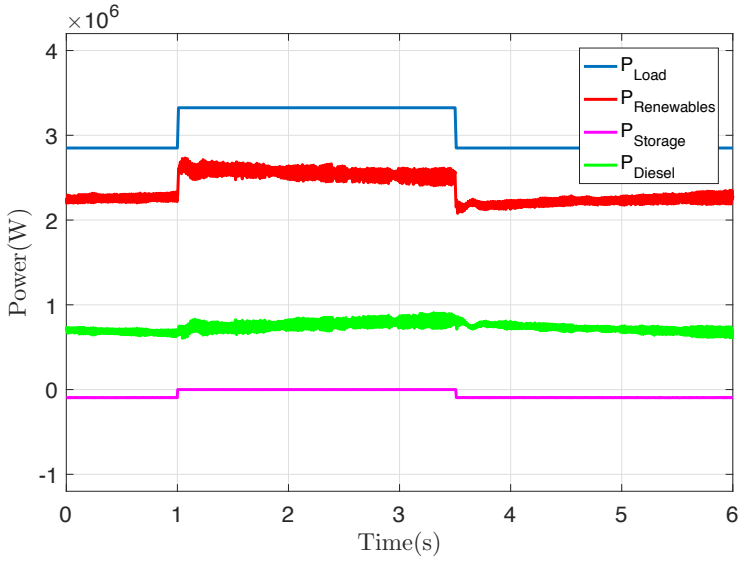


FIGURE 4.47: Power variations for the full system transient state test, with a SOC of 0%.

- For a SOC of 0%, figures 4.47, 4.48, and 4.49 illustrate the power of the different elements of the system, the grid voltage and frequency respectively.

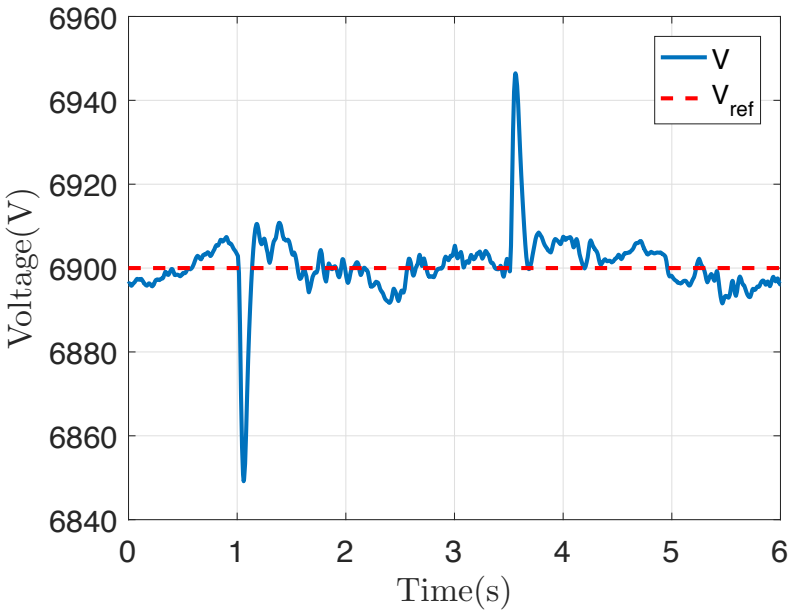


FIGURE 4.48: Voltage variations for the full system transient state test, with a SOC of 0%.

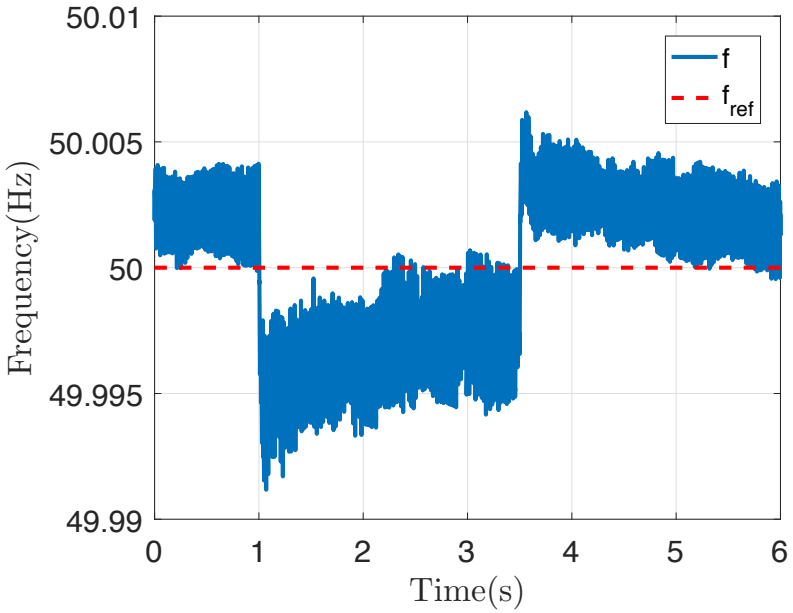


FIGURE 4.49: Frequency variations for the full system transient state test, with a SOC of 0%.

In fact, with a $0\%$ SOC, the ESS generator will be turned off (the ESS will only charge), and the system will present a renewable/diesel state. The results present a high stability. Furthermore, and similar to the renewable/storage state presented earlier, figure 4.49 shows frequency variation margin smaller then $0.1\%$. As for the voltage, figure 4.48 shows a voltage variation margin around $1\%$. Such variations are largely acceptable, and illustrates a high system stability, even under harsh conditions.

## 4.5 Conclusion

In this chapter, multiple hybrid energy production system control strategies were evaluated. In the first part, three inverter control strategies were developed and tested. The $P/Q$ control strategy aims to regulate the power production of the system, where the $V/f$ control strategy regulates the signal voltage and frequency. The $IVSG$ control strategy present the capability to combine the regulation of the power production as well as the signal voltage and frequency.

In the second part, two renewable energy system control strategy were developed and compared for basic cases including several renewable sources production. The traditional droop control strategy has the advantage of a non-privileged master source. In fact all sources help in maintaining the grid power balance. This regulation strategy presents fast dynamics and a high voltage stability. Finally, the $VSG$ control strategy, which is based on the $IVSG$ regulation, presents a high frequency stability, but slower dynamics compared to the traditional droop control.

In the final part, a full hybrid system was simulated using the $VSG$ control strategy. This system combined two wind turbines of $1\ MW$ each, one tidal turbine of $0.5\ MW$, four diesel generators (two of $1.2\ MW$ and two of $1\ MW$), and a PHS with a capacity of $40\ MWh$. The achieved simulation results have clearly highlight the high stability of the hybrid system from power generation, voltage, and frequency perspectives.

# Conclusion and Perspectives

This PhD thesis has focused on some important challenges that renewables-based hybrid power supply systems will face in the near future, when applied in stand-alone sites. First, up-to-date information on renewable energy technologies and energy storage systems technologies were presented. These technologies were compared and scaled depending on their maturity, farm projects, and applicability on the chosen islanded site. Three main sources were therefore chosen: solar, wind, and tidal energies. Several ESS technologies were also described, where a pumped hydroelectric storage system was chosen as a possible ESS. Afterwards, a state of the art concerning offshore energy transmission and renewable energy systems regulation was presented. Furthermore, and considering the site characteristics, a MVAC transmission method was chosen for the offshore elements. Such method is suitable for the power level and the distance of the system elements from the shore. As for the renewable energy system regulation, two main regulation method families were identified: vector control-based and observer-based methods.

In the second chapter, a study of the chosen site (Ouessant island) characteristics is presented. The three mature renewable energy sources already discussed in the first chapter were considered to supply this stand-alone site. From these potential sources, the solar one was not considered view its low efficiency on the island compared to the other renewable sources.

In the third chapter, a sizing method of the hybrid system elements was presented. The sizing was based on a rough optimization, where a power exchange network between the different elements was developed. The results show a clear advantage for the usage of such hybrid system. In fact, a well chosen hybrid system can reduce significantly the cost as well as the $CO_2$ emissions for the Ouessant island.

The fourth chapter is devoted to the regulation of the system. In a first part, three regulation methods of a single inverter connected to the grid were presented. The $P/Q$ control strategy is based on a vector control and focuses on

a power regulation of the system. The $V/f$ control strategy is based on a vector control strategy as well and aims to regulate the voltage and frequency of the electrical signal. The $IVSG$ control strategy is based on an observer regulation strategy and presents the advantage of regulating the power production of the system, as well as the voltage and the frequency. In the second part, a multi-source renewable energy production system is regulated using two control strategies. The traditional droop control strategy present faster dynamics and better voltage stability compared to the $VSG$, which presents a better frequency stability. This is why this last control solution seems interesting in the context of a stand-alone island. In a final part, a full hybrid system was simulated using the $VSG$ control strategy. The achieved simulation results have clearly highlighted a high voltage and frequency stability.

The perspectives following the above presented studies can be divided between energy management and hybrid system regulation aspects. Indeed, some perspectives can be highlighted for future studies. For the energy management:

- It is possible to include other renewable energy sources, even if they present low efficiency. For example, solar panels can present the advantage of a better production potential in seasons when the wind potential is low.
- The cost estimation studies can be improved by adding adding the cable costs (among others) and taking into consideration an interval of cost variation.

For the hybrid system regulation:

- Adding a synchronization for the different elements regulation, when they are to be connected to an already running system.
- It will be useful and interesting to validate the proposed approaches experimentally, in a low power system or even in a real islanded site. This will allow to improve and validate the proposed solutions and choices.

# A. Power Scheme of the Full System

| | |
|---|---|
| PMU | Power Management Unit |
| DGPM | Diesel Generators Power Manager |
| $DG_n$ | Diesel Generator ($n$) |
| $WT_n$ | Wind Turbine ($n$) |
| $TT_n$ | Tidal Turbine ($n$) |
| ESS | Energy Storage System |
| SOC | State Of Charge |
| $Vel_W$ | Wind velocity |
| $Vel_T$ | Tidal velocity |
| $P_l$ | Load |
| $cos(\varphi)$ | Power factor |
| $P_{WTn}$ | Wind turbine ($n$) power potential |
| $N_w$ | Number of wind turbines |
| $P_{TTn}$ | Tidal turbine ($n$) power potential |
| $N_t$ | Number of tidal turbines |
| $P_{RE}$ | Renewable energy total power potential ($P_{RE} = \sum_{n=1}^{N_w} P_{WT_n} + \sum_{n=1}^{N_t} P_{TT_n}$) |
| $P_{lim}$ | Renewable energy power potential limitation |
| $P_D$ | Diesel generators total power |
| $P_Dn$ | Diesel generator ($n$) power |
| $P_{ESS}$ | Energy storage system power |

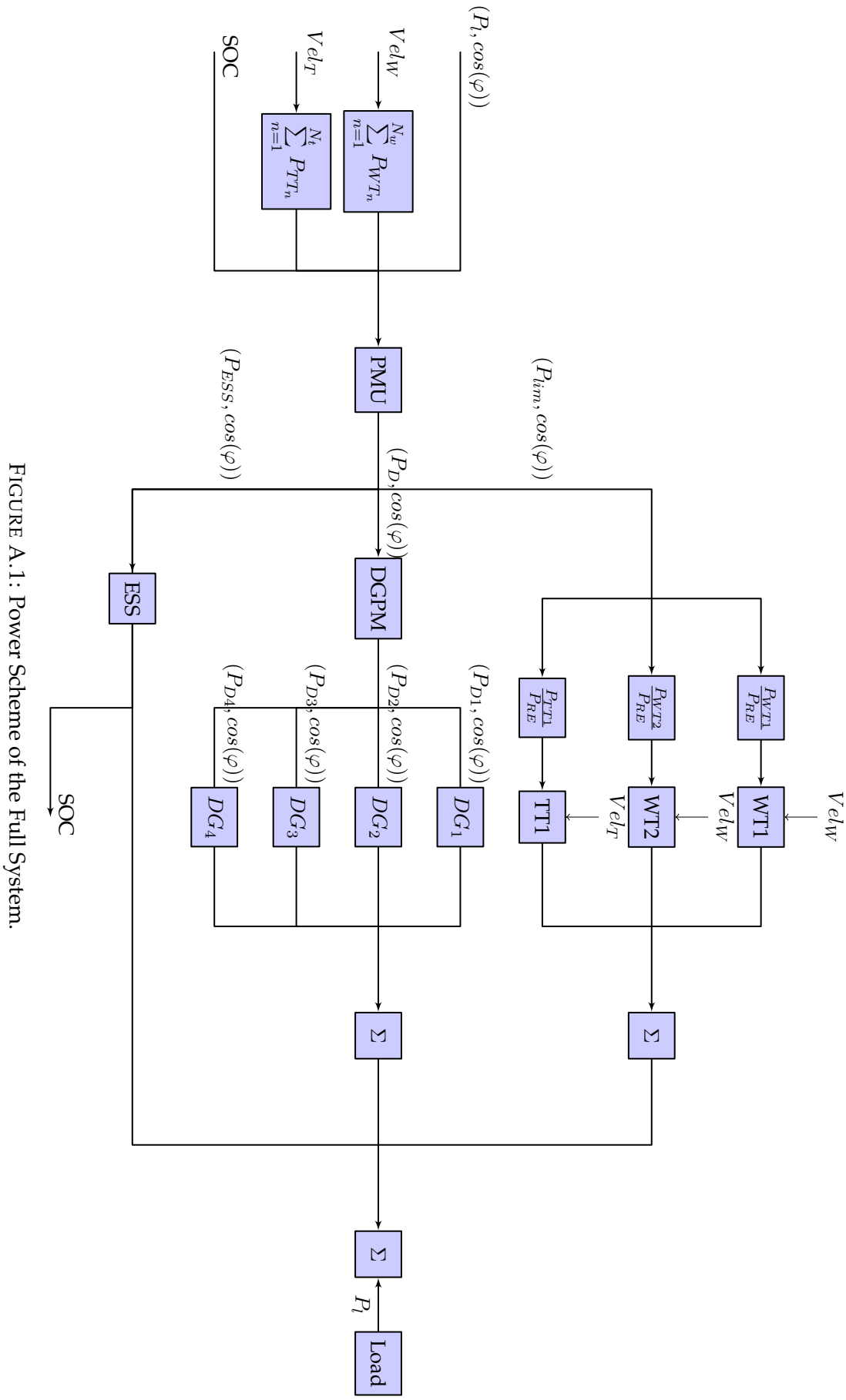


FIGURE A.1: Power Scheme of the Full System.

# B. IVSG Block Diagram

| | |
|---|---|
| Meas | Measurements |
| PWM | Pulse Width Modulated |
| PI | Proportional integral regulator |
| $K_f$ | Frequency droop parameter |
| $K_V$ | Voltage droop parameter |
| $J$ | Virtual inertia |
| $D$ | Virtual Damping |
| $Z$ | Virtual impedance |
| $\omega^*$ | Rotational speed reference value |
| $\omega$ | Virtual rotational speed |
| $f^*$ | Frequency reference value |
| $f$ | Signal frequency |
| $\Theta$ | virtual angular position |
| $\Phi$ | Three phased signal phasing difference |
| $U^*$ | Voltage reference value |
| $U$ | Voltage |
| $P^*$ | Reference active power |
| $P$ | Active power |
| $Q^*$ | Reference reactive power |
| $Q$ | Reactive power |

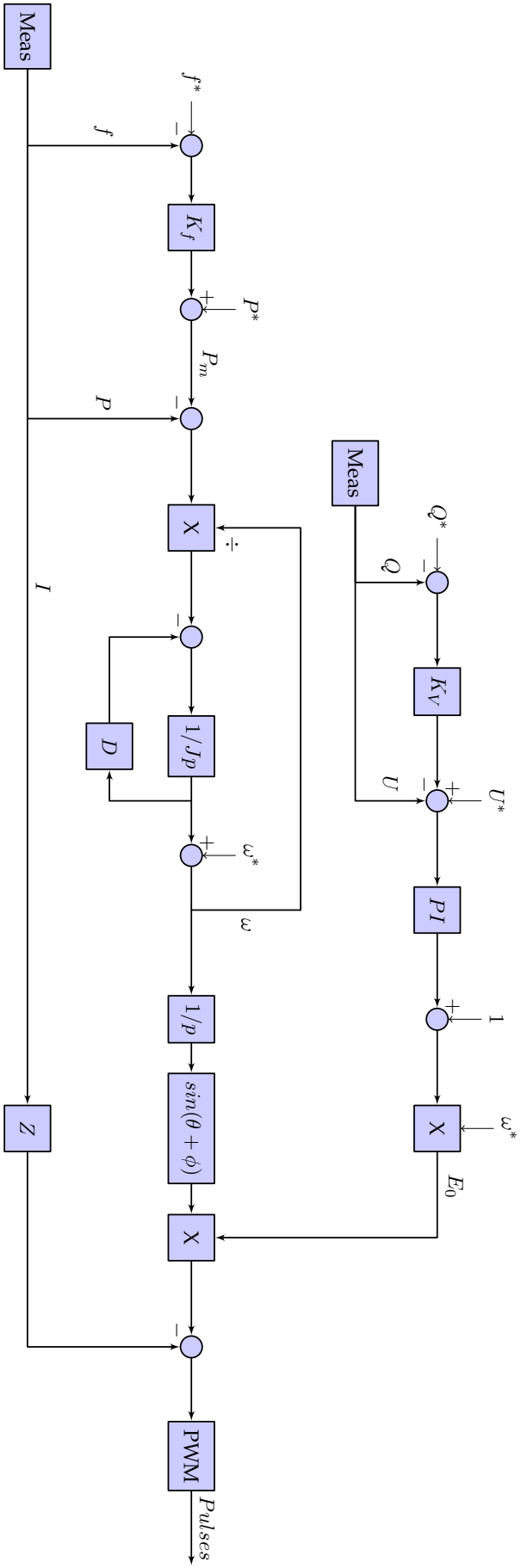


FIGURE B.1: *IVSG* block diagram.

# References


[1] R. V. V. Petrescu, R. Aversa, A. Aonio, and F. I. T. Petrescu, "Green energy to protecting the environment/energia verde para proteger o meio ambiente," *Revista GEINTEC-Gestão, Inovação e Tecnologias*, vol. 7, no. 1, pp. 3722–3743, 2017.

[2] S. Butterfield, W. Musial, J. Jonkman, and P. Sclavounos, "Engineering challenges for floating offshore wind turbines," tech. rep., National Renewable Energy Laboratory (NREL), Golden, CO., 2007.

[3] J. Zhang, *Optimization design and control strategies of a double stator permanent magnet generator for tidal current energy application*. PhD thesis, Ecole Polytechnique de l'Université de Nantes, Laboratory IREENA, 2015.

[4] B. Drew, A. R. Plummer, and M. N. Sahinkaya, "A review of wave energy converter technology," 2009.

[5] A. Sciacovelli, Y. Li, H. Chen, Y. Wu, J. Wang, S. Garvey, and Y. Ding, "Dynamic simulation of adiabatic compressed air energy storage (a-caes) plant with integrated thermal storage–link between components performance and plant performance," *Applied Energy*, vol. 185, pp. 16–28, 2017.

[6] M. De Jong, "Commercial grid scaling of energy bags for underwater compressed air energy storage," *International Journal of Environmental Studies*, vol. 71, no. 6, pp. 804–811, 2014.

[7] X. Hu, C. Zou, C. Zhang, and Y. Li, "Technological developments in batteries: A survey of principal roles, types, and management needs," *IEEE Power and Energy Magazine*, vol. 15, no. 5, pp. 20–31, 2017.

[8] M. Zubiaga, *Energy transmission and grid integration of AC offshore wind farms*. Ph.D. dissertation, Escuela Politecnica Superior de Mondragon, July 2011.

[9] S. D. Wright, A. L. Rogers, J. F. Manwell, and A. Ellis, "Transmission options for offshore wind farms in the united states," in *Proceedings of the American Wind Energy Association Annual Conference*, pp. 1–12, 2002.

[10] REN21, "Renewables 2015 global status report," *REN21 Secretariat, Paris, ISBN: 978-1-84919-561-4*, 2015.

[11] C. Ozoegwu, C. Mgbemene, and P. Ozor, "The status of solar energy integration and policy in nigeria," *Renewable and Sustainable Energy Reviews*, vol. 70, pp. 457–471, 2017.

[12] M. M. Herrera, I. Dyner, and F. Cosenz, "Effects of the penetration of wind power in the brazilian electricity market," *Revista Ingeniería Industrial*, vol. 15, no. 3, pp. 309–319, 2017.

[13] A. Masmoudi, A. Tankari Mahamadou, B. Camara Mamadou, B. Dakyo, and C. Nichita, "Wind power integration in hybrid power system with active energy management," *COMPEL-The international journal for computation and mathematics in electrical and electronic engineering*, vol. 30, no. 1, pp. 246–264, 2011.

[14] "Wärtsilä auxpac product guide," *in WÄRTSILÄ AUXPAC PRODUCT GUIDE*, October 2014.

[15] P. Komor and J. Glassmire, "Electricity storage and renewables for island power," *IRENA*, May 2009.

[16] G. Sinden, "Wind power and the uk wind resource," *the Environmental Change Institute, University of Oxford*, 2005.

[17] M. M. Alam, S. Rehman, J. P. Meyer, and L. M. Al-Hadhrami, "Review of 600–2500kw sized wind turbines and optimization of hub height for maximum wind energy yield realization," *Renewable and Sustainable Energy Reviews*, vol. 15, no. 8, pp. 3839–3849, 2011.

[18] Z. Zhou, *Modeling and power control of a marine current turbine system with energy storage devices*. PhD thesis, Université de Bretagne Occidentale, 2014.

[19] S. Stubkier and H. C. Pedersen, "Design, optimization and analysis of hydraulic soft yaw system for 5 mw wind turbine," *Wind Engineering*, vol. 35, no. 5, pp. 529–549, 2011.

[20] S. Djebarri, J. F. Charpentier, F. Scuiller, and M. E. H. Benbouzid, "A systemic design methodology of pm generators for fixed-pitch marine current turbines," in *Green Energy, 2014 International Conference on*, pp. 32–37, IEEE, 2014.

[21] J. Weber, "Wec technology readiness and performance matrix–finding the best research technology development trajectory," in *4th International Conference on Ocean Energy, Dublin*, 2012.

[22] W. Ji, L. Yuxin, C. Libo, and T. Jiuting, "Using the technology readiness levels to support technology management in the special funds for marine renewable energy," in *OCEANS 2016 - Shanghai*, pp. 1–5, April 2016.

[23] H. Shien, W. Weizhou, J. Huaisen, C. Gang, W. Fujun, and L. Jun, "Integration of wind farm into gansu power grid and its operation," in *2009 International Conference on Sustainable Power Generation and Supply*, pp. 1–5, April 2009.

[24] M. Kheshti, X. Kang, G. Song, and Z. Jiao, "Modeling and fault analysis of doubly fed induction generators for gansu wind farm application," *Canadian Journal of Electrical and Computer Engineering*, vol. 38, no. 1, pp. 52–64, 2015.

[25] G. Dolf, "Power sector costing study update," *IRENA Working Paper*, January 2012.

[26] A. Myhr, C. Bjerkseter, A. Ågotnes, and T. A. Nygaard, "Levelised cost of energy for offshore floating wind turbines in a life cycle perspective," *Renewable Energy*, vol. 66, pp. 714–728, 2014.

[27] T. R. Wilbert, D. A. S. Woollett, A. Whitelaw, J. Dart, J. R. Hoyt, S. Galen, K. Ralls, D. E. Meade, and J. E. Maldonado, "Non-invasive baseline genetic monitoring of the endangered san joaquin kit fox on a photovoltaic solar facility," *Endangered Species Research*, vol. 27, no. 1, pp. 31–41, 2015.

[28] V. Badescu, *Modeling solar radiation at the earth's surface*. Springer, 2014.

[29] A. Hübler, B. Trnovec, T. Zillger, M. Ali, N. Wetzold, M. Mingebach, A. Wagenpfahl, C. Deibel, and V. Dyakonov, "Printed paper photovoltaic cells," *Advanced Energy Materials*, vol. 1, no. 6, pp. 1018–1022, 2011.

[30] E. Klugmann-Radziemska, P. Ostrowski, K. Drabczyk, P. Panek, and M. Szkodo, "Experimental validation of crystalline silicon solar cells recycling by thermal and chemical methods," *Solar energy materials and solar cells*, vol. 94, no. 12, pp. 2275–2282, 2010.

[31] Q. Vanhellemont and K. Ruddick, "Turbid wakes associated with offshore wind turbines observed with landsat 8," *Remote Sensing of Environment*, vol. 145, pp. 105–115, 2014.

[32] S.-P. Breton and G. Moe, "Status, plans and technologies for offshore wind turbines in europe and north america," *Renewable Energy*, vol. 34, no. 3, pp. 646 – 654, 2009.

[33] T. Utsunomiya, T. Shiraishi, I. Sato, E. Inui, and S. Ishida, "Floating offshore wind turbine demonstration project at goto islands, japan," in *OCEANS 2014 - TAIPEI*, pp. 1–7, April 2014.

[34] J. Zhang, L. Moreau, M. Machmoum, and P.-E. Guillerm, "State of the art in tidal current energy extracting technologies," in *Green Energy, 2014 International Conference on*, pp. 1–7, IEEE, 2014.

[35] M. R. Hashemi, S. P. Neill, P. E. Robins, A. G. Davies, and M. J. Lewis, "Effect of waves on the tidal energy resource at a planned tidal stream array," *Renewable Energy*, vol. 75, pp. 626–639, 2015.

[36] N. Maslov, J.-F. Charpentier, and C. Claramunt, "A modelling approach for a cost-based evaluation of the energy produced by a marine energy farm," *International Journal of Marine Energy*, vol. 9, pp. 1–19, 2015.

[37] T. El Tawil, J. F. Charpentier, and M. Benbouzid, "Tidal energy site characterization for marine turbine optimal installation: Case of the ouessant island in france," *International Journal of Marine Energy*, vol. 18, pp. 57–64, 2017.

[38] H. Titah-Benbouzid and M. Benbouzid, "Marine renewable energy converters and biofouling: A review on impacts and prevention," in *EWTEC 2015*, pp. Paper–09P1, 2015.

[39] N. Maslov, D. Brosset, C. Claramunt, and J.-F. Charpentier, "A geographical-based multi-criteria approach for marine energy farm planning," *ISPRS International Journal of Geo-Information*, vol. 3, no. 2, pp. 781–799, 2014.

[40] H. C. Smith and I. Ashton, "Modelling changes to physical environmental impacts due to wave energy array layouts," *Environmental Interactions of Marine Renewable Energy Technologies*, 2014.

[41] J. P. Deane, B. Ó. Gallachóir, and E. McKeogh, "Techno-economic review of existing and new pumped hydro energy storage plant," *Renewable and Sustainable Energy Reviews*, vol. 14, no. 4, pp. 1293–1302, 2010.

[42] C. Bueno and J. A. Carta, "Wind powered pumped hydro storage systems, a means of increasing the penetration of renewable energy in the canary islands," *Renewable and Sustainable Energy Reviews*, vol. 10, no. 4, pp. 312–340, 2006.

[43] L. Belhadji, S. Bacha, I. Munteanu, A. Rumeau, and D. Roye, "Adaptive mppt applied to variable-speed microhydropower plant," *IEEE Transactions on Energy Conversion*, vol. 28, no. 1, pp. 34–43, 2013.

[44] S. M. Schoenung, "Characteristics and technologies for long-vs. short-term energy storage," *United States Department of Energy*, 2001.

[45] D. A. Katsaprakakis, D. G. Christakis, K. Pavlopoylos, S. Stamataki, I. Dimitrelou, I. Stefanakis, and P. Spanos, "Introduction of a wind powered pumped storage system in the isolated insular power system of karpathos–kasos," *Applied Energy*, vol. 97, pp. 38–48, 2012.

[46] A. V. Ntomaris and A. G. Bakirtzis, "Stochastic scheduling of hybrid power stations in insular power systems with high wind penetration," *IEEE Transactions on Power Systems*, vol. 31, no. 5, pp. 3424–3436, 2016.

[47] A. Silver, "4 new ways to store renewable energy with water," *IEEE Spectrum*, pp. 13–15, 2017.

[48] S. Shalaby, "Reverse osmosis desalination powered by photovoltaic and solar rankine cycle power systems: A review," *Renewable and Sustainable Energy Reviews*, vol. 73, pp. 789–797, 2017.

[49] N. Flourentzou, V. G. Agelidis, and G. D. Demetriades, "Vsc-based hvdc power transmission systems: An overview," *IEEE Transactions on power electronics*, vol. 24, no. 3, pp. 592–602, 2009.

[50] H. G. Svendsen, J. I. Marvik, and S. C. Recio, "Report on deep offshore wind farm grid integration aspects including a case study: Hiprwind wp5-deliverable d5. 2," 2015.

[51] M. Aguirre and G. Ibikunle, "Determinants of renewable energy growth: A global sample analysis," *Energy Policy*, vol. 69, pp. 374–384, 2014.

[52] E. Martinot *et al.*, "Renewables 2005: Global status report," *Washington, DC: Worldwatch Institute*, 2005.

[53] J. P. Dorian, H. T. Franssen, and D. R. Simbeck, "Global challenges in energy," *Energy Policy*, vol. 34, no. 15, pp. 1984–1991, 2006.

[54] M. Bragard, N. Soltau, S. Thomas, and R. W. De Doncker, "The balance of renewable sources and user demands in grids: Power electronics for

modular battery energy storage systems," *IEEE Transactions on Power Electronics*, vol. 25, no. 12, pp. 3049–3056, 2010.

[55] J. P. Painuly, "Barriers to renewable energy penetration; a framework for analysis," *Renewable energy*, vol. 24, no. 1, pp. 73–89, 2001.

[56] E. Figueres, G. Garcerá, J. Sandia, F. Gonzalez-Espin, and J. C. Rubio, "Sensitivity study of the dynamics of three-phase photovoltaic inverters with an LCL grid filter," *IEEE Transactions on Industrial Electronics*, vol. 56, no. 3, pp. 706–717, 2009.

[57] Y. Yin, R. Zane, R. Erickson, and J. Glaser, "Direct modeling of envelope dynamics in resonant inverters," in *IEEE Power Electronics Specialist Conference*, vol. 3, pp. 1313–1318, IEEE, 2003.

[58] J. Rodriguez, J.-S. Lai, and F. Z. Peng, "Multilevel inverters: a survey of topologies, controls, and applications," *IEEE Transactions on industrial electronics*, vol. 49, no. 4, pp. 724–738, 2002.

[59] T. Sukegawa, K. Kamiyama, T. Matsui, and T. Okuyama, "Fully digital, vector-controlled PWM VSI-fed AC drives with an inverter dead-time compensation strategy," in *In proceeding of the IEEE Industry Applications Society Annual Meeting*, pp. 463–469, IEEE, 1988.

[60] G. Yao, Z. Lu, M. E. H. Benbouzid, T. Tang, and J. Han, "A virtual synchronous generator based inverter control method for distributed generation systems," in *Proceedings of the 2015 IEEE IECON*, Yokohama (Japan), pp. 002112–002117, Nov 2015.

[61] C. Schauder, "Adaptive speed identification for vector control of induction motors without rotational transducers," *IEEE Transactions on Industry Applications*, vol. 28, no. 5, pp. 1054–1061, 1992.

[62] T. Ohtani, N. Takada, and K. Tanaka, "Vector control of induction motor without shaft encoder," *IEEE Transactions on Industry Applications*, vol. 28, no. 1, pp. 157–164, 1992.

[63] F.-Z. Peng and T. Fukao, "Robust speed identification for speed-sensorless vector control of induction motors," *IEEE Transactions on Industry Applications*, vol. 30, no. 5, pp. 1234–1240, 1994.

[64] Y.-R. Kim, S.-K. Sul, and M.-H. Park, "Speed sensorless vector control of induction motor using extended kalman filter," *IEEE Transactions on Industry Applications*, vol. 30, no. 5, pp. 1225–1233, 1994.

[65] J. N. Nash, "Direct torque control, induction motor vector control without an encoder," *IEEE Transactions on Industry Applications*, vol. 33, no. 2, pp. 333–341, 1997.

[66] P. Cortés, G. Ortiz, J. I. Yuz, J. Rodríguez, S. Vazquez, and L. G. Franquelo, "Model predictive control of an inverter with output LC filter for UPS applications," *IEEE Transactions on Industrial Electronics*, vol. 56, no. 6, pp. 1875–1883, 2009.

[67] M. Kojima, K. Hirabayashi, Y. Kawabata, E. C. Ejiogu, and T. Kawabata, "Novel vector control system using deadbeat-controlled PWM inverter with output LC filter," *IEEE Transactions on Industry Applications*, vol. 40, no. 1, pp. 162–169, 2004.

[68] N. Hur, J. Jung, and K. Nam, "A fast dynamic dc-link power-balancing scheme for a pwm converter-inverter system," *IEEE Transactions on industrial electronics*, vol. 48, no. 4, pp. 794–803, 2001.

[69] E. Bayoumi, A. Maamoun, O. Pyrhönen, M. Khalil, and A. Mhfouz, "Enhanced method for controlling dependent integrated PWM converter-inverter system," in *Proc. of the IASTED International Conf. of Power and Energy Systems*, pp. 425–430, 2002.

[70] A. L. Shenkman, B. Axelrod, and V. Chudnovsky, "A new simplified model of the dynamics of the current-fed parallel resonant inverter," *IEEE Transactions on Industrial Electronics*, vol. 47, pp. 282–286, Apr 2000.

[71] Y. Pei, G. Jiang, X. Yang, and Z. Wang, "Auto-master-slave control technique of parallel inverters in distributed ac power systems and UPS," in *Power Electronics Specialists Conference, 2004. PESC 04. 2004 IEEE 35th Annual*, vol. 3, pp. 2050–2053, IEEE, 2004.

[72] M. Prodanovic, T. Green, and H. Mansir, "A survey of control methods for three-phase inverters in parallel connection," in *proceedings of the Eighth International Conference on Power Electronics and Variable Speed Drives*, pp. 472–477, IET, 2000.

[73] T. Green and M. Prodanović, "Control of inverter-based micro-grids," *Electric Power Systems Research*, vol. 77, no. 9, pp. 1204–1213, 2007.

[74] H. Laaksonen, P. Saari, and R. Komulainen, "Voltage and frequency control of inverter based weak LV network microgrid," in *proceedings of the International Conference on Future Power Systems*, IEEE, 2005.

[75] K. De Brabandere, B. Bolsens, J. Van den Keybus, A. Woyte, J. Driesen, and R. Belmans, "A voltage and frequency droop control method for parallel inverters," *IEEE Transactions on power electronics*, vol. 22, no. 4, pp. 1107–1115, 2007.

[76] L. Malesani and P. Tenti, "A novel hysteresis control method for current-controlled voltage-source PWM inverters with constant modulation frequency," *IEEE Transactions on Industry Applications*, vol. 26, no. 1, pp. 88–92, 1990.

[77] F. Poitiers, T. Bouaouiche, and M. Machmoum, "Advanced control of a doubly-fed induction generator for wind energy conversion," *Electric Power Systems Research*, vol. 79, no. 7, pp. 1085–1096, 2009.

[78] A. M. Howlader, Y. Izumi, A. Uehara, N. Urasaki, T. Senjyu, A. Yona, and A. Y. Saber, "A minimal order observer based frequency control strategy for an integrated wind-battery-diesel power system," *Energy*, vol. 46, no. 1, pp. 168–178, 2012.

[79] B. Beltran, T. Ahmed-Ali, and M. E. H. Benbouzid, "High-order sliding-mode control of variable-speed wind turbines," *IEEE Transactions on Industrial electronics*, vol. 56, no. 9, pp. 3314–3321, 2009.

[80] M. Torres and L. A. Lopes, "Virtual synchronous generator control in autonomous wind-diesel power systems," in *Electrical Power & Energy Conference (EPEC), 2009 IEEE*, pp. 1–6, IEEE, 2009.

[81] K. Sakimoto, Y. Miura, and T. Ise, "Stabilization of a power system with a distributed generator by a virtual synchronous generator function," in *proceedings of the 8th IEEE International Conference on Power Electronics and ECCE Asia (ICPE & ECCE)*, pp. 1498–1505, IEEE, 2011.

[82] Y. Du, J. M. Guerrero, L. Chang, J. Su, and M. Mao, "Modeling, analysis, and design of a frequency-droop-based virtual synchronous generator for microgrid applications," in *Proceedings of the 2013 IEEE ECCE*, Melbourne Victoria (Australia), pp. 643–649, June 2013.

[83] K. Visscher and S. W. H. De Haan, "Virtual synchronous machines (VSG's) for frequency stabilisation in future grids with a significant share of decentralized generation," in *SmartGrids for Distribution, 2008. IET-CIRED. CIRED Seminar*, pp. 1–4, IET, 2008.

[84] H. Levrel, M. Etienne, C. Kerbiriou, C. L. Page, and M. Rouan, "Comodeling process, negotiations, and power relationships: Some outputs from a MAB project on the island of ouessant," *Society & Natural Resources*, vol. 22, no. 2, pp. 172–188, 2009.

[85] J. M. Carrasco, L. G. Franquelo, J. T. Bialasiewicz, E. Galvan, R. C. PortilloGuisado, M. A. M. Prats, J. I. Leon, and N. Moreno-Alfonso, "Power-electronic systems for the grid integration of renewable energy sources: A survey," *IEEE Transactions on Industrial Electronics*, vol. 53, pp. 1002–1016, June 2006.

[86] J. Yuan, C. Na, Y. Xu, and C. Zhao, "Wind turbine manufacturing in china: A review," *Renewable and Sustainable Energy Reviews*, vol. 51, pp. 1235–1244, 2015.

[87] M. R. Islam, Y. Guo, and J. Zhu, "A review of offshore wind turbine nacelle: technical challenges, and research and developmental trends," *Renewable and Sustainable Energy Reviews*, vol. 33, pp. 161–176, 2014.

[88] L. Joerissen, J. Garche, C. Fabjan, and G. Tomazic, "Possible use of vanadium redox-flow batteries for energy storage in small grids and stand-alone photovoltaic systems," *Journal of Power Sources*, vol. 127, no. 1, pp. 98–104, 2004.

[89] D. P. Kaundinya, P. Balachandra, and N. Ravindranath, "Grid-connected versus stand-alone energy systems for decentralized power—a review of literature," *Renewable and Sustainable Energy Reviews*, vol. 13, no. 8, pp. 2041–2050, 2009.

[90] E. K. Akpinar and S. Akpinar, "An assessment on seasonal analysis of wind energy characteristics and wind turbine characteristics," *Energy Conversion and Management*, vol. 46, no. 11, pp. 1848 – 1867, 2005.

[91] R. Baker, S. Walker, and J. Wade, "Annual and seasonal variations in mean wind speed and wind turbine energy production," *Solar Energy*, vol. 45, no. 5, pp. 285 – 289, 1990.

[92] "Observations météo à ouessant - stiff," *http://www.meteo-bretagne.fr/observations-station-meteo-Ouessant-Stiff*, (last accessed: June 2016).

[93] M. E. Soberanis and W. Mérida, "Regarding the influence of the van der hoven spectrum on wind energy applications in the meteorological

mesoscale and microscale," *Renewable Energy*, vol. 81, pp. 286 – 292, 2015.

[94] O. Rodriguez-Hernandez, J. del Río, and O. Jaramillo, "The importance of mean time in power resource assessment for small wind turbine applications," *Energy for Sustainable Development*, vol. 30, pp. 32 – 38, 2016.

[95] L. Yanjie and W. Jun, "A large time scale wind velocity simulation method," in *2010 International Conference On Computer Design and Applications*, vol. 4, pp. V4–282–V4–286, June 2010.

[96] P. Drobinski, C. Coulais, and B. Jourdier, "Surface wind-speed statistics modelling: alternatives to the weibull distribution and performance evaluation," *Boundary-Layer Meteorology*, vol. 157, no. 1, pp. 97–123, 2015.

[97] J. Chen, J. Chen, and C. Gong, "New overall power control strategy for variable-speed fixed-pitch wind turbines within the whole wind velocity range," *IEEE Transactions on Industrial Electronics*, vol. 60, no. 7, pp. 2652–2660, 2013.

[98] Z. Zhou, F. Scuiller, J. F. Charpentier, M. E. H. Benbouzid, and T. Tang, "Power smoothing control in a grid-connected marine current turbine system for compensating swell effect," *IEEE Transactions on Sustainable Energy*, vol. 4, no. 3, pp. 816–826, 2013.

[99] F. O. Rourke, F. Boyle, and A. Reynolds, "Tidal energy update 2009," *Applied Energy*, vol. 87, no. 2, pp. 398–409, 2010.

[100] M. E. H. Benbouzid, J. A. Astolfi, S. Bacha, J. F. Charpentier, M. Machmoum, T. Maître, and D. Roye, "Concepts, modeling and control of tidal turbines," *Marine Renewable Energy Handbook*, pp. 219–278, 2013.

[101] A. Bahaj and L. Myers, "Fundamentals applicable to the utilisation of marine current turbines for energy production," *Renewable energy*, vol. 28, no. 14, pp. 2205–2211, 2003.

[102] S. Benelghali, J. Charpentier, and M. E. H. Benbouzid, "Resource to wire modelling for tidal turbines, electrical design for ocean waves and tidal energy systems," *Chap. 9, p. 303-313, ISBN: 978-1-84919-561-4, Renewable Energy Series, IET, London*, 2013.

[103] A. Uihlein and D. Magagna, "Wave and tidal current energy – a review of the current state of research beyond technology," *Renewable and Sustainable Energy Reviews*, vol. 58, pp. 1070–1081, 2016.

[104] C. Johnstone, D. Pratt, J. Clarke, and A. Grant, "A techno-economic analysis of tidal energy technology," *Renewable Energy*, vol. 49, pp. 101–106, 2013.

[105] A. S. Bahaj, "Generating electricity from the oceans," *Renewable and Sustainable Energy Reviews*, vol. 15, no. 7, pp. 3399–3416, 2011.

[106] Z. Zhou, F. Scuiller, J. F. Charpentier, M. Benbouzid, Mohamed El Hachem, and T. Tang, "Power control of a nonpitchable PMSG-based marine current turbine at overrated current speed with flux-weakening strategy," *IEEE Journal of Oceanic Engineering*, vol. 40, no. 3, pp. 536–545, 2015.

[107] Z. Zhou, F. Scuiller, J. F. Charpentier, M. E. H. Benbouzid, and T. Tang, "An up-to-date review of large marine tidal current turbine technologies," in *IEEE 2014 International Electronics and Application Conference and Exposition (PEAC)*, pp. 480–484, IEEE, 2014.

[108] S. Djebarri, J. F. Charpentier, F. Scuiller, and M. E. H. Benbouzid, "Design and performance analysis of double stator axial flux PM generator for rim driven marine current turbines," *IEEE Journal on Oceanic Energy*, vol. 41, pp. 50–66, January 2016.

[109] A. Nicolle, *Modélisation des marées et des surcotes dans les Pertuis Charentais*. PhD thesis, Université de La Rochelle, 2006.

[110] SHOM (Service Hydrographique et Océanographique de la Marine), *3D Marine Tidal Currents in Fromveur (Ouessant island)*. 2014.

[111] S. Masami, "Numerical analysis of horizontal-axis wind turbine characteristics in yawed conditions," *Open Journal of Fluid Dynamics*, vol. 2012, 2012.

[112] M. Adaramola and P.-Å. Krogstad, "Experimental investigation of wake effects on wind turbine performance," *Renewable Energy*, vol. 36, no. 8, pp. 2078–2086, 2011.

[113] A. Darmani, N. Arvidsson, A. Hidalgo, and J. Albors, "What drives the development of renewable energy technologies? toward a typology for the systemic drivers," *Renewable and Sustainable Energy Reviews*, vol. 38, pp. 834 – 847, 2014.

[114] "Soleil à Brest en 2014," *Online; available at: http://www.linternaute.com/voyage/climat/brest/ville-29019/2014*, (last accessed: June 2016).

[115] G. O. Löf, J. Duffie, and C. Smith, "World distribution of solar radiation," *Solar Energy*, vol. 10, no. 1, pp. 27 – 37, 1966.

[116] N. Lidula and A. Rajapakse, "Microgrids research: A review of experimental microgrids and test systems," *Renewable and Sustainable Energy Reviews*, vol. 15, no. 1, pp. 186 – 202, 2011.

[117] D. A. Katsaprakakis, D. G. Christakis, I. Stefanakis, P. Spanos, and N. Stefanakis, "Technical details regarding the design, the construction and the operation of seawater pumped storage systems," *Energy*, vol. 55, pp. 619–630, 2013.

[118] H. Ibrahim, A. Ilinca, and J. Perron, "Energy storage systems—characteristics and comparisons," *Renewable and sustainable energy reviews*, vol. 12, no. 5, pp. 1221–1250, 2008.

[119] A. Woyte, V. Van Thong, R. Belmans, and J. Nijs, "Voltage fluctuations on distribution level introduced by photovoltaic systems," *IEEE Transactions on energy conversion*, vol. 21, no. 1, pp. 202–209, 2006.

[120] P. D. N. Ngoc, T. T. H. Pham, S. Bacha, and D. Roye, "Optimal operation for a wind-hydro power plant to participate to ancillary services," in *Industrial Technology, 2009. ICIT 2009. IEEE International Conference on*, pp. 1–5, IEEE, 2009.

[121] A. Canova, G. Chicco, G. Genon, and P. Mancarella, "Emission characterization and evaluation of natural gas-fueled cogeneration microturbines and internal combustion engines," *Energy Conversion and Management*, vol. 49, no. 10, pp. 2900–2909, 2008.

[122] L. Fingersh, M. Hand, and A. Laxson, "Wind turbine design cost and scaling model," tech. rep., National Renewable Energy Laboratory (NREL), Golden, CO., 2006.

[123] G. Dolf, "Renewable energy technologies: Cost analysis series," *Volume 1: Power Sector, Issue 5/5 Wind Power*, June 2012.

[124] L. Castro-Santos, E. Martins, and C. G. Soares, "Cost assessment methodology for combined wind and wave floating offshore renewable energy systems," *Renewable Energy*, vol. 97, pp. 866 – 880, 2016.

[125] Lazard, "Lazard's levelized cost of energy analysis version 8.0," *Online; available at: https://www.lazard.com/media/1777/levelized_cost_of_energy_-_version_80.pdf*, (last accessed: September 2016).

[126] K. Salevid, "Market requirements for pumped storage profitability: Expected costs and modelled price arbitrage revenues, including a case study of juktan," *PhD Thesis, Uppsala University, Uppsala (Sweden)*, December 2013.

[127] C. R. Hallam and C. Contreras, "Evaluation of the levelized cost of energy method for analyzing renewable energy systems: A case study of system equivalency crossover points under varying analysis assumptions," *IEEE Systems Journal*, vol. 9, no. 1, pp. 199–208, 2015.

[128] S. Giorgio and K. Ruud, "Electricity storage: Technology brief," *Technology Policy Brief E18*, April 2012.

[129] F. Geth, T. Brijs, J. Kathan, J. Driesen, and R. Belmans, "An overview of large-scale stationary electricity storage plants in europe: Current status and new developments," *Renewable and Sustainable Energy Reviews*, vol. 52, pp. 1212–1227, December 2015.

[130] S. Benelghali, M. E. H. Benbouzid, and J. F. Charpentier, "Marine tidal current electric power generation technology: State of the art and current status," in *2007 IEEE International Electric Machines Drives Conference*, vol. 2, pp. 1407–1412, May 2007.

[131] S. Diaf, G. Notton, M. Belhamel, M. Haddadi, and A. Louche, "Design and techno-economical optimization for hybrid PV/wind system under various meteorological conditions," *Applied Energy*, vol. 85, no. 10, pp. 968 – 987, 2008.

[132] L. Cao, K. H. Loo, and Y. M. Lai, "Systematic derivation of a family of output-impedance shaping methods for power converters a case study using fuel cell-battery-powered single-phase inverter system," *IEEE Transactions on Power Electronics*, vol. 30, pp. 5854–5869, Oct 2015.

[133] M. Yazdanian and A. Mehrizi-Sani, "Distributed control techniques in microgrids," *IEEE Transactions on Smart Grid*, vol. 5, no. 6, pp. 2901–2909, 2014.

[134] J. Sun, "Impedance-based stability criterion for grid-connected inverters," *IEEE Transactions on Power Electronics*, vol. 26, pp. 3075–3078, Nov 2011.

[135] M. Liserre, R. Teodorescu, and F. Blaabjerg, "Stability of photovoltaic and wind turbine grid-connected inverters for a large set of grid impedance values," *IEEE Transactions on Power Electronics*, vol. 21, pp. 263–272, Jan 2006.

[136] L. Gyugyi, C. D. Schauder, S. L. Williams, T. R. Rietman, D. R. Torgerson, and A. Edris, "The unified power flow controller: a new approach to power transmission control," *IEEE Transactions on Power Delivery*, vol. 10, pp. 1085–1097, Apr 1995.

[137] D.-C. Lee and G.-M. Lee, "A novel overmodulation technique for space-vector PWM inverters," *IEEE Transactions on Power Electronics*, vol. 13, pp. 1144–1151, Nov 1998.

[138] K. Sakimoto, Y. Miura, and T. Ise, "Stabilization of a power system with a distributed generator by a virtual synchronous generator function," in *Proceedings of the 2011 ICPE ECCE*, Jeju (South Korea), pp. 1498–1505, May 2011.

[139] S. S. Sorkhabi and A. Bakhshai, "Microgrid control system based on an adaptive notch filter power processor," in *2016 IEEE 7th International Symposium on Power Electronics for Distributed Generation Systems (PEDG)*, pp. 1–6, June 2016.

[140] T. Caldognetto, S. Buso, P. Tenti, and D. I. Brandao, "Power-based control of low-voltage microgrids," *IEEE Journal of Emerging and Selected Topics in Power Electronics*, vol. 3, pp. 1056–1066, Dec 2015.

[141] J. T. Bialasiewicz, "Renewable energy systems with photovoltaic power generators: Operation and modeling," *IEEE Transactions on Industrial Electronics*, vol. 55, pp. 2752–2758, July 2008.

[142] J. M. Guerrero, L. Hang, and J. Uceda, "Control of distributed uninterruptible power supply systems," *IEEE Transactions on Industrial Electronics*, vol. 55, pp. 2845–2859, Aug 2008.

[143] M. Borrega, L. Marroyo, R. González, J. Balda, and J. L. Agorreta, "Modeling and control of a master slave PV inverter with n-paralleled inverters and three-phase three-limb inductors," *IEEE Transactions on Power Electronics*, vol. 28, pp. 2842–2855, June 2013.

[144] K. Sun, L. Zhang, Y. Xing, and J. M. Guerrero, "A distributed control strategy based on dc bus signaling for modular photovoltaic generation systems with battery energy storage," *IEEE Transactions on Power Electronics*, vol. 26, no. 10, pp. 3032–3045, 2011.

[145] F. Bignucolo, R. Caldon, M. Coppo, F. Pasut, and M. Pettinà, "Integration of lithium-ion battery storage systems in hydroelectric plants for supplying primary control reserve," *Energies*, vol. 10, no. 1, p. 98, 2017.

[146] H. Zhou, T. Bhattacharya, D. Tran, T. S. T. Siew, and A. M. Khambadkone, "Composite energy storage system involving battery and ultracapacitor with dynamic energy management in microgrid applications," *IEEE transactions on power electronics*, vol. 26, no. 3, pp. 923–930, 2011.

[147] C. Abbey and G. Joos, "Supercapacitor energy storage for wind energy applications," *IEEE Transactions on Industry Applications*, vol. 43, no. 3, pp. 769–776, 2007.

[148] J. Morren, S. W. De Haan, W. L. Kling, and J. Ferreira, "Wind turbines emulating inertia and supporting primary frequency control," *IEEE Transactions on power systems*, vol. 21, no. 1, pp. 433–434, 2006.

[149] P. Tielens and D. Van Hertem, "Grid inertia and frequency control in power systems with high penetration of renewables," 2012.

[150] M. A. Vallet, S. Bacha, I. Munteanu, A. I. Bratcu, and D. Roye, "Management and control of operating regimes of cross-flow water turbines," *IEEE Transactions on Industrial Electronics*, vol. 58, pp. 1866–1876, May 2011.

[151] S. Bacha, I. Munteanu, A. I. Bratcu, *et al.*, "Power electronic converters modeling and control," *Advanced Textbooks in Control and Signal Processing*, vol. 454, 2014.

[152] S. Hazra and P. S. Sensarma, "Self-excitation and control of an induction generator in a stand-alone wind energy conversion system," *IET Renewable Power Generation*, vol. 4, pp. 383–393, July 2010.

[153] S. Srilad, S. Tunyasrirut, and T. Suksri, "Implementation of a scalar controlled induction motor drives," in *2006 SICE-ICASE International Joint Conference*, pp. 3605–3610, Oct 2006.

[154] J. M. Guerrero, J. C. Vasquez, J. Matas, L. G. de Vicuna, and M. Castilla, "Hierarchical control of droop-controlled ac and dc microgrids; a general approach toward standardization," *IEEE Transactions on Industrial Electronics*, vol. 58, pp. 158–172, Jan 2011.

[155] J. M. Guerrero, J. Matas, L. G. de Vicuna, M. Castilla, and J. Miret, "Decentralized control for parallel operation of distributed generation inverters using resistive output impedance," *IEEE Transactions on Industrial Electronics*, vol. 54, pp. 994–1004, April 2007.

[156] H. Zhao, Q. Yang, and H. Zeng, "Multi-loop virtual synchronous generator control of inverter-based DGs under microgrid dynamics," *IET Generation, Transmission & Distribution*, 2016.

[157] W. Wu, Y. Chen, A. Luo, L. Zhou, X. Zhou, L. Yang, Y. Dong, and J. M. Guerrero, "A virtual inertia control strategy for DC microgrids analogized with virtual synchronous machines," *IEEE Transactions on Industrial Electronics*, 2016.

[158] K. D. Brabandere, B. Bolsens, J. V. den Keybus, A. Woyte, J. Driesen, and R. Belmans, "A voltage and frequency droop control method for parallel inverters," *IEEE Transactions on Power Electronics*, vol. 22, pp. 1107–1115, July 2007.

[159] M. Athari and M. Ardehali, "Operational performance of energy storage as function of electricity prices for on-grid hybrid renewable energy system by optimized fuzzy logic controller," *Renewable Energy*, vol. 85, pp. 890 – 902, 2016.

[160] W. Li, "Design of a hybrid fuzzy logic proportional plus conventional integral-derivative controller," *IEEE Transactions on Fuzzy Systems*, vol. 6, pp. 449–463, Nov 1998.

[161] N. J. Schouten, M. A. Salman, and N. A. Kheir, "Fuzzy logic control for parallel hybrid vehicles," *IEEE Transactions on Control Systems Technology*, vol. 10, pp. 460–468, May 2002.

[162] K. Yeager and J. Willis, "Modeling of emergency diesel generators in an 800 megawatt nuclear power plant," *IEEE Transactions on Energy Conversion*, vol. 8, no. 3, pp. 433–441, 1993.

[163] M. Rezkallah, *Amélioration de la qualité d'énergie fournie au réseau autonome hybride éolien-diesel*. PhD thesis, École de technologie supérieure, 2010.

[164] I. Vechiu, *Modélisation et analyse de l'intégration des énergies renouvelables dans un réseau autonome*. PhD thesis, Université du Havre, 2005.

[165] V. Slenduhhov and J. Kilter, "Modeling and analysis of the synchronous generators excitation systems," *Publication of Doctoral School of Energy and Geotechnology, Pärnu, Estonia*, 2013.

[166] B. Badrzadeh and S. Salman, "Enhancement of fault ride-through capability and damping of torsional oscillations for a distribution system comprising induction and synchronous generators," in *proceedings of the IEEE PES/IAS Conference on Sustainable Alternative Energy (SAE)*, pp. 1–7, IEEE, 2009.

[167] T. Zabaiou, L.-A. Dessaint, and P. Brunelle, "Development of a new library of IEEE excitation systems and its validation with PSS/E," in *Power and Energy Society General Meeting, 2012 IEEE*, pp. 1–8, IEEE, 2012.

[168] F. Demello, R. Koessler, J. Agee, P. Anderson, J. Doudna, J. Fish, P. Hamm, P. Kundur, D. Lee, G. Rogers, *et al.*, "Hydraulic-turbine and turbine control-models for system dynamic studies," *IEEE Transactions on Power Systems*, vol. 7, no. 1, pp. 167–179, 1992.

[169] S.-M. Yang and S.-J. Ke, "Performance evaluation of a velocity observer for accurate velocity estimation of servo motor drives," *IEEE Transactions on Industry Applications*, vol. 36, no. 1, pp. 98–104, 2000.

[170] A. Elfizy, G. Bone, and M. Elbestawi, "Design and control of a dual-stage feed drive," *International Journal of Machine Tools and Manufacture*, vol. 45, no. 2, pp. 153–165, 2005.

[171] O. Akhrif, F.-A. Okou, L.-A. Dessaint, and R. Champagne, "Application of a multivariable feedback linearization scheme for rotor angle stability and voltage regulation of power systems," *IEEE Transactions on Power Systems*, vol. 14, no. 2, pp. 620–628, 1999.

# Dimensionnement et réglage d'un système d'alimentation hybride à base d'énergies marines appliqué dans un contexte insulaire

***Résumé*** - L'objectif de cette thèse est de dimensionner et régler un système hybride de production d'énergie pour un site isolé de type insulaire, basé sur des énergies renouvelables marines. De manière préliminaire divers systèmes de production d'énergie renouvelable marine ont d'abord été étudiés et comparés de manière qualitative à des systèmes de production d'énergie classiques. Plusieurs types de système de stockage d'énergie ont également été étudiés, comparés et évalués dans le cas du site considéré. Cette analyse préliminaire a été étendue aux différents types de transmissions d'énergie offshore et de méthodes de réglage des convertisseurs associés aux sources renouvelables. A partir de l'étude des caractéristiques du site et de l'analyse statistique des ressources renouvelables (vents, courants marins) une méthode de dimensionnement des éléments du système de production est présentée, dans l'objectif de minimiser les émissions de $CO_2$ et le coût du système sur son cycle de vie. Pour cela, une solution de gestion de la puissance basée sur la logique floue est proposée pour le type de site considéré et comparée à une solution plus classique basée sur des règles logiques. Pour finir, une étude détaillée des différents méthodes de réglage du système hybride coté réseau est présentée. Trois niveaux de réglage sont considérés : réglage d'une source unique, réglage d'une ferme de plusieurs sources et réglage global du système hybride. Plusieurs modes de réglage sont considérés pour chaque niveau.

# On sizing and control of a renewables-based hybrid power supply system for stand-alone applications in an island context

***Abstract*** - This PhD thesis models a renewable-based hybrid power supply system applied in an islanded context and investigates sizing and regulation strategies of such a hybrid system. First, various marine energy production technologies were reviewed and compared to common renewable resources. As well, various energy storage technologies were reviewed, compared, and evaluated to fit the chosen site characteristics. A brief investigation on offshore energy transmission and inverter regulations methods is presented. Then, a study of the site characteristics, and the availability of the different renewable energy resources in the area are presented. This energy study constitutes the basis of the proposed system sizing method, where minimizing the cost and the CO2 emissions are considered as the main objectives. Furthermore, a fuzzy logic power management approach is proposed for the islanded microgrid. Finally, a detailed study of the system components grid-side inverter regulation is presented. Three regulation levels were investigated: the single inverter, the renewable farm, and the hybrid system. In this context, different regulation strategies are considered at each level.